Development of Key Technologies for Transitioning of Direct Digital Manufacturing for Repair and Remanufacturing of High Value DoD Components

Prepared by:

R. P. Martukanitz and F. Lia

Applied Research Laboratory
Pennsylvania State University
P.O. Box 30, State College, PA, 16804

Program Conducted for:

Army Aviation and Missile Research Development and Engineering Center

Benet Laboratories

July 25, 2014

REPORT DOCUMENTATION PAGE

Form Approved
OMB No. 0704-0188

1. REPORT DATE *(DD-MM-YYYY)*	2. REPORT TYPE	3. DATES COVERED *(From - To)*
25-04-2014	Final	28 Sept 2012-28 March 2014

4. TITLE AND SUBTITLE
Direct Digital Manufacturing (DDM) for the Defense Industrial Base

5a. CONTRACT NUMBER
W15QKN-12-2-0004

5b. GRANT NUMBER

5c. PROGRAM ELEMENT NUMBER

6. AUTHOR(S)
Richard Martukanitz

5d. PROJECT NUMBER
19864

5e. TASK NUMBER

5f. WORK UNIT NUMBER

7. PERFORMING ORGANIZATION NAME(S) AND ADDRESS(ES)
The Pennsylvania State University Applied Research Labotatory
Office of Sponsored Programs
110 Technology Center Building
University Park, PA 16802-7000

8. PERFORMING ORGANIZATION REPORT NUMBER

9. SPONSORING/MONITORING AGENCY NAME(S) AND ADDRESS(ES)
Benet Laboratories
1 Buffington St.
BLDG 40
Watervliet Arsenal, NY 12189-4000

10. SPONSOR/MONITOR'S ACRONYM(S)

11. SPONSORING/MONITORING AGENCY REPORT NUMBER

12. DISTRIBUTION AVAILABILITY STATEMENT
"Approved for Public Release; distribution is Unlimited"

13. SUPPLEMENTARY NOTES

14. ABSTRACT
Laser deposition processes for repairing components representing Ti-6Al-4V alloy, 8620 steel having a carburized surface, and Inconel 718® having chromium electroplated surface were evaluated. The objective was to establish processing parameters and deposition materials that could emulate the characteristics of the various surfaces for use as a repair process. Actual parts representing engine drive train components were utilized for these evaluations, and the areas for repair primarily represented bearing surfaces. Evaluations were conducted with deposition materials representing Inconel 718®, martensitic SS 431, and martensitic SS 431 with TiC to form a metal matrix composite system. All deposition materials were used in powder form, and the evaluations included detailed characterization of the deposits produced from these materials on Ti-6Al-4V, 8620 steel, and Inconel 718®

15. SUBJECT TERMS

16. SECURITY CLASSIFICATION OF:			17. LIMITATION OF ABSTRACT	18. NUMBER OF PAGES	19a. NAME OF RESPONSIBLE PERSON
a. REPORT	b. ABSTRACT	c. THIS PAGE			Richard Martukanitz
u	u	u	u	123	19b. TELEPONE NUMBER (*Include area code*) 814-863-7282

INSTRUCTIONS FOR COMPLETING SF 298

1. REPORT DATE. Full publication date, including day, month, if available. Must cite at lest the year and be Year 2000 compliant, e.g., 30-06-1998; xx-08-1998; xx-xx-1998.

2. REPORT TYPE. State the type of report, such as final, technical, interim, memorandum, master's thesis, progress, quarterly, research, special, group study, etc.

3. DATES COVERED. Indicate the time during which the work was performed and the report was written, e.g., Jun 1997 - Jun 1998; 1-10 Jun 1996; May - Nov 1998; Nov 1998.

4. TITLE. Enter title and subtitle with volume number and part number, if applicable. On classified documents, enter the title classification in parentheses.

5a. CONTRACT NUMBER. Enter all contract numbers as they appear in the report, e.g. F33615-86-C-5169.

5b. GRANT NUMBER. Enter all grant numbers as they appear in the report, e.g. 1F665702D1257.

5c. PROGRAM ELEMENT NUMBER. Enter all program element numbers as they appear in the report, e.g. AFOSR-82-1234.

5d. PROJECT NUMBER. Enter al project numbers as they appear in the report, e.g. 1F665702D1257; ILIR.

5e. TASK NUMBER. Enter all task numbers as they appear in the report, e.g. 05; RF0330201; T4112.

5f. WORK UNIT NUMBER. Enter all work unit numbers as they appear in the report, e.g. 001; AFAPL30480105.

6. AUTHOR(S). Enter name(s) of person(s) responsible for writing the report, performing the research, or credited with the content of the report. The form of entry is the last name, first name, middle initial, and additional qualifiers separated by commas, e.g. Smith, Richard, Jr.

7. PERFORMING ORGANIZATION NAME(S) AND ADDRESS(ES). Self-explanatory.

8. PERFORMING ORGANIZATION REPORT NUMBER. Enter all unique alphanumeric report numbers assigned by the performing organization, e.g. BRL-1234; AFWL-TR-85-4017-Vol-21-PT-2.

9. SPONSORING/MONITORS AGENCY NAME(S) AND ADDRESS(ES). Enter the name and address of the organization(s) financially responsible for and monitoring the work.

10. SPONSOR/MONITOR'S ACRONYM(S). Enter, if available, e.g. BRL, ARDEC, NADC.

11. SPONSOR/MONITOR'S REPORT NUMBER(S). Enter report number as assigned by the sponsoring/ monitoring agency, if available, e.g. BRL-TR-829; -215.

12. DISTRIBUTION/AVAILABILITY STATEMENT. Use agency-mandated availability statements to indicate the public availability or distribution limitations of the report. If additional limitations/restrictions or special markings are indicated, follow agency authorization procedures, e.g. RD/FRD, PROPIN, ITAR, etc. Include copyright information.

13. SUPPLEMENTARY NOTES. Enter information not included elsewhere such as: prepared in cooperation with; translation of; report supersedes; old edition number, etc.

14. ABSTRACT. A brief (approximately 200 words) factual summary of the most significant information.

15. SUBJECT TERMS. Key words or phrases identifying major concepts in the report.

16. SECURITY CLASSIFICATION. Enter security classification in accordance with security classification regulations, e.g. U, C, S, etc. If this form contains classified information, stamp classification level on the top and bottom of this page.

17. LIMITATION OF ABSTRACT. This block must be completed to assign a distribution limitation to the abstract. Enter UU (Unclassified Unlimited) or SAR (Same as Report). An entry in this block is necessary if the abstract is to be limited.

EXECUTIVE SUMMARY

The objective of the IBIF program was to provide a sound foundation to accelerate implementation of DDM technology for sustainment activities that cut across various DoD organizations and platforms. Goals of the project included developing and validation of laser-based repair process for critical DoD components, developing a repair selection criteria, developing methods for quality assurance of parts, and to disseminate knowledge of laser-based direct digital manufacturing (DDM) technology to members of the defense industrial base.

A laser deposition process simulating Ti-6Al-4V, carburized, and chromium electroplated surfaces for bearing applications was investigated in this program. Three components including the T700 Power Turbine Shaft, the Input Bevel Pinion Gear, and the Cooling Fan Shaft were selected for repair. The substrate material selected for laser processing included, Ti-6Al-4V, carburized AISI 8620 steel (8620 steel), and Inconel 718® with a chromium electroplated surface. Deposition materials that were evaluated during these work included Inconel 718®, AISI stainless steel 431 (SS431), and SS 431 with various level of titanium carbide as a composite deposit. The various materials were deposited onto the selected components using the directed laser deposition process.

Scanning electron microscopy (SEM), energy dispersive spectrometry (EDS), and a particle size analyzer were used to characterize selected powders used during the laser deposition experiment. Microstructural analysis, Vickers micro hardness testing, and EDS-mapping were used for deposited material evaluations. Performance testing of the laser deposited composite material was also conducted and included rolling contact fatigue testing and tribological analysis.

Vickers Hardness tests indicated the validity of the Ti-6Al-4V and AISI stainless steel TiC deposits, with hardness values greater than or equal to the hardness of the original components. SEM images showed that some of the TiC particles dissolved and the Ti and C were reprecipitated in the SS 431 matrix. The higher carbon within the matrix material enhanced the overall hardness of the laser deposit. The dissolved TiC phase that surrounded the original TiC particle formed a secondary phase in the matrix alloy by reprecipitation during cooling. Rolling contact fatigue tests, which represented an aggressive rolling and sliding wear, indicated that the composite deposit exhibited slightly greater wear, due to hard particle expulsion, that resulted in lower rolling contact fatigue life when compared to the carburized 8620 steel.

The program provided great insight into the validity of laser-based DDM technology for component repair. Specifically, it was concluded that laser-based repair offers full metallurgical bonding at the deposit/substrate interface. Repair of Ti-6Al-4V components using Ti-6Al-4V additions provided properties of the deposit that were slightly better than the original material. Aside from very minor microporosity, the deposit exhibited excellent quality. Martensitic stainless steel alloy with 20% (wt.) TiC deposit provides hardness similar to a carburized surface. The deposit also exhibited excellent quality. Laser deposition for repair of Inconel 718® appears to require very low heat input that minimizes dilution of the nickel base material into the deposit. It is believed that lower heat input with stainless steel 431 and/or 431 with TiC may match the hardness of the chromium electroplated surface on

Inconel 718®. Laser-based repair using like alloys or alternate deposition materials may be used to repair a wide range of high value components.

TABLE OF CONTENTS

LIST OF FIGURES

LIST OF TABLES

1. PROGRAM OBJECTIVE

The objective of the program was to provide a sound foundation to accelerate implementation of direct digital manufacturing (DDM) technology for sustainment activities that cut across various DoD organizations and platforms. It is hoped that providing this foundation will lead to broader adoption of DDM technology for repair and restoration of worn, damaged, or reconfigured components for critical DoD assets.

1.1 Program Goals and Metrics

1) To establish methods that the DoD may utilized for categorizing common part families for repair based on similar characteristics and requirements and to identify and evaluate DDM technology in at least three of these categories.

2) To develop methods and implement procedures for quality assurance that relies on process controls, qualification, and documentation.

3) To broadly disseminate knowledge of DDM technology to members of the defense industrial base, that includes its selection and proper use for repair and refurbishment through integrated project teams, forums, and hands-on training.

The metrics for the program are to identify at least three component families containing at least five components each. Certification strategies and qualification plans for each family will be identified and developed. Quality assurance methods will be developed that ensure the repair procedures and the remanufactured components meet or exceed the original design intent. Through annual forums, the proposed program will initially provide training to at least three key personnel from each of the depots and research, development, and engineering centers, with plans to expand the dissemination of information to other DoD depots, facilities, and commercial interests supporting the supply chain in the later years of the program.

2. STATEMENT OF WORK

2.1 Additive Manufacture and Laser Deposition

Task 1.1 Establish Integrated Program Team (IPT). Identify Part Categories and Representative Components for Laser-Based Repair Evaluations

The integrated project team will consist of key representatives responsible for the development and insertion of technology across the supply chain. At the depot level, this will include representatives from both engineering and manufacturing, component owners and cognizant authorities for parts and systems. Supply chain team members (i.e. Genesis, LLC, depot suppliers, and commercial repair facilities) are included to provide a supplier perspective, specialized testing and fabrication. The Applied Research Laboratory, the Pennsylvania State University (ARL Penn State) and Benet Laboratories as the research organizations provide expertise in metal DDM process technology, the associated impact of DDM processes on performance, various material and process models, and past and leveraged research in metal DDM technology applicable to the proposed effort. Once established, the IPT will identify part categories and representative components for laser-based repair evaluations. The categories will include material, service criticality, geometry, current fabrication method, supply chain status, and required performance metrics. It is anticipated that each depot will supply information on at least ten component parts for the first year of program execution. The component parts will include both infrequent and frequent repairs. The AMRDEC Aviation Engineering Directorate (AED) Maintenance Engineering Division (MED) Storage, Analysis, Failure evaluation and Reclamation (SAFR) program co-located at Corpus Christi Army Depot will be used as a source of candidate parts, failure analysis and technical data in support of DDM repair process development.

Task 1.2 Establish Repair Process Planner for DDM

The DDM repair process must consider the form, fit and function of the subject component. One of the key components of this effort is to develop a standardized method by which a component may be repaired. The intent is not to restrict depots or commercial suppliers to repair of a component in a specific manner, but to develop the necessary controls to ensure those components repaired by DDM by multiple suppliers meet the intended service requirements. To this end, a process planning strategy will be developed that defines requirements for CAD models, tolerancing, surface finish, material, deposition path planning, surface preparation, post machining, post heat treatment, and inspection. As part of the repair process plan, an approval methodology will be developed that will enable a broad supply network to be established within existing DoD criteria.

Task 1.3 Establish quality assurance requirements and automated quality control functionality

In conjunction with the repair process planner, quality assurance will be addressed through the establishment of quality assurance requirements and equipment quality control functionality. The proposed effort will establish the guidelines, databases, and in-process monitoring components (laser power, powder flow, vision system) that may be interfaced with commercially available laser deposition systems. Relevant existing standards (ASTM, MIL, AMS, ISO etc) will be used.

Task 1.4 Evaluate Repair Process for Representative Components

From the list of potential components to be repaired by DDM, at least three components per depot will be evaluated for repair by ARL Penn State. This will entail at least 9 potential repair applications of high value DoD components. It is anticipated that these components will span the range of material and repair situations identified during the first task. The evaluation will follow the method established in task 1.2 and 1.3 for process planning and quality assurance. These evaluations will provide a proving ground for the development and refinement of the laser-based repair methods applicable to a wide range of DoD components.

Task 1.5 Characterization and Validation of Laser-Based Repair Processes

Actual repaired components from task 1.4 will be extensively analyzed to provide performance data to the integrated project team to determine the effectiveness of the methods established. Specimens representing these repaired components will be analyzed to determine material–process characteristics.

Task 1.6 Conduct IPT Forum and Develop "Best DDM Practices for Repair"

The forum will present to the IPT and potential supply chain organizations the results of the first year effort and will include technical training, process demonstrations, and feedback for the developed Best Practices for Direct Digital Manufacturing for Repair. Commercial organizations having leadership roles in DDM technology will also participate with the objective of developing a commercially-based supply chain for repair and remanufacturing during surge production or to address defense industrial base shortfalls. This will include aspects needed to support Tasks 2.4, 3.1, and 3.2.

3. STATEMENT OF WORK FOR OPTIONAL YEARS 2 AND 3 TASKS

Task 2.1: Expand repair components to include remanufacturing as an additional option for obtaining the necessary component.

The IPIT will (a) incorporate lessons learned year one into the part family categorization guidelines, (b) expand the list of components and part families to include decision criteria to repair or remanufacture a component and (c) update the Repair Process Planner to include remanufacturing

Task 2.2: Reproduce Tasks 1.3 and 1.4 at depots and/or repair facilities with wider selection of components applicable to laser-based repair.

Continue repair and begin remanufacture process development at ARL Penn State, Benet Labs, and include inter-facility studies between ARL Penn State, Anniston, Benet and other supply chain partners.

Task 2.3: Begin qualification and verification process for laser-based repair.

Further testing, verification and analysis of the methods established and component repaired during year two, supporting qualifications, will be conducted by ARL Penn State, Benet, and Genesis.

Task 2.4: Identify process metrics for expanded categories of parts and determine viable repair supply chain.

A forum will be held at ARL Penn State to present to the IPT and supply chain organizations the results of the second year of effort which will include technical training, process demonstrations, and feedback for the developed.

Task 3.1: Disseminate repair technology and establish supply chain for support of depots.

Disseminate standards and guidelines developed conduct extensive training at ARL Penn State at their facilities, extending invitations to all Sustainment Defense Industrial Base entities (depots, technical authorities, and commercial interests).

Task 3.2: Conduct certification of supply chain functions.

ARL Penn State will conduct further component testing and analysis in support of the certification of the part families and components repaired.

4. PROGRAM TEAM

Because of the necessity to engage a variety of organizations required for broad and successful implementation of laser-based repair technology, program direction is guided through an Integrated Program Team (IPT) encompassing, shown as Figure 1:

- Research, Development, and Engineering Centers of the Army (ARDEC, AMRDEC and TARDEC) and Navy (NAVAIR),
- Major DoD depots (Corpus Christi, Anniston, MCLC Albany, and Fleet Readiness Center East),
- Process development and applications organizations (Applied Research Laboratory, Pennsylvania State University, Benét Laboratories, and Genesis Engineering Associates), and
- Commercial organizations specializing in DDM for repair and remanufacturing (Alabama Laser, Preco Corporation, and Morris Technologies).

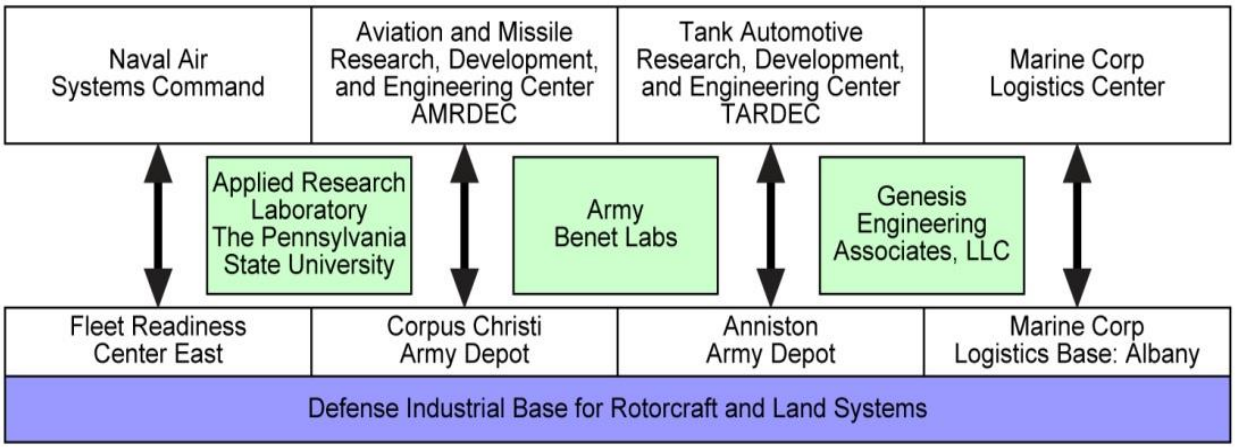

Figure 1 – Program team organization showing institutional interactions.

5. DDM INTRODUCTION

Direct Digital Manufacturing (DDM) is a novel additive manufacturing process by which volumes of material are added to selectively restore dimensions and features for repair or to directly produce components via a digital representation of the part through a CAD file or point cloud. In contrast to conventional formative and subtractive manufacturing processes, all DDM technologies fabricate features or the component in an additive manner through the layer wise addition of material. The desired component dimensions or shape are achieved through coordinated motion of the heat source and the material feedstock addition to repeatedly produce layers of fused material. Volumes of material ranging from a 1 mm^3 repair to a 1 m^3 component can be produced with the technology. The process is well suited for repair of high value components or the production of small lots of components, and has the potential to address supply chain issues associated with surge production and long lead times. Thus, DDM has great potential for addressing availability of parts and components for critical DoD assets, increased affordability, and surge capacity for sustainment activities within the defense industrial base.

There have been several instances of demonstrated DDM repairs in the DoD to date. For example Anniston Army Depot demonstrated the use of Laser Engineered Net Shaping (LENS) to repair gas turbine engine components on the M1A1. The Applied Research Laboratory, Pennsylvania State University (ARL Penn State) and its partners have demonstrated DDM repair for titanium compressor blade tips in the F402 engine, valves and shaft components for submarines, gear components for aviation, and aluminum shells used in undersea systems for the Navy. [1] Researchers at Rolls-Royce developed a LENS repair for high performance Ti-6Al-4V blisk aerofoils. In addition, many aerospace OEM's are pursuing DDM technology for new manufacture. [2] Despite these often positive, dispersed, technical success, there are still engineering challenges that exist, preventing the widespread adoption of DDM as a tool for improving sustainment in the defense industrial base. [3-8]

Current issues facing DDM prior to acceptance by the DoD are lack of methods and guidance for process qualification and component certification for a wide range of metals. The only existing specification available is the Aerospace Materials Specification, "Titanium Alloy Direct Deposited Products 6Al – 4V Annealed". [9,10] This document (AMS 4999A) considers deposition of Ti-6Al-4V in terms of testing requirements, minimum properties, and reporting requirements to achieve certification to this standard. [11] The American Society for Testing and Materials F42 Committee on Additive Manufacturing Technologies is in the process of developing a range of standards for DDM processes. From a qualification and certification standpoint, Boeing and Lockheed Martin have conducted a multitude of testing, valued at $10M, to obtain certified components through the development of "design allowable" for DDM processed Ti-6Al-4V. While both companies are on the verge of implementing this technology, much of the information surrounding properties and process are proprietary. The extensive testing performed to satisfy conventional design and engineering requirements is often used as a yardstick by organizations wishing to implement the technology for their own components; however, the desire to maintain data as proprietary serves as an impediment to wider implementation of DDM technology to the defense industrial base. The process for DDM development is shown in Figure 2.

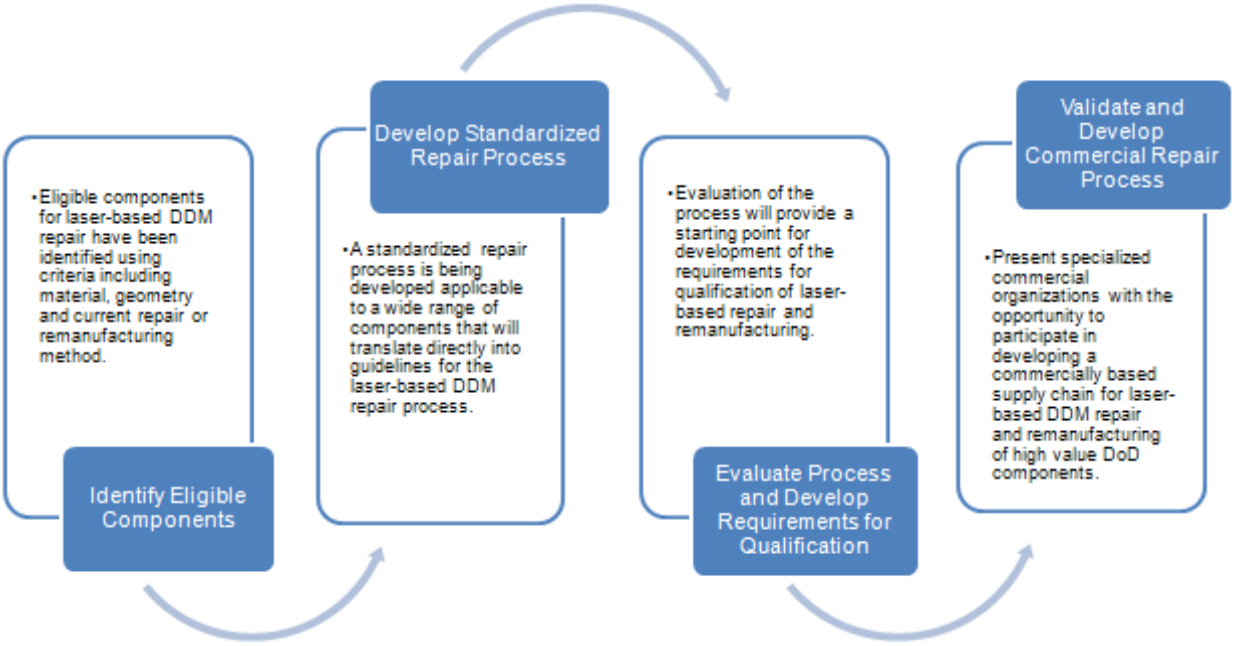

Figure 2 – Ideal process for DDM development.

6. SELECTION OF COMPONENTS AND PLANNING FOR LASER-BASED REPAIR

An extremely important aspect of meeting technical and economic metrics for the laser-based repair process is the selection of applicable components. General considerations during the selection process should include cost for replacement, and requirements for meeting the component and system performance. Typically, these factors are directly dependent; whereas, critical components dictate high replacement costs. Since it has been shown that laser-based repair, by providing full metallurgical bonding of the repair material and substrate, can provide performance equivalent to or better than original material, high value items should be considered potential candidates for laser-based repair technologies. Obviously, the ability to compress the time required for system repair or overhaul, which may be influenced by repair verses acquisition of a component, may also provide incentive for implementation of laser-based repair processes.

Specific consideration for laser-based repair include the original substrate material, the loading conditions and/or environment while in service, and the spatial attributes of the area to be repaired. The original substrate material may be repaired by adding a material identical in composition to the substrate or a different material that may meet the requirements and provide metallurgical compatibility of the original material. Even if the original material composition is used for repair, post process heat treatment may be required to ensure that the microstructure in the repair area provides the properties necessary for meeting the requirements for service. Post processing may be required when heat treating has been used to obtain a specific microstructure, and mechanical properties of the original component. However, in many instance laser-based repair may provide characteristic of the deposition material that meet the attributes of the original material without post process heat treatment, which may increase cost of the repair process, be difficult to implement due to size or part configuration, and may impart dimensional variability due to induced thermal distortion or relaxation.

Shown in Figure 3 is a proposed flowchart for initial selection of components for repair through directed laser deposition. The flowchart provides a formalized method to determine the potential performance requirements for a candidate components for repair and the difficulty in instituting the repair process based on the material and geometry for the repair. The difficulty in meeting the performance requirements based on the repair material and the anticipated loading conditions, derived from the designer or the technical authority for the component, is captured using individual repair indices that are totaled to provide a Component Repair Index. Based on the a qualitative analysis, a cumulative Component Repair Index above 5 would be considered a difficult laser-based repair process for implementation.

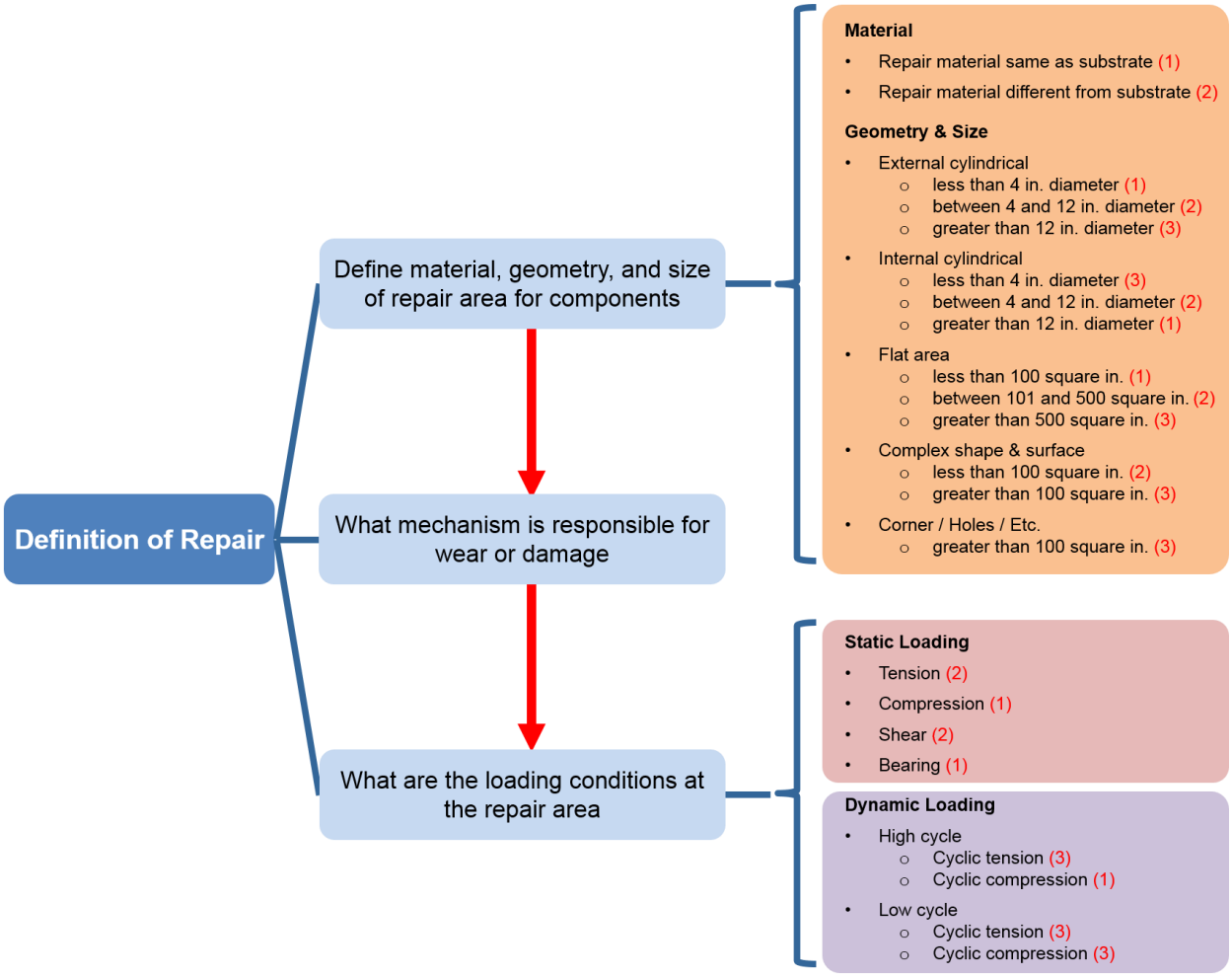

Where (#) is the individual repair indices. The cumulative score of the individual indices is the Component Repair Index. A Component Repair Index above 5 would be considered a difficult repair process for implementation.

Figure 3 – Flowchart for selection of components and conditions for laser-based repair process.

7. SELECTION OF COMPONENTS FOR DDM EVALUATIONS

Initial material selection was conducted with laser deposits of four different materials on low carbon steel substrate. The four selected deposition materials were: SS 431, SS 431 with 28.13 vol% (20 wt%) of TiC (SS 431/20 TiC), SS 431 with 53.07 vol% (40 wt%) of TiC (SS 431/40 TiC), and SS 431 with 70.14 vol% (60 wt%) of TiC (SS 431/60 TiC). The SS 431 – TiC powders were mixed by the weight percentage ratio before laser processing.

All selected materials were laser deposited with a single layer and a multi-layer deposition on to a low carbon steel substrate. All samples were examined by microstructural images and measured using Vickers micro hardness testing. Two selected materials were determined for laser deposition on the carburized 8620 steel substrates. The exact deposition parameters were also developed to optimize deposition quality.

Based on the results of initial material selection, deposition material SS 431/20 TiC and SS 431/40 TiC were selected for further evaluations on carburized 8620 steel substrates using a single layer deposition. Both samples were analyzed using microstructural images and micro hardness testing. A final deposition material was chosen for RCF test specimen production. The RCF test specimen was not only tested by rolling contact fatigue, but also examined using microstructural images, micro hardness testing, and SEM and EDS analysis. Finally, the RCF specimen was measured for surface roughness after surface roller grinding.

Four different materials were also selected for simulating chromium electroplating on Inconel 718®. The selected powder materials were Inconel 718®, SS 431, SS 431/20 TiC, and SS 431/40 TiC. All samples were examined by microstructural images and Vickers micro hardness testing. Surface roughness testing was also conducted on these specimens after surface roller grinding.

7.1 AISI 8620 Steel

AISI 8620 steel contains a wide range of alloying additions that typically include C, Mo, Cr, Mn, Mo, Ni, and Si, fixed for carbon steels. The chemical composition of 8620 steel is shown in Table 1. [12] These types of steels are more responsive to mechanical and heat treatments than plain carbon steels. Alloy 8620 steel is a common, carburizing alloy steel. This steel is flexible during hardening treatments, thus enabling improvement of case/core properties. Normalized 8620 steel has a hardness of approximately at 270 HV; however, carburization of 8620 steel develops an excellent wear resistant surface in the range of 700 to 760 HV (60 – 63 HRC). Properties of interest for the 8620 steel for this study are shown in Table 2, [12] and a comparison chart of various hardness values are shown in Appendix A. The raw data for hardness measurements obtain during the evaluations are shown in Appendix B.

Table 1 – Chemical composition of 8620 steel alloy. [12]

	Fe	Cr	Ni	Mn	Mo	C	Si
8620 Steel	96.9-98.02	0.4-0.6	0.4-0.7	0.7-0.9	0.15-0.25	0.18-0.23	0.15-0.35

Table 2 – Properties of interest for 8620 steel alloy. [12]

Theoretical Density (g/cm^3)	Melting Temperature (°C)	Normalized Hardness (HV)	Carburized Hardness (HV)
7.85	1427	272	697 – 763

7.2 AISI Stainless Steel 431

AISI stainless steel alloy 431 (SS 431) is a case hardenable steel that exhibits excellent corrosion resistance. Martensitic stainless steels contain more than 10.5 wt% Cr along with other austenite-stabilizing elements, such as carbon, nitrogen, nickel, and manganese, to expand the austenite phase field and permit heat treatment. The nominal composition of alloy 431 is Fe-0.2C-1Si-1Mn-16Cr (wt%). [13] The composition must be carefully balanced to prevent delta-ferrite formation at the austenitizing temperature. Delta-ferrite in the hardened structure should be avoided for embrittlement and attain the best mechanical properties. Alloy 431 also has excellent tensile and torque strength, and good toughness.

The stainless steel alloy 431 powder was acquired from Carpenter Technology, with a particle size of between 45 to 149 μm (-100/+325 mesh). The powder was gas atomized. As shown in Figure 4, the particles are spherical. The image of Figure 5 shows the topography of a particle, which indicated a rough texture. The sub particle structure was small and densely formed. The mean particle size (d_{50}) was found to be 87 μm with a standard deviation of 45.4 μm, which is shown in Figure 6. The EDS spectrum for the SS 431 is shown in Figure 7. A chemical composition comparison is shown in Table 3, and matches the nominal reference composition. [13] However, relatively high levels of carbon were found to be present and may be due to sample preparation with carbon tape. Properties of interest for SS 431 are shown in Table 4. [13]

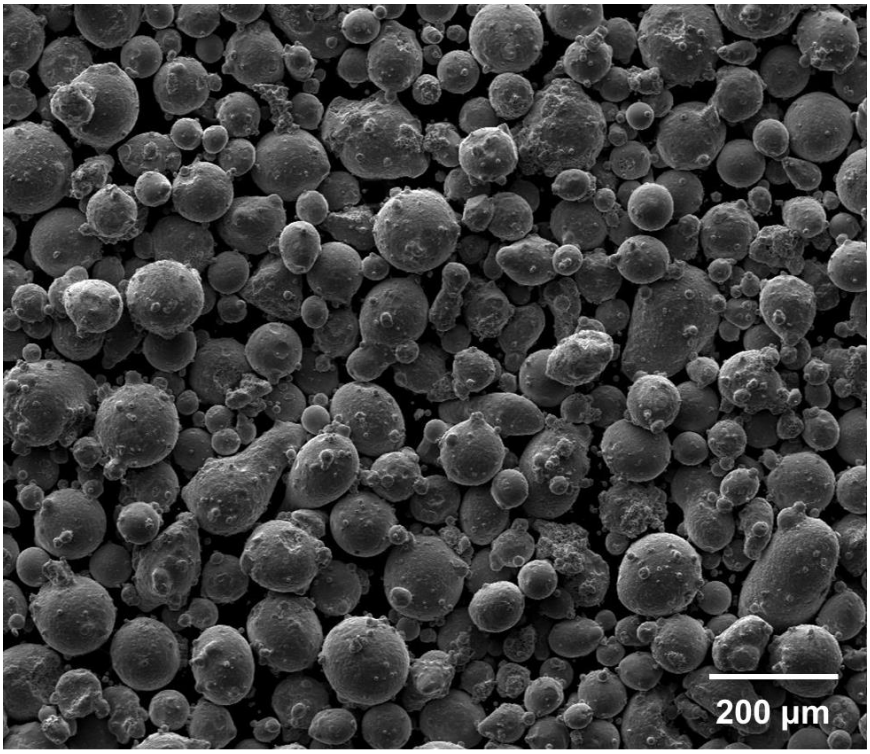

Figure 4 – SEM image of SS 431 particles of powder obtained from Carpenter Technology.

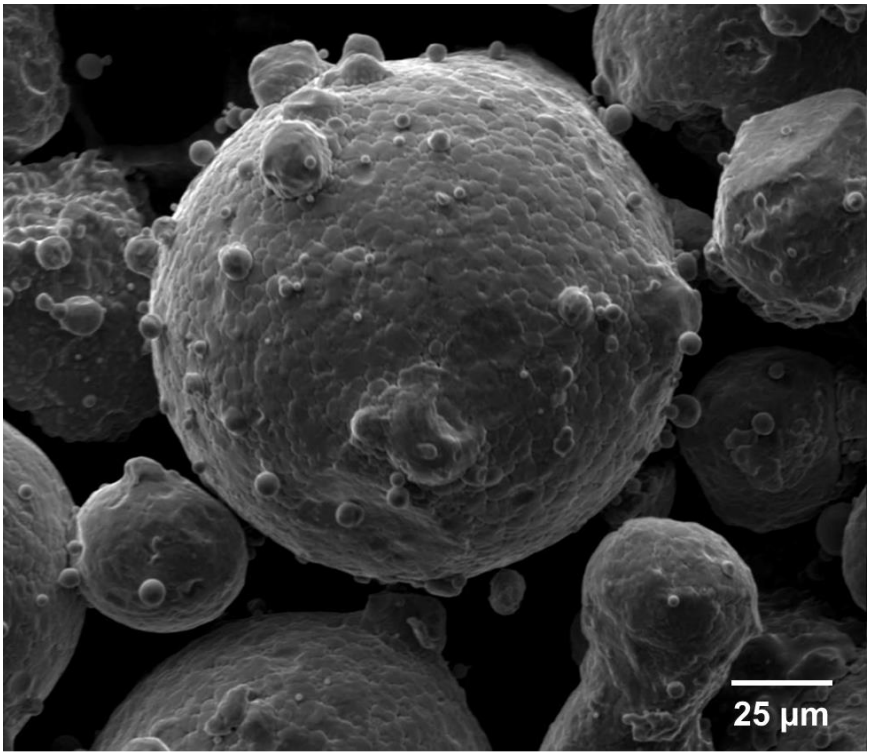

Figure 5 – SEM image of SS 431 particle with satellites around the dense spherical particle of powder obtained from Carpenter Technology.

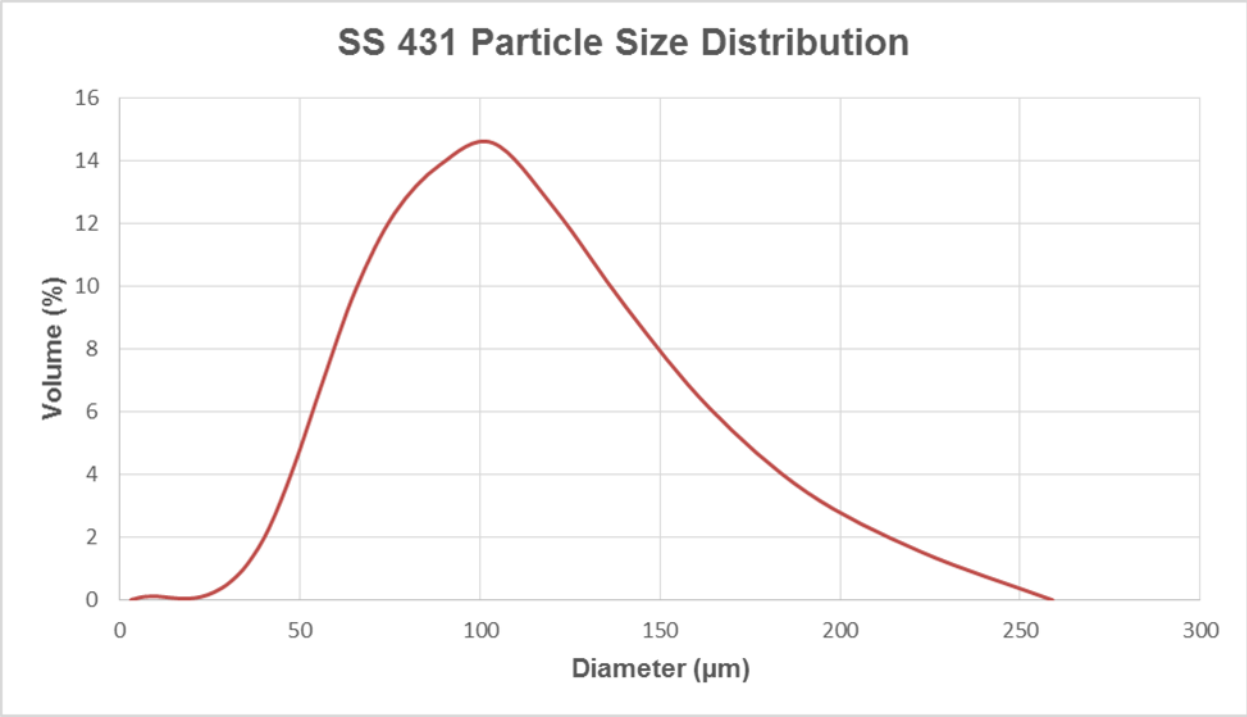

Figure 6 – Particle size distribution of SS 431 powder.

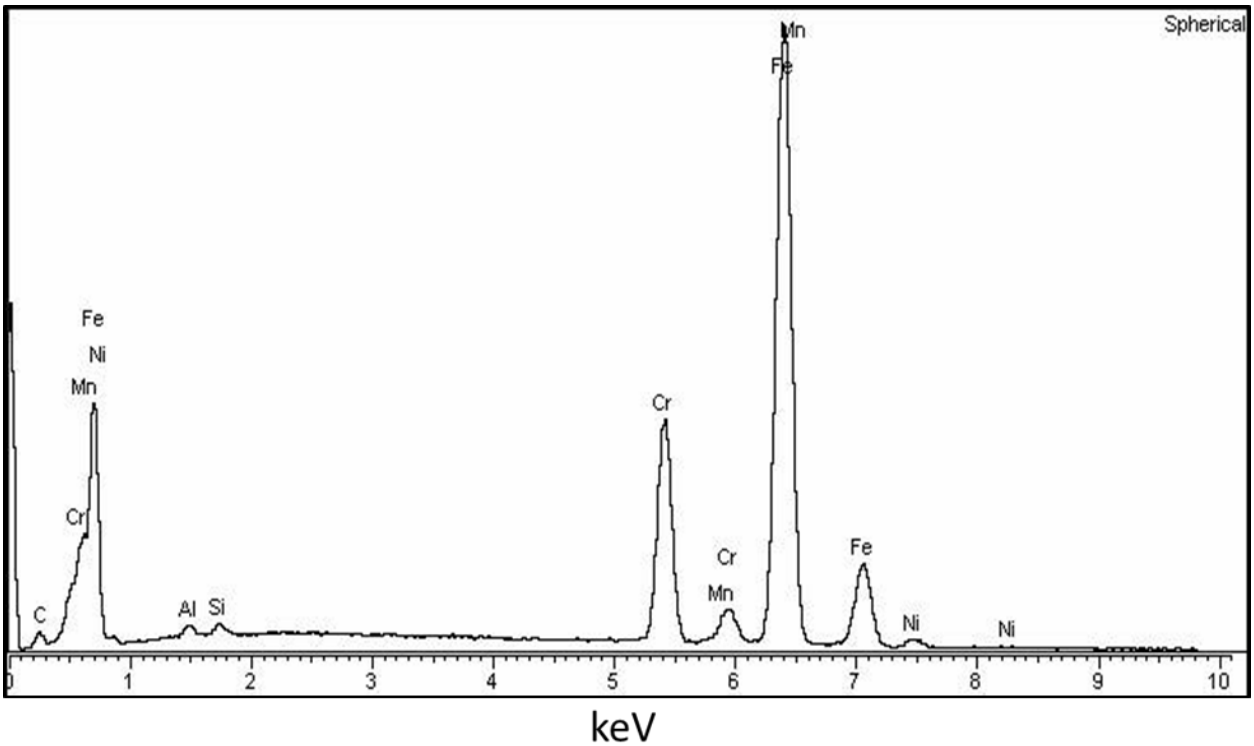

Figure 7 – EDS spectrum of SS 431 powder.

Table 3 – Measured and reported nominal chemical compositions for SS 431 powder.

wt%	Fe	Cr	Ni	Mn	C	Si	Al
SS 431	79.17	15.58	1.36	0.44	2.5	0.4	0.54
Reference[13]	80	15-17	1.25-2.25	1	0.2	1	-

Table 4 – Properties of interest for SS 431. [13]

Theoretical Density (g/cm^3)	Melting Temperature (°C)	Hardness (HV)
7.8	1482	392

7.3 Titanium Carbide

The titanium carbide (TiC) powder is an extremely hard ceramic material. Titanium carbide has excellent properties for wear and corrosion resistance, which aided the decision to utilize this material within the metal matrix.

The TiC powder was obtained from AEE Corporation, with a particle size of 45 to 149 μm (-100/+325 mesh). The AEE TiC powder was found to be irregular in shape, and is shown as Figure 8. The particles exhibited pores and debris on the surface and this is shown as Figure 9. The mean particle size (d_{50}) was found to be 88 μm with a standard deviation of 41.5 μm, which is shown in Figure 10. The EDS spectrum for the TiC is shown in Figure 11. A comparison of measured and reported composition is shown in Table 5, and the measured composition was similar to the nominal composition. [14] There was also a small amount of vanadium (V), approximately 0.3%, that was observed in the TiC powder, and was probably in the TiC raw material. Properties of interest for the TiC are shown in Table 6. [14]

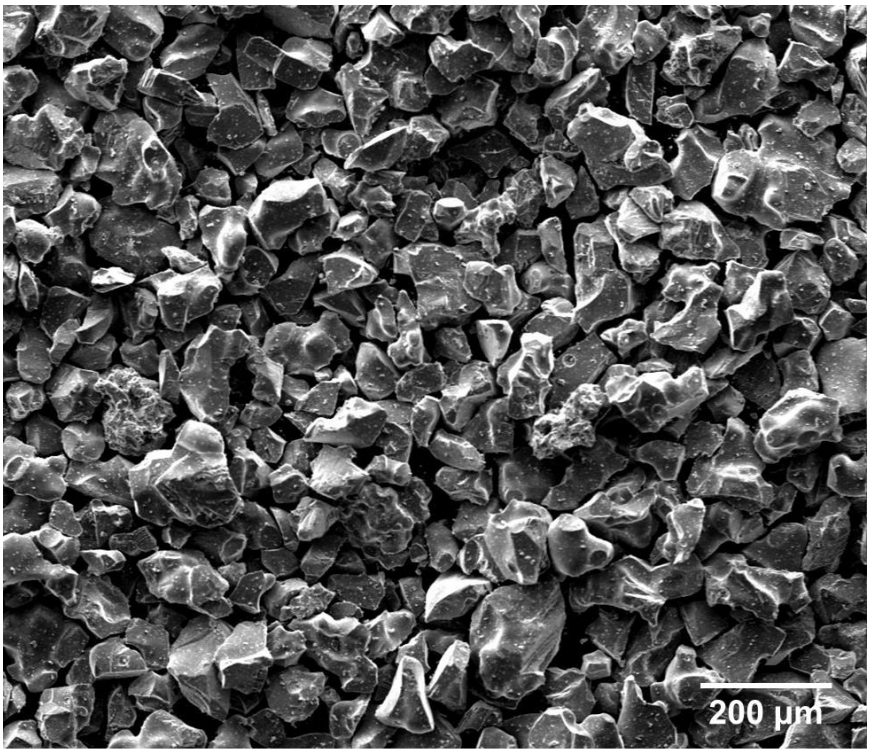

Figure 8 – SEM image of TiC particles of powder obtained from AEE Corporation.

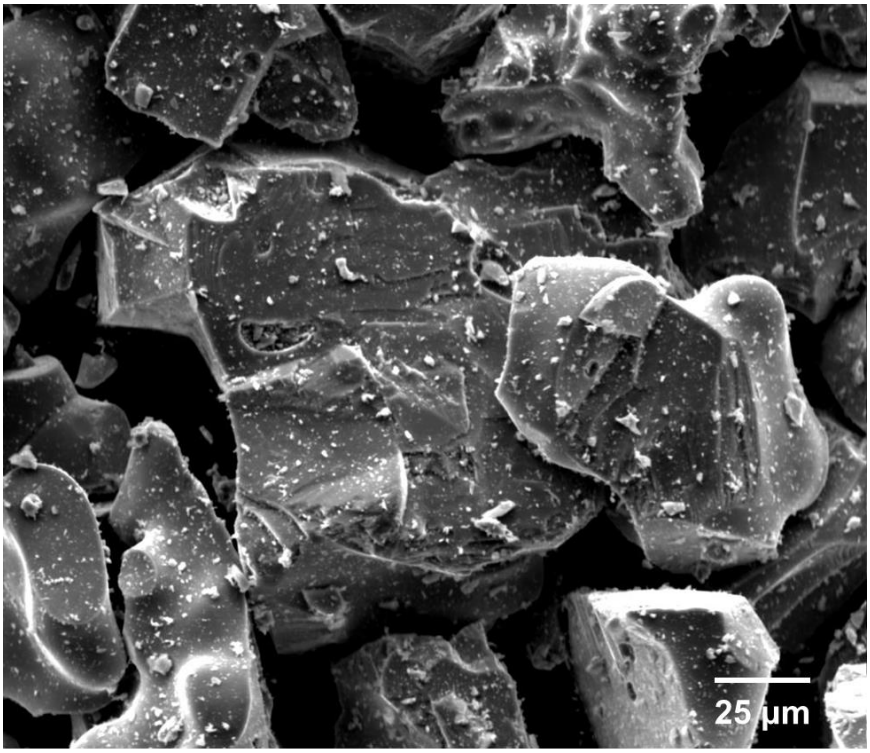

Figure 9 – SEM image of TiC particle with pores at the surface of powder obtained from AEE Corporation.

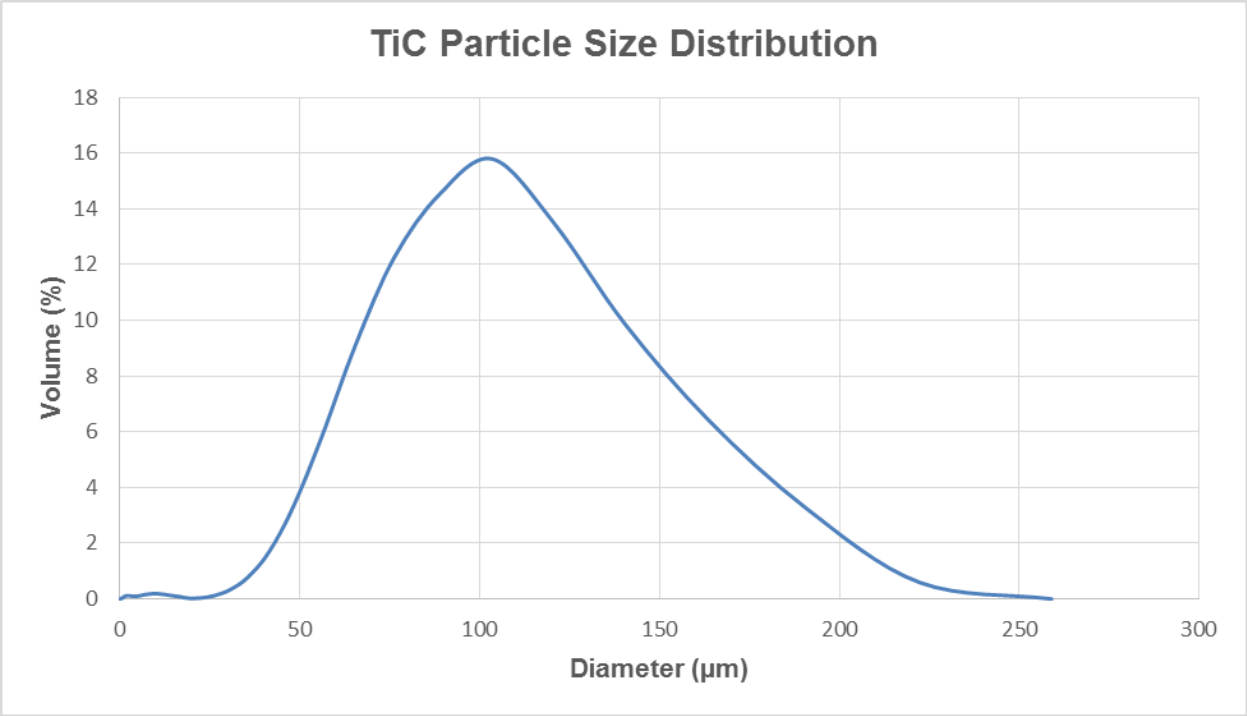

Figure 10 – Particle size distribution of TiC powder.

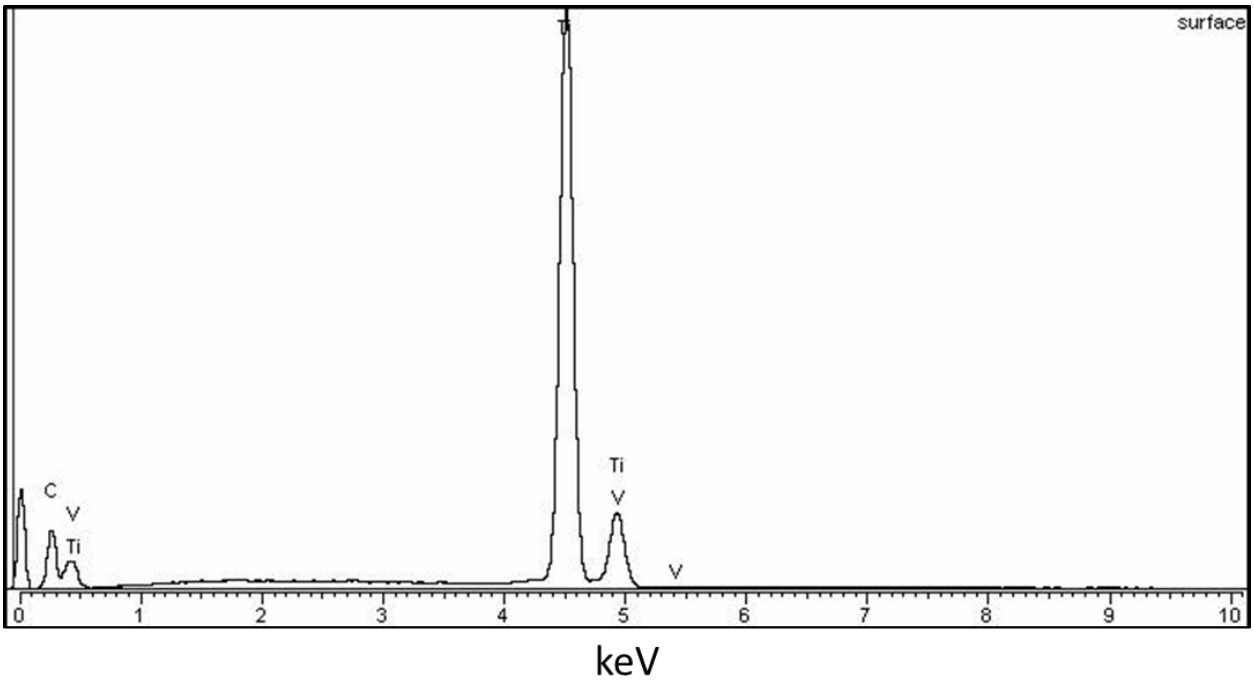

Figure 11 – EDS spectrum of TiC powder.

Table 5 – Measured and reported nominal chemical compositions for TiC powder.

wt%	Ti	C	V
TiC	83.81	15.85	0.34
Theoretical [14]	79.9	20.1	–

Table 6 – Properties of interest for TiC. [14]

Theoretical Density (g/cm^3)	Melting Temperature (°C)	Hardness (HV)
4.93	3140	3500

7.4 Inconel 718®

Inconel alloy 718® is a high-strength, corrosion-resistant, nickel chromium material used in the temperature range of -252.8°C to 704°C. The nominal composition of Inconel 718® is Ni-19.0Cr-18.0Fe-3.0Mo-5.0Nb+Ta-1.0Ti (wt %). [15] The strength of alloy 718 is dependent on the precipitation of secondary phases, such as gamma prime (γ') and gamma double prime (γ''). Inconel 718® is used in a variety of applications because of the ease and economy with which it can be fabricated, combined with its good tensile, fatigue, creep, and rupture strength.

Inconel 718® powder was acquired from Sulzer Metco with a particle size of between 45 to 125 μm (-120/+325 mesh). The powder was gas atomized, and spheroidal in shape. Most of the particles were similar in size, which is illustrated in Figure 12. The powder appeared to have no signs of contamination; however, a small amount of satellites are observed in Figure 13. The mean particle size (d_{50}) is 78 μm with a standard deviation of 30.0 μm. The measured size distribution is shown in Figure 14. The EDS spectrum is shown in Figure 15, and a complete compositional comparison is listed as Table 7. The measured composition is similar to the reported nominal composition of Inconel 718®. [16,17] Properties of interest for Inconel 718® are shown in Table 8. [16,17]

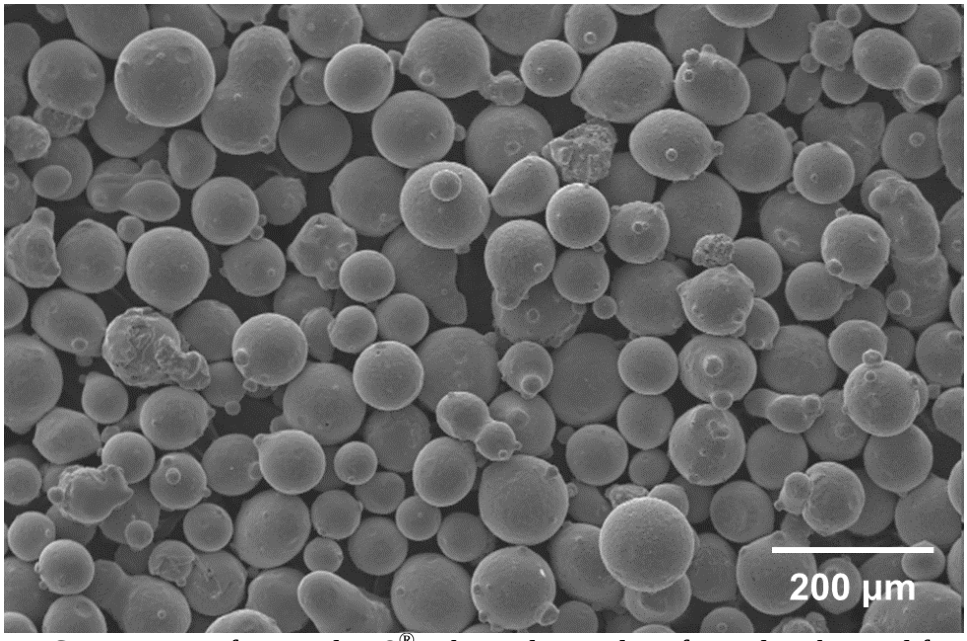

Figure 12 – SEM image of Inconel 718® spherical particles of powder obtained from Sulzer Metco.

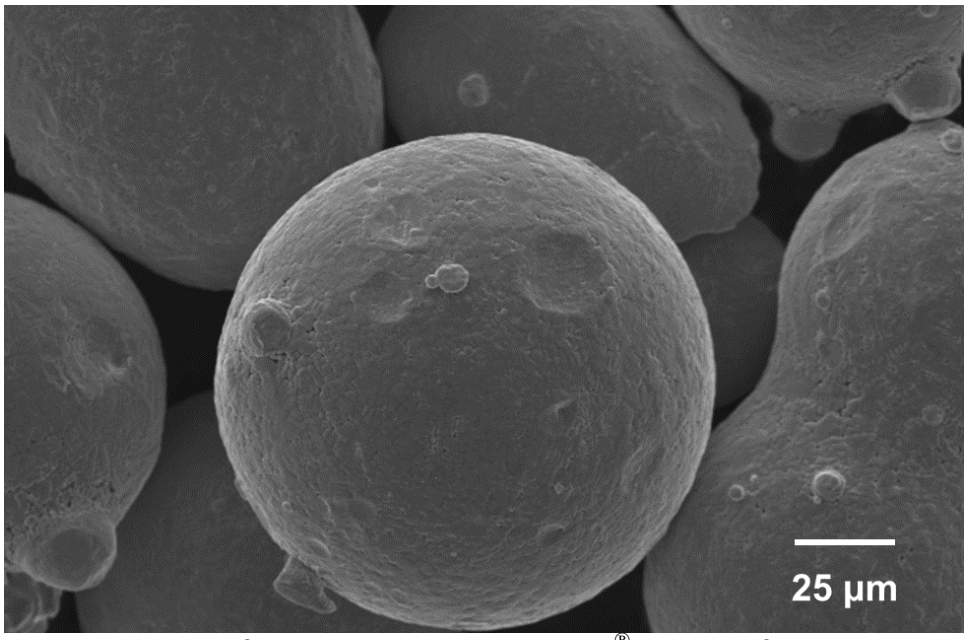

Figure 13 – SEM image of dense spherical Inconel 718® particle of powder obtained from Sulzer Metco.

Table 7 – Measured and reported nominal chemical compositions for Inconel 718® powder.

wt%	Ni	Cr	Fe	Nb+Ta	Mo	Ti	Al	Cu	Co
Inconel 718®	50.78	19.08	18.87	4.6	3.35	1.32	0.83	0.78	0.42
Reference[15]	53	19	18	5	3	1	0.5	–	1

Table 8 – Properties of interest for Inconel 718®. [16,17]

Theoretical Density (g/cm^3)	Melting Temperature (°C)	Hardness (HV)
8.19	1260 – 1343	272

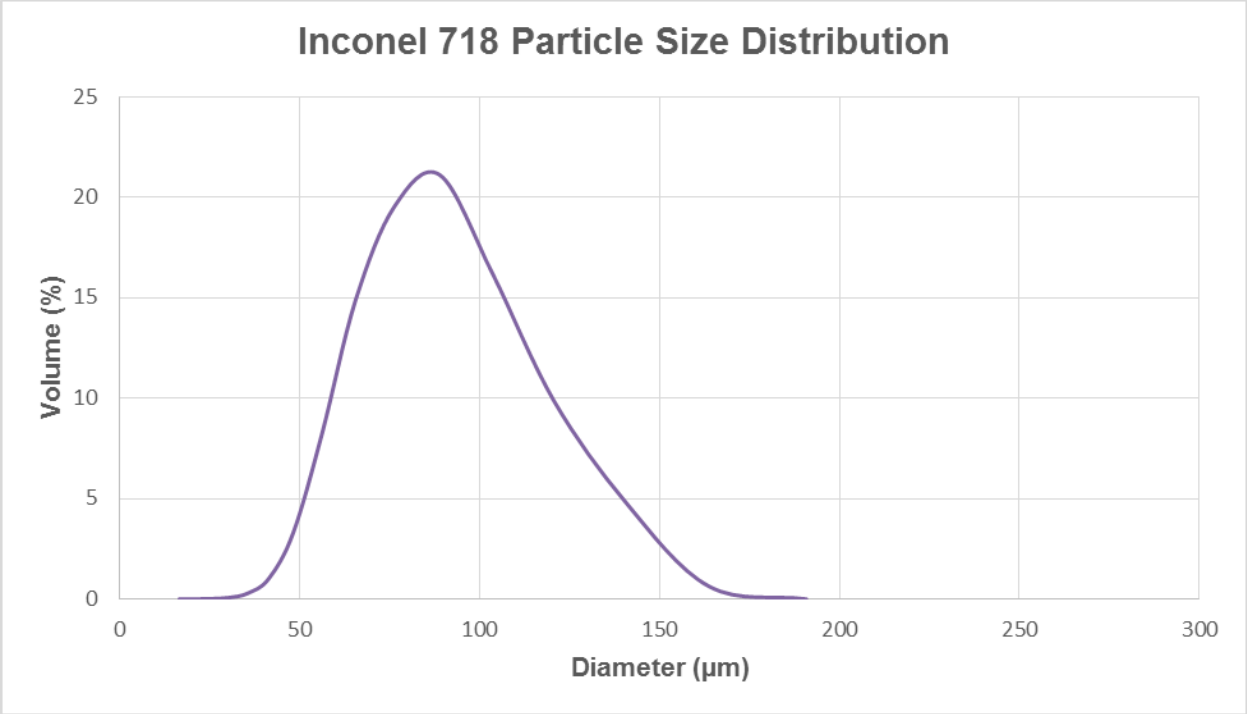

Figure 14 – Particle size distribution of Inconel 718® powder.

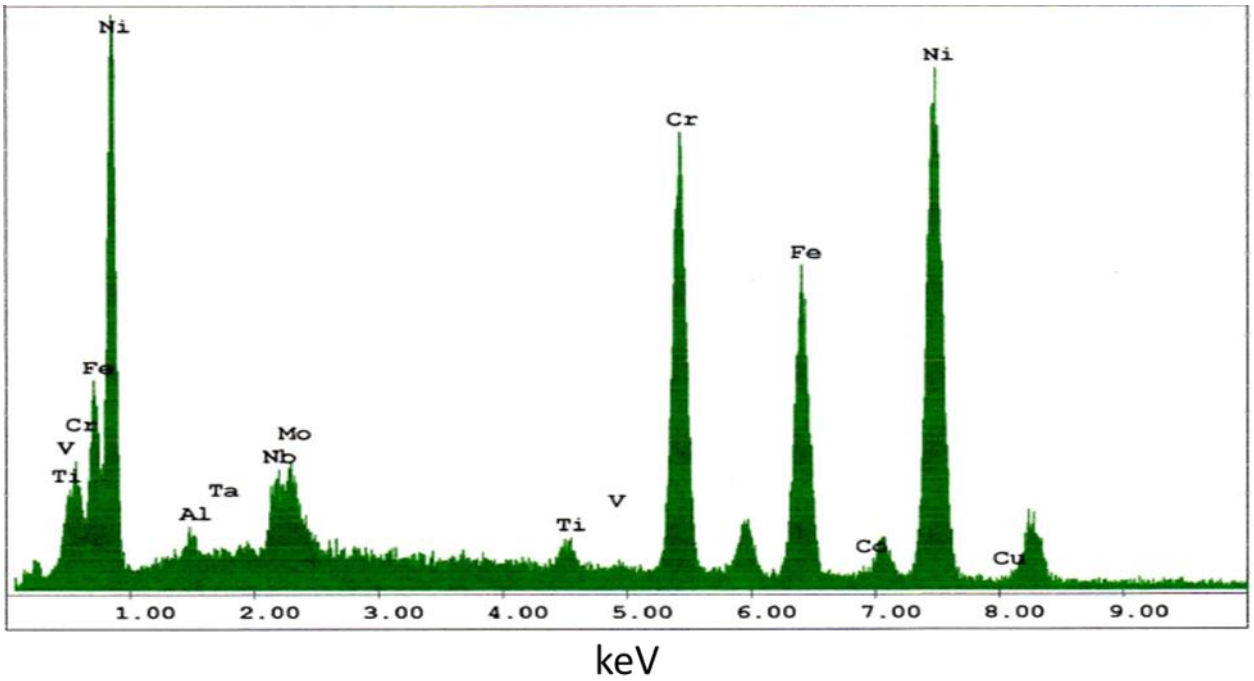

Figure 15 – EDS spectrum of Inconel 718® powder.

7.5 Ti-6Al-4V

Ti-6Al-4V ELI grade powder was acquired from Phelly Materials with a particle size of between 45 to 149 μm (-100/+325 mesh). The powder was plasma rotating electrode process (PREP) processed, and spheroidal in shape. Most of the particles were similar in size, which is illustrated in Figure 16. The powder appeared to have no signs of contamination in Figure 17. The mean particle size (d_{50}) is 127 μm with a standard deviation of 40.9 μm. The measured size distribution is shown in Figure 18. The EDS spectrum is shown in Figure 19, and a complete compositional comparison is listed as Table 9. The measured composition is similar to the reported nominal composition of Ti-6Al-4V. [18] Properties of interest for Ti-6Al-4V are shown in Table 10. [18]

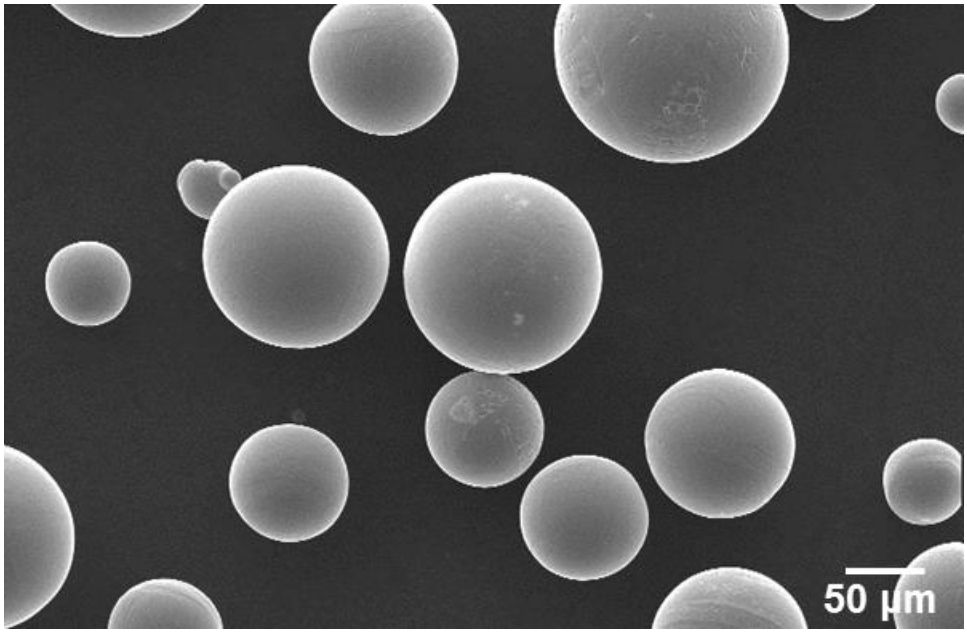

Figure 16 – SEM image of Ti-6Al-4V ELI grade spherical particles of powder obtained from Phelly Materials.

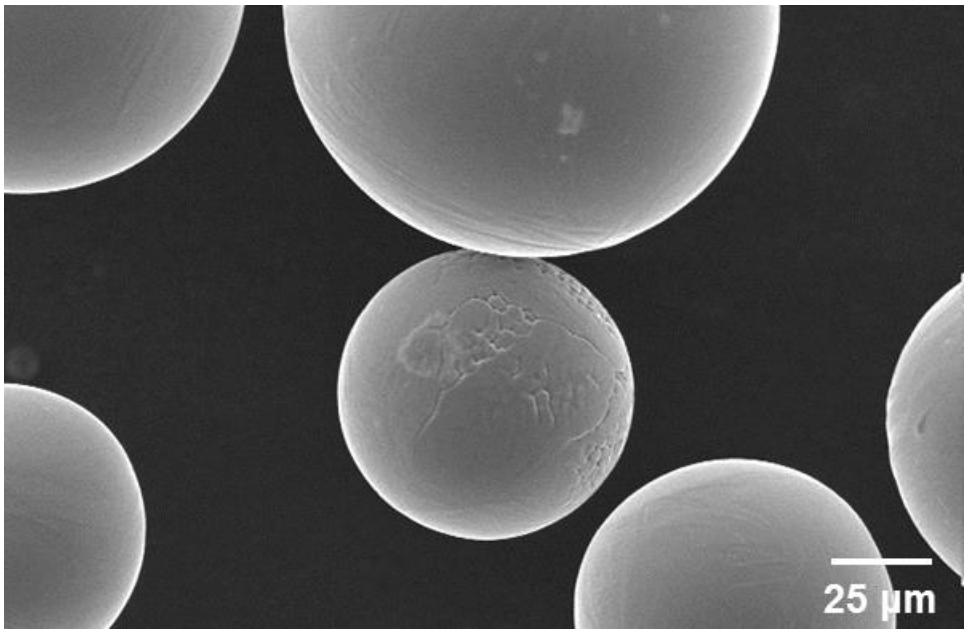

Figure 17 – SEM image of dense spherical Ti-6Al-4V ELI grade particle of powder obtained from Phelly Materials.

Table 9 – Measured and reported nominal chemical compositions for Ti-6Al-4V ELI grade powder.

wt%	Ti	Al	V	Fe	O
Ti-6Al-4V	89.68	6.94	3.338	-	-
Reference[18]	90	6	4	Max. 0.25	Max. 0.2

Table 10 – Properties of interest for Ti-6Al-4V ELI grade. [18]

Theoretical Density (g/cm^3)	Melting Temperature (°C)	Hardness (HV)
4.43	1604 – 1660	349

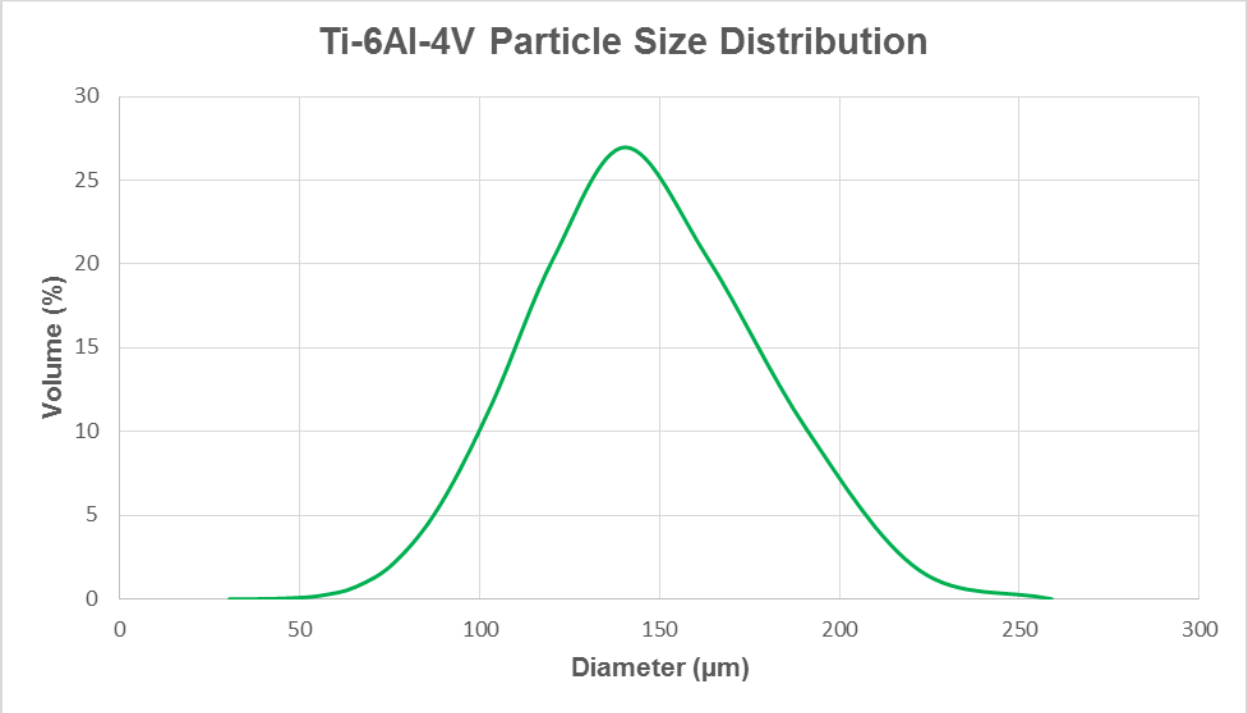

Figure 18 – Particle size distribution of Ti-6Al-4V ELI grade powder.

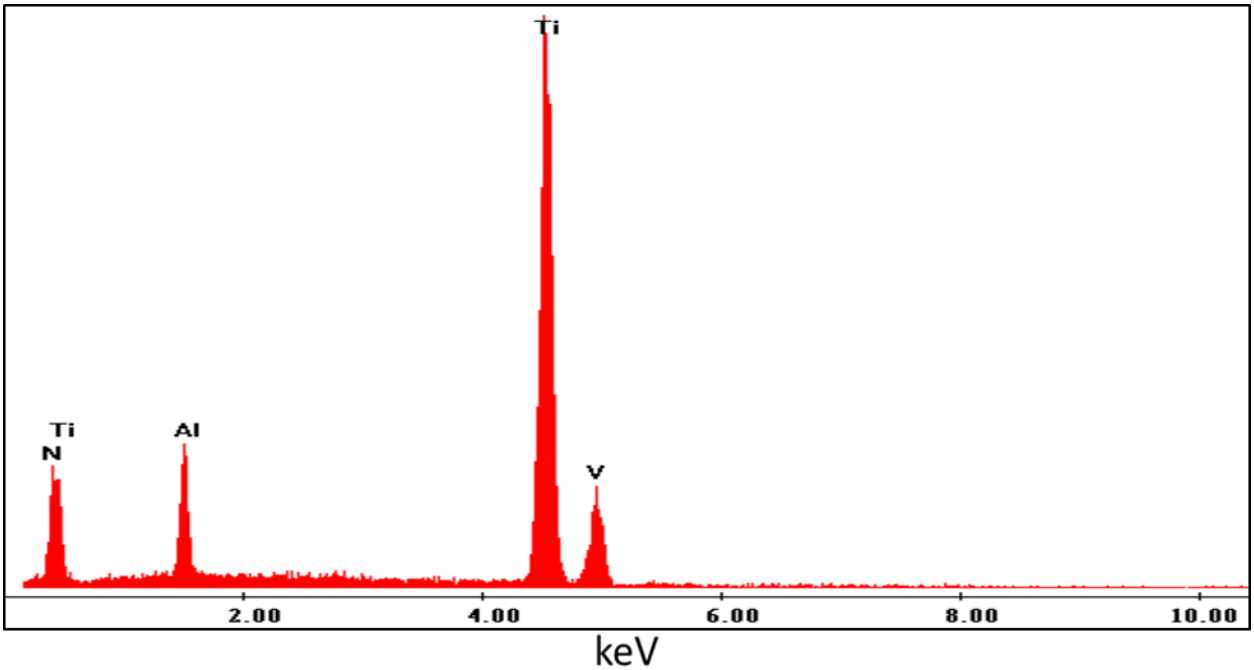

Figure 19 – EDS spectrum of Ti-6Al-4V ELI grade powder.

7.6 Recent Research on the AISI 431- TiC Composite System

R.P. Martukanitz and S.S. Babu [19] suggested that the stability of the hard reinforcement phase during the rapid heating and cooling cycle experienced in the laser deposition process is critical in developing affordable coatings having improved wear resistance, because dissolution of the reinforcement particles result in the loss of their ability to improved wear resistance. Carbide materials also create brittle microstructures that increase the sensitivity of the matrix to cracking upon cooling. The solubility of the particle may be estimated by its enthalpy of formation, ΔH_f. In general, lower values of ΔH_f denote decreased solubility of the particle and greater stability. The enthalpy of formation for various carbides, nitrides, and borides is shown in Figure 20. [19]

Microstructural observations shown in Figure 21, also indicate that dissolution of tungsten carbide particles in iron-rich liquids was faster than that in nickel-rich liquids for identical laser traversing speeds. [19] The dissolution of tungsten carbide particles in iron-rich liquid became less pronounced with an increase in laser traversing speed. Tungsten carbide particles developed complex, faceted surfaces in the nickel-rich structure.

Figure 22(a) shows the thermodynamic stability diagram at 1600 °C, and Figure 22(b) shows the solid volume fraction during cooling for a system represented by titanium or tungsten with carbon in stainless steel alloy 431. The greater stability, based on composition, was associated with TiC in the stainless steel alloy 431 when compared to WC and may be seen in the figure by the larger region showing TiC stability.

The stability diagram for the Fe-Ti-C-N system at 1800 K is shown in Figure 23. The calculations considered different extents of dissolved nitrogen as a function of titanium and carbon concentrations in the liquid iron. Since the TiC, TiN and Ti(CN) all have face centered cubic (FCC) crystal structure, in thermodynamic calculations the three phases are denoted as MX. The first set of calculations was performed in a simple Fe-C-T-N system with no dissolved nitrogen. The calculations showed a limited stability of the MX phase as shown by the shaded region. However, with an increase in nitrogen concentration to 0.003 wt%, the calculations showed increased stability of MX phase indicating that the MX phase is progressively changing from TiC to Ti(CN). At high concentrations of nitrogen, the calculations showed that the MX phase is stable even with low-carbon concentrations. This showed that by the combined additions of titanium, carbon and nitrogen, the MX particles could be stabilized in the Fe-rich laser melt pool.

The stability of a phase is governed by its free energy, which can be described as Equation 1. The free energy contribution(G^{ϕ}) equals the pure components in that phase(G_o^{ϕ}) plus the contribution from ideal mixing($G_{idea-mix}^{\phi}$) plus the contribution due to non-ideal interactions between the components($G_{excess-mix}^{\phi}$). Equation 1 can be substituted by the chemical potential of element, μ_i^{ϕ} to obtain Equation 2.

$$\mathrm{G}^{\Phi} = \mathrm{G}_{\mathrm{o}}^{\Phi} + \mathrm{G}_{\mathrm{ideal+mix}}^{\Phi} + \mathrm{G}_{\mathrm{excess-mix}}^{\Phi} \qquad \text{Eq. (1)}$$

$$\mu_{\mathrm{A}}^{\Phi} = \mathrm{G}^{\Phi} - \mathrm{X}_{\mathrm{B}}^{\Phi} \frac{\partial \mathrm{G}^{\Phi}}{\partial \mathrm{X}_{\mathrm{B}}^{\Phi}}; \mu_{\mathrm{B}}^{\Phi} = \mathrm{G}^{\Phi} - (1 - \mathrm{X}_{\mathrm{B}}^{\Phi}) \frac{\partial \mathrm{G}^{\Phi}}{\partial \mathrm{X}_{\mathrm{B}}^{\Phi}} \qquad \text{Eq. (2)}$$

A two-phase Gibbs energy diagram is shown in Figure 24. The Gibbs energy diagram indicates that some mixture of α+β is the stable state for an alloy between the two tangent points. [20] The lower enthalpy governs lower free energy and chemical potential, which means the material with lower enthalpy in Figure 20, has a greater stability in the matrix.

The results of the research showed carbides in the form of TiC dendrites and also fine titanium carbonitrides, Ti(CN), formed within the SS 431 matrix. [19] The dissolved titanium, carbon and nitrogen reacted to precipitate as TiC and Ti(CN). The presence of the dendritic shaped TiC particles indicate these precipitates were forming before the primary solidification of the SS 431 matrix. The research also reported that the laser deposits of the SS 431 with the addition of TiC powder significantly increased the surface hardness of laser deposits.

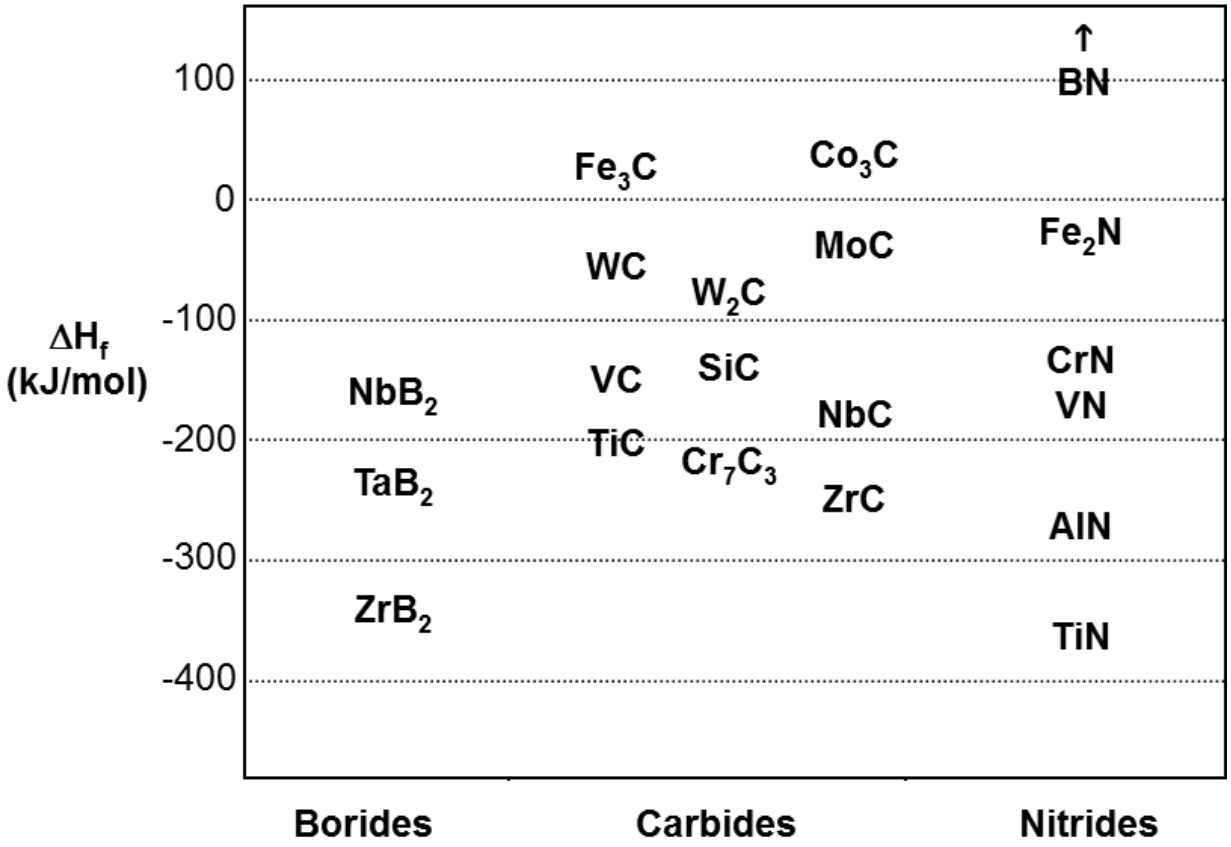

Figure 20 – Enthalpy of formation, ΔH_f, of various hard phases. [19]

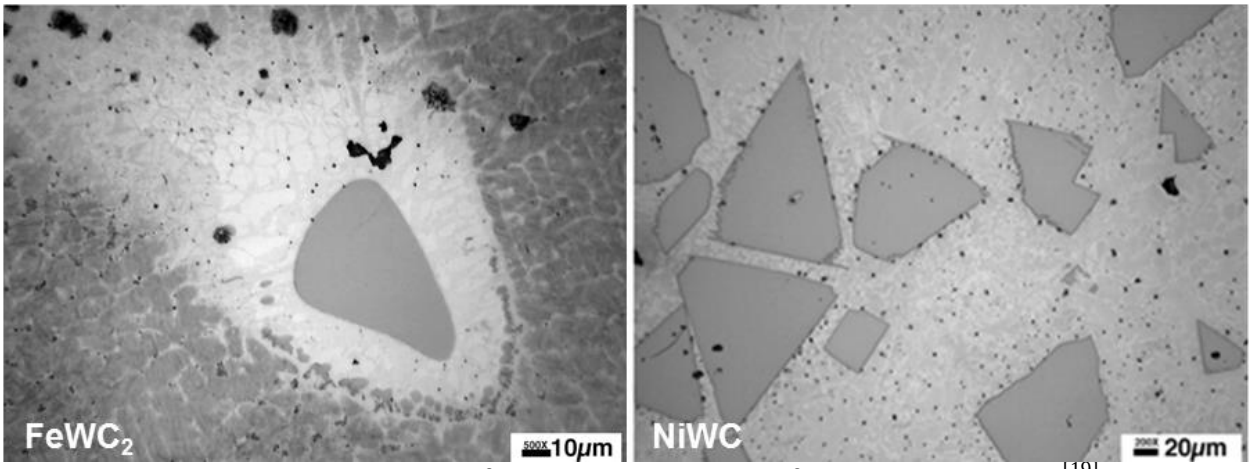

Figure 21 – Dissolution of WC particle in iron (left) and nickel (right). [19]

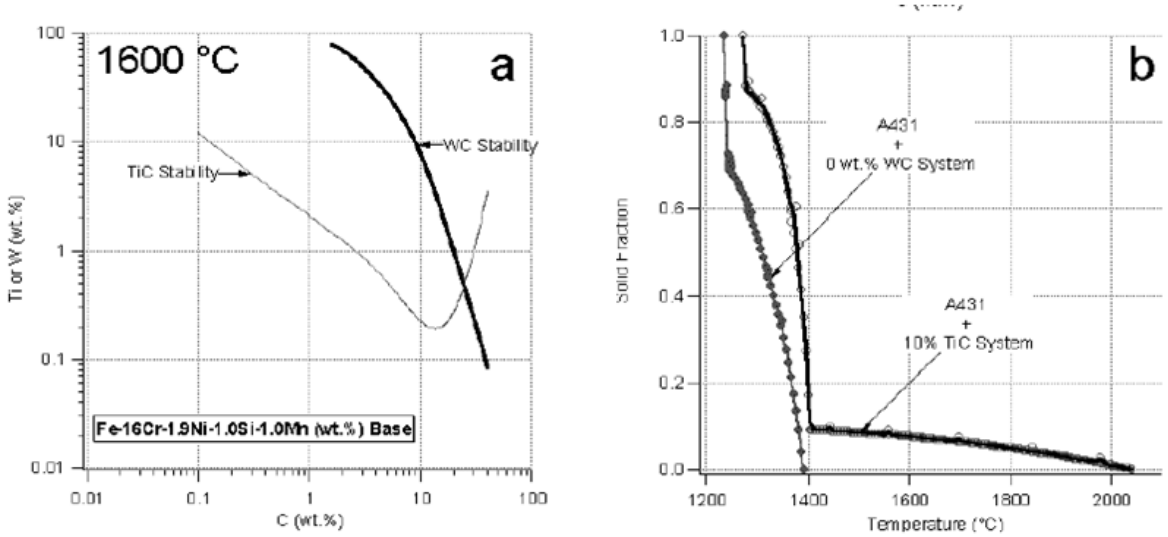

Figure 22 – Thermodynamic stability diagram (a) and solid volume fraction during cooling (b) for a system represented by titanium or tungsten with carbon in SS 431. [19]

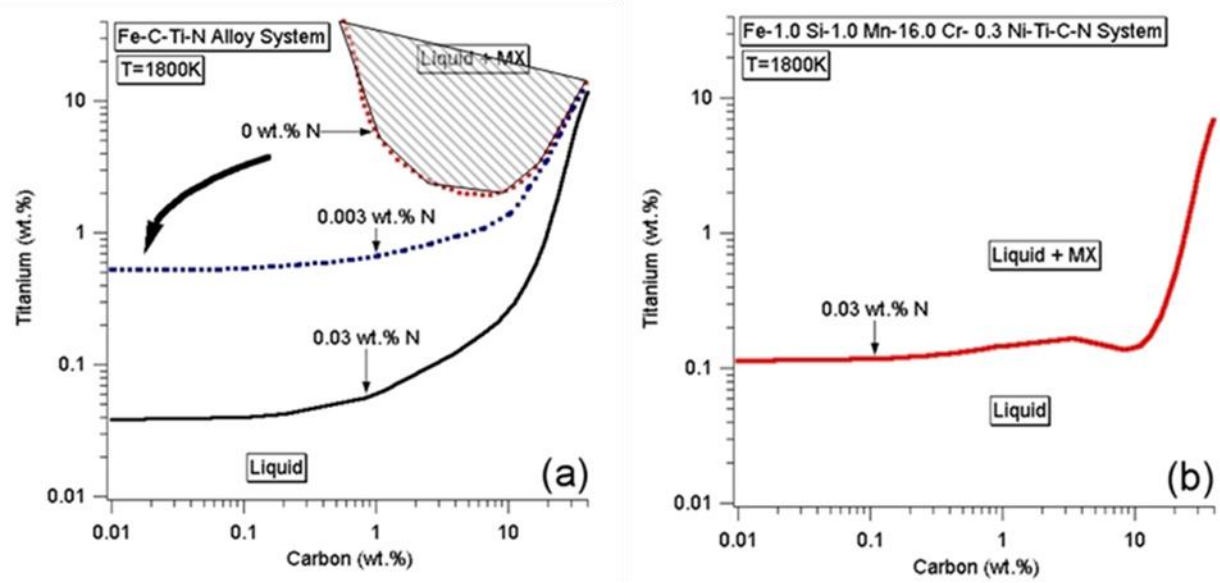

Figure 23 – Thermodynamic calculations of MX stability as a function of carbon and nitrogen for (a) a simple Fe-based and (b) complex Fe-base alloy. [19]

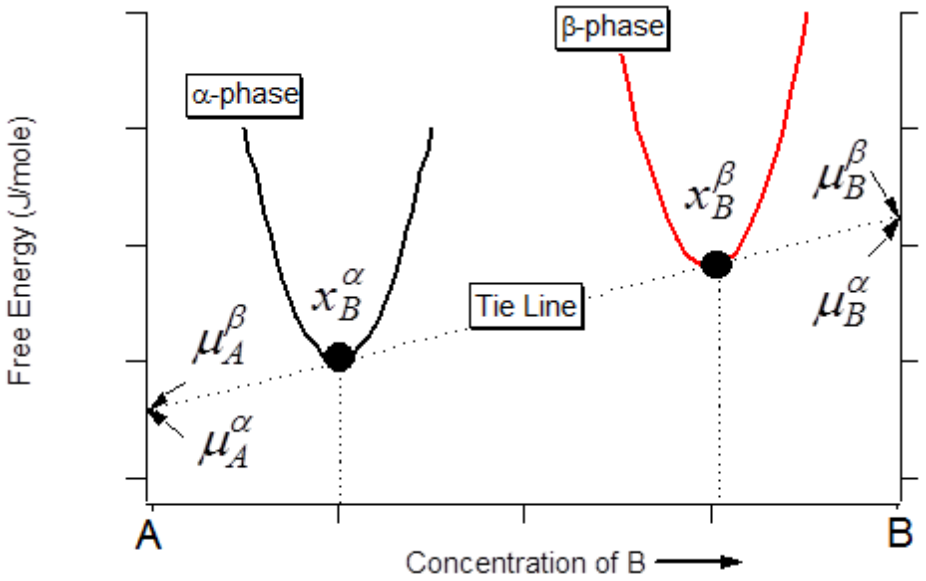

Figure 24 – Two-phase molar Gibbs energy diagram. [19]

7.7 Target Properties after Deposition

The results of the investigation should provide deposition properties that are comparable to gear components produced from AISI 8620 steel (8620 steel) that have been carburized and chromium electroplated Inconel 718®. The conclusion of this research should be based on two considerations: the hardness of the experimental deposits must be equal or higher than the carburized 8620 steel surface and the chromium electroplated Inconel 718®, and the results of rolling contact fatigue (RCF) testing of the laser deposited material on carburized 8620 steel should be equivalent to an 8620 carburized surface. The carburized 8620 steel surface is reported to have a hardness of between 700 and 750 Vickers hardness (HV). [12] Because of the wide range of hardness reported for chromium electroplated surfaces, hardness of the chromium electroplating on the Inconel 718® surface would be measured during this research. The RCF testing of laser deposit material on carburized 8620 steel will be directly compared with prior RCF test results of carburized 8620 steel. The RCF test simulates the rolling/sliding action that occurs in a gear mesh, the testing results typically determine the surface durability performance of the material by comparing the lives to failure of the tested specimens. [21] The occurrence of wear in an RCF test is not typical, but can be used to compare the wear resistance of a material by measuring the wear rate or total time to a maximum wear interval of the test specimen. The prior RCF test results of carburized 8620 steel would be provided by the Drivetrain Technology Center at the Applied Research Laboratory. These prior results are shown in Table 11. [22]

Additionally, the finished specimens require a surface finish finer than Ra equal to 1.63 µm (64 µin) after grinding and preferably an Ra equal to 0.406 – 0.813 µm (16 – 32 µin). When the surface roughness of the bearing surface is greater than Ra equal to 64 µin, the component is considered non-serviceable. The ability of the deposited material to meet these tribology requirements after grinding is an important consideration for bearing surfaces under rotation.

Table 11 – Carburized 8620 steel RCF testing results. [22]

Specimen #	Roller #	Stress (ksi)	Load (lbs)	Speed (rpm)	Hours	Cycles (x 10^6)	Specimen Ra (µin)	Roller Ra (µin)	Observations
341-1	341-30	300	1249	2922	135.4	23.738	30.25	3.3	Surface Origin Pitting
341-37	341-33	300	1249	2922	188.1	32.978	27.5	4	Surface Origin Pitting
341-33	341-36	300	1249	2919	84.2	14.747	26.5	13	Surface Origin Pitting
341-55	341-44	300	1249	2925	207.9	36.486	35.75	14.25	Surface Origin Pitting

Conditions		
	Speed	3000 rpm, High
	Temperature	70 °C (158 °F), Low
	Ra	High
	Sliding	High

8. DDM PROCESS

8.1 DDM Process Development

Process development was conducted at the Center for Innovative Materials Processing through Direct Digital Deposition (CIMP-3D) at the Pennsylvania State University. The center currently houses three DLD systems, the Laser Engineered Net Shaping (LENS) MR-7 system, a Precitec laser deposit head on the Laser Articulating Robotic System (LARS), and the High Power High Deposition (HPHD) system. All systems represent the same process technologies, and process parameters are approximately interchangeable between the various machines. The distinction between the LENS and the LARS system is build envelop and laser power. The LENS has a build envelop of 30 cm x 30 cm x 30 cm, with a maximum power of 500 watts using an ytterbium fiber laser. The LARS system has a larger build envelop of 3.35 m x 3.35 m x 1.07 m, with a maximum laser power of 12000 watts through an ytterbium fiber laser with a 200 μm fiber optic cable.

The initial laser deposition trials involved development of parameters that met the required deposition quality followed by detailed characterization involving optical microscopy and micro hardness testing. Process parameter for the initial laser deposition trials were based on a review of the literature [23] and prior experience. This resulted in a recommended contact angle between the deposition track and the substrate of 140 degrees. [23] This contact angle was found to be most suited for all of the powders that would be evaluated.

The original process parameters were developed for the LENS machine, with a powder feed rate of 0.826 cm^3/min with Ar carrier gas at 1.89 l/min (4 cfh), laser power at 350 watts at a wavelength of 1.07 microns, spot size of 2 mm, coaxial powder nozzle at 9.27 mm away from the substrate, a travel speed of 1.06 cm per second (25 in/min), and Ar shielding gas at 18.88 l/min (40 cfh). The resultant tracks produced beads having a contact angle of 141 degrees, being 0.711 mm (0.028 in.) in width, and 0.127 mm (0.005 in.) in height. The spacing between tracks, Δw_{track}, calculated using Equation 3 [23], was 1.905 mm (0.075 in.). Equation 3 may be used to determine the spacing between tracks that will result in a flat deposit which is necessary to prevent the formation of inter-track and inter-pass lack of fusion defects. The h is the height of the deposit track above the substrate, and the w is the width of the deposit track.

$$\Delta w_{track} = \frac{4hw\left(-2w^2 + h\left(8h + \sqrt{\frac{\left(-4h^2 + w^2\right)^2}{h^2}}\right)\right) + \left(4h^2 + w^2\right)^2 \mathrm{ArcSin}\left[\frac{4hw}{4h^2 + w^2}\right]}{64h^3} \qquad \text{Eq. (3)}$$

Based on prior experience and adjustments of the LARS process parameters for the SS 431 powder, it was concluded that applicable parameters for achieving good deposition quality were a powder feed rate of 1.0 cm^3/min with Ar carrier gas at 9.44 l/min (20 cfh), 2000 Watts of laser power, spot size of 4 mm, coaxially powder nozzle at 10 mm away from the substrate, a travel speed of 1.06 cm per second (25 in/min), Ar shielding gas at 9.44 l/min (20 cfh), and additional trailing Ar gas at the melt pool to prevent oxidation during laser deposition at 14.16 l/min (30 cfh). The build size of the single track deposition was 3.2 mm (0.126 in) wide, height above

substrate was 0.267 mm (0.0105 in), contact angle at 161°, and Δw_{track} spacing was 1.905 mm (0.075 in), which is shown in Figure 25.

For the contact fatigue samples or cylindrical specimens, a "helical" pattern was employed, with the tracks starting against the profile of the filet in the reduced section. The specimen was rotated during deposition at a speed (RPM) calculated with respect to the increased radius of the bar, which is shown in Equation 4. Therefore, the tangential velocity of the surface being deposited was maintained at a travel speed of 1.06 cm per second (25 in/min).

$$RPM = \frac{25}{2\pi\,[radius\ of\ bar + (layer\ thinckness \times number\ of\ layers)]} \qquad \text{Eq. (4)}$$

Parameters (laser power, travel speed, mass flow rate, track spacing, and layer thickness) were established using the SS 431 powder and remained consistent with the other deposition materials. The powder flow rate was adjusted to provide the same volumetric flow rate of material to the melt pool between materials of different density.

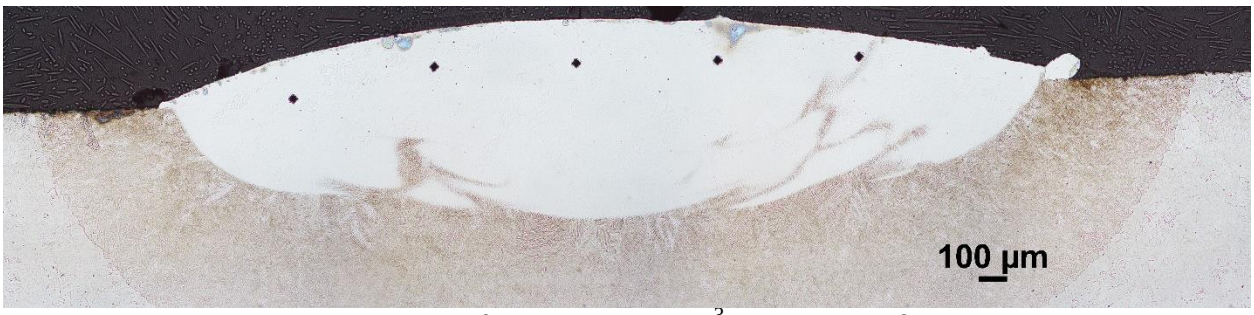

Figure 25 – Single track deposit of SS 431 at 1.0 cm^3/min powder flow rate and 2 kW laser power.

8.2 DDM Analysis

8.2.1 Microstructural analysis

All samples were removed from the cylindrical specimens by wet cutting using a Struers Labotom-3 and were then hot mounted in epoxy resin using a Struers Pronto-Press 2. All samples were ground and polished on a Struers Pedomax-2. Grinding utilized various grits including 240, 320, 400, 500, 600, 800, 1000, 1200, and 2400. Each grit size was used for two minutes, followed by a rinse prior to the subsequent paper. After the samples were ground, they were polished using a 3 micron diamond suspension and 1 micron diamond suspension. The samples were polished for 3 minutes each with the diamond suspensions, alternating the use of the diamond suspension and a polishing lubricant (Blue Lube) every 15 seconds. The colloidal silica was used for 3 minutes, alternating between silica and distilled water being sprayed on the polishing pad every 15 seconds.

All samples were etched for microstructural imaging after polishing using a 2% Nital solution. The Nital solution was applied for 5 seconds to etch the 8620 steel substrate and HAZ. Deposit materials, Inconel 625, SS 431, and SS 431/TiC composite, required electrolytic etching with 10% oxalic acid solution. Due to electrolytic etching of the deposited materials, over etching of the HAZ and 8620 steel substrate occurred. Therefore, both 8620 steel substrate and HAZ microstructural images were taken before electrolytic etching.

8.2.2 Vickers hardness test

After metallographic analysis, micro hardness measurements were conducted based on the ASTM-E384 specification [24] using a Leco M-400-G1 micro hardness tester in the Vickers scale. This was conducted by applying a 300 gram load. Before micro hardness testing, samples were re-ground, re-polished, and etched lightly with the 2% Nital solution to reveal the heat affected zone (HAZ). Since the HAZ was so narrow, hardness samples were taken in a staggered procedure using two rows separated by 0.5 mm and depth spacing of 0.125 and 0.25 mm from the top surface of the deposit, and resulting in 4 to 6 rows on each sample. Figure 26 demonstrates the location and spacing for micro hardness testing. This was performed to ensure that prior indentations and deformation zones were at least 2.5 times away from prior indentations, and would not affect the results of the current hardness measurement. A hardness conversion chart, Appendix A, was used to convert the reference hardness in Rockwell C (HRC) unit to Vickers hardness (HV) units. The complete Vickers hardness testing for each test indent is listed in Appendix B. [25]

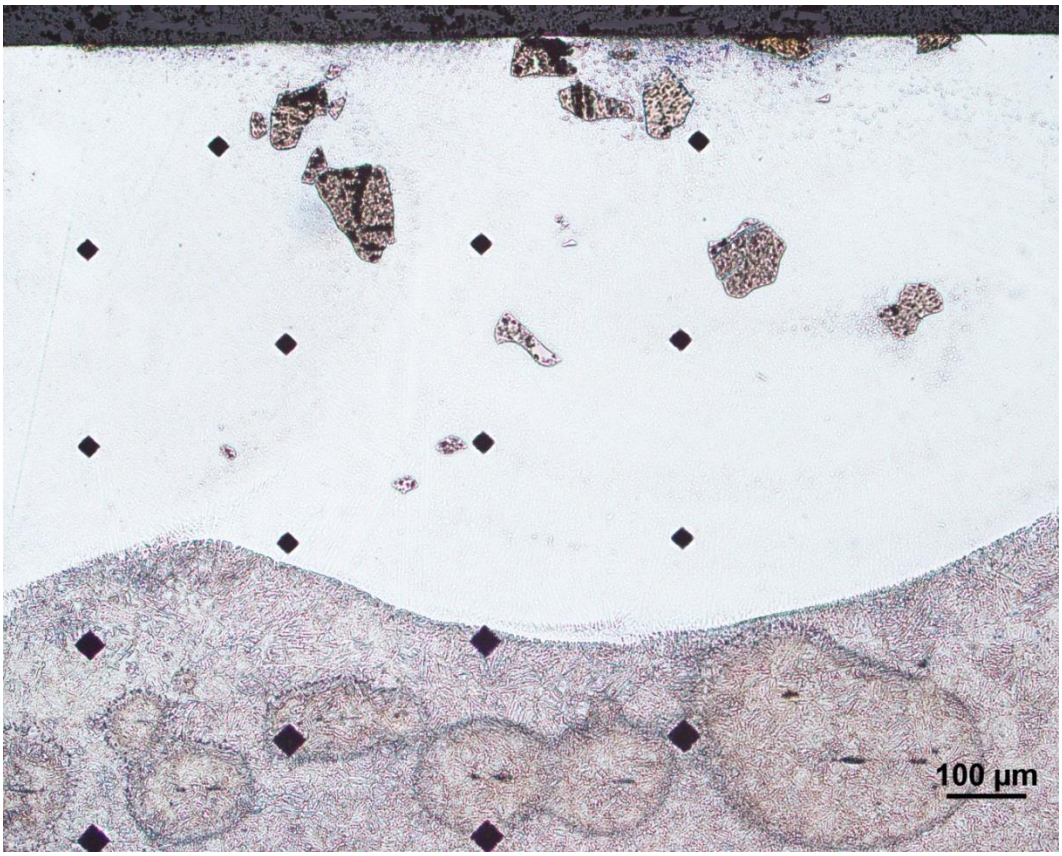

Figure 26 – Demonstrating the staggered procedure for measuring micro hardness.

8.3 Selection of Components for Contact Fatigue Testing

Upon selection of the stainless steel alloy 431 and the 431/20TiC composite material, specimens were prepared for further characterization of deposit attributes, such as rolling/sliding contact fatigue (RCF) testing. Four RCF test specimen were laser deposited with SS 431/20 TiC on carburized 8620 steel bars. These specimens were produced at CIMP-3D using the LARS laser deposition system. The process parameters were adjusted to reduce heat input and dilution of the substrate during the deposition. The new process parameters were powder feed rate of 1.0 cm^3/min with Ar carrier gas at 9.44 l/min (20 cfh), 1000 Watts of laser power at a wavelength of 1.07 microns, spot size of 2.5 mm, coaxially powder nozzle at 10 mm away from substrate, a travel speed of 1.06 cm per second (25 in/min), Ar shielding gas at 9.44 l/min (20 cfh), and additional trailing Ar gas at the melt pool at 14.16 l/min (30 cfh). The build size of the single track deposition was 3.1 mm (0.122 in) wide, height above substrate was 0.378 mm (0.015 in), contact angle at 151°, and Δw_{track} spacing was 1.27 mm (0.05 in), Complete process parameters for both process development and specimen production are listed as Appendix C.

Shown in Figure 27a and Figure 27b are the carburized 8620 base material and deposition specimens that were used for producing samples for RCF testing. As shown in Figure 27a, the carburized 8620 steel specimens for contact fatigue tests were 2.515 cm (0.9905 in.) in diameter and 12.42 cm (4.89 in.) in length. A small recess approximately 0.0318 mm (0.00125

in.) in depth and 2.29 cm (0.9 in.) wide was machined into the bar at the center. Deposits approximately 3.43 cm (1.35 in.) in width and 0.254 mm (0.010 in.) thick were deposited circumferentially onto the recess at the midpoint of the bar, shown in Figure 27b. Photographs of the specimens produced for characterization are shown in Figure 28. After deposition, the final dimensions, shown in Figure 29, were obtained by roller grinding at Quala-Die, Inc. at St Marys, PA to the dimensions shown in Figure 30.

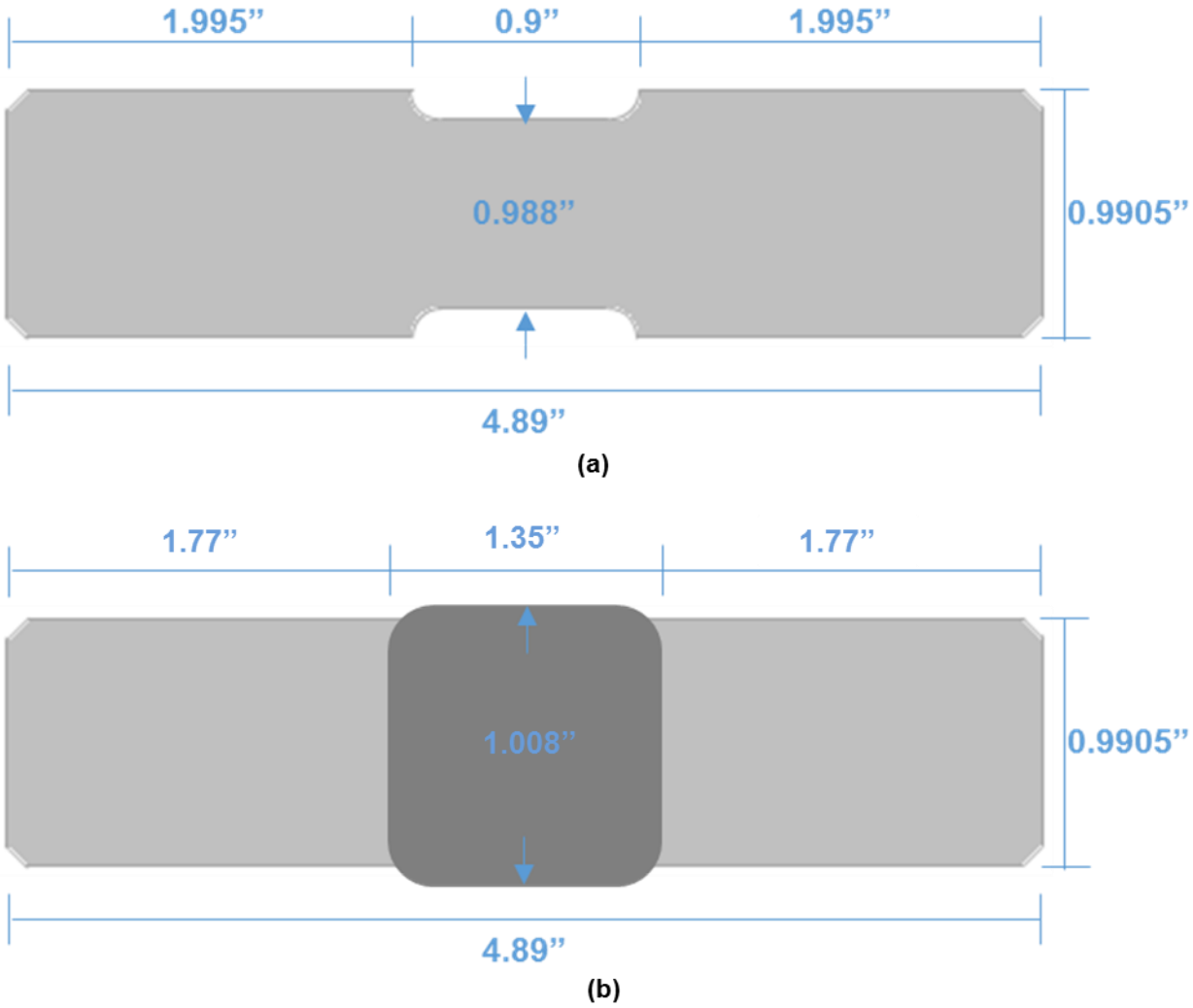

Figure 27 – Schematics of the specimen produced for RCF testing (a) initial machined specimen. (b) Specimen after with laser deposition materials over the center of carburized 8620 steel bar (Units are inches).

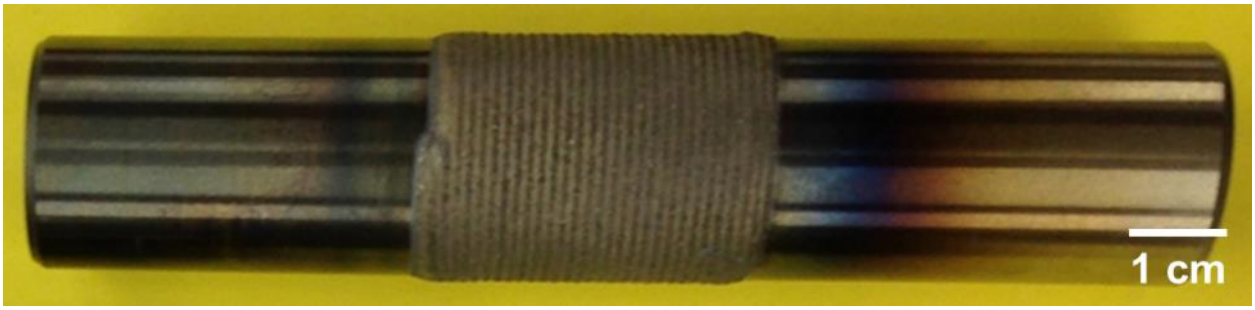

Figure 28 – Carburized 8620 steel specimen that had been laser deposited with SS 431/20 TiC.

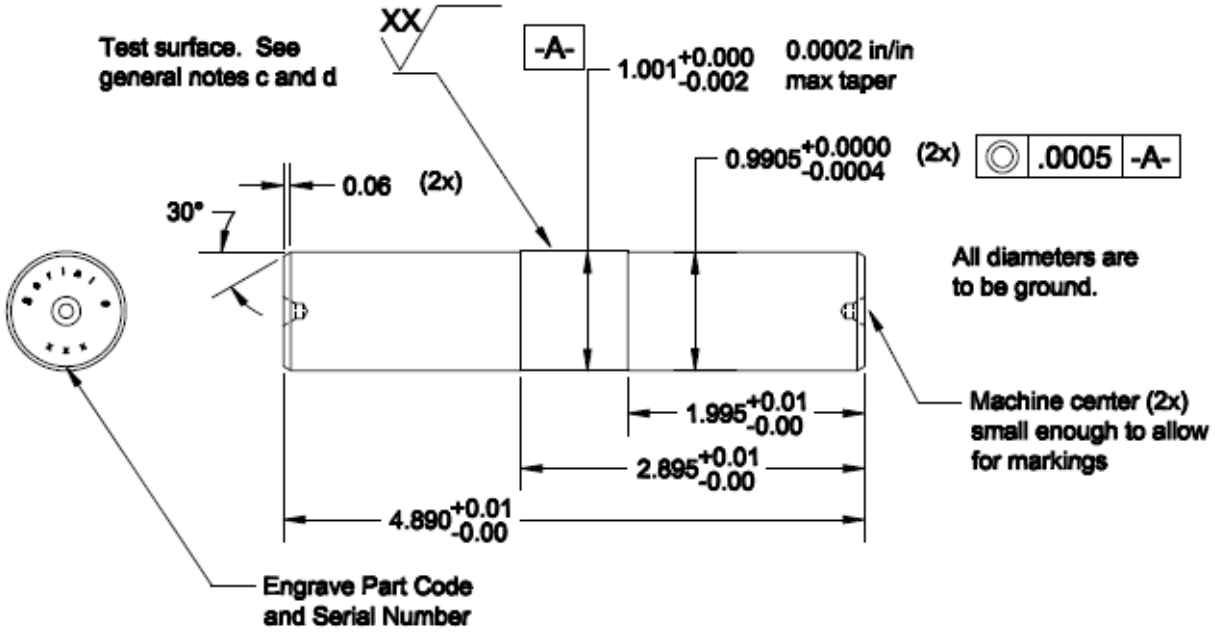

Figure 29 – The final dimension of the RCF test specimen.

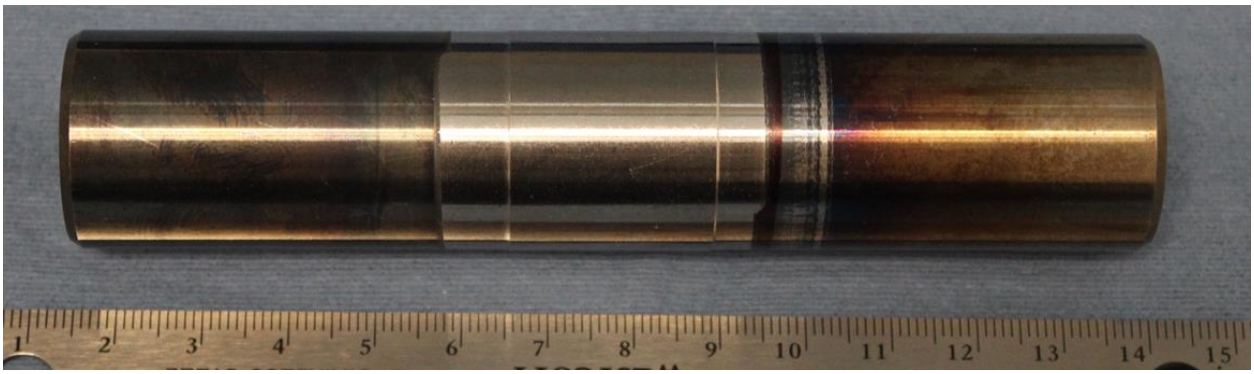
Figure 30 – The RCF test specimen with laser deposited SS 431/20 TiC (scale in cm).

9. COMPONENTS FOR REPAIR

Based on discussions with various DoD depot personnel a vast number of high value components may be applicable to laser-based repair technology. Analyses have shown that not only does laser repair result in significant cost savings when compared to replacement, but also may lead to dramatically decreased lead times and increased readiness. The three components that have been tested and that may fit the criteria for DoD are shown below.

9.1 T700 Power Turbine Shaft

The Power Turbine (PT) Shaft (PN: 5125T92G01/RE, NSN: 2840-01-473-3556 & PN: 6043T35G01), shown in Figure 31, is founded in the T700 Engine Series used on H60 (Blackhawk, Pavehawk & Seahawk), AH-1W(Z – Cobra) and UH-1Y (Huey) Helicopter Systems serviced at Corpus Christi Army Depot (CCAD). This part is scheduled to be removed from the RECAP Kitting Parts Replacement Package and go to a 100% overhaul. Current repair turnaround time is 110 days. Current chromium electroplating repair is 50% of total overhaul cost (~$8,000/ea.) for the part. The proposed application of DDM is to replace chromium electroplating for repair on various bearing journals and lands of the PT shaft, which has been determined viable by the Army. However, testing and authorization of DDM repair on this Critical Safety Item (CSI) is needed. Material and part repair testing at bearing contact/working surfaces would be required to approve this Non-Critical Safety Item (CSI). DDM represents an alternative repair to chrome at the seal journal to increasing repair damage tolerance limits beyond current repair process limits. Material and part repair testing at bearing contact/working surface are required for approval. The SAFR team estimates savings can be obtained if the part can be repaired or remanufactured by DDM. The Fedlog Part Cost is $14,432.00, and repair cost savings of approximately $2,000/ea is anticipated (i.e. 25% of Total PT shaft overhaul cost). An estimate of $1 Million in Cost Savings is expected based on DDM repair of 50% of the SAFR inventory (1,000 ea.). The estimate cost savings for the CCAD US Army engine and power turbine module programs is at least $300k/per program year, and would reduce CCAD overhaul by at least 10% (~10+ days). Implementation would reduce overhaul cost for this CSI, and would also result in an Environmental Waste Stream Reduction and associated handling and processing costs by eliminating chromium electroplating for repair.

Figure 31 – T700 Power Turbine Shaft for the H60, AH-1W, and UH-1Y.

9.2 Input Bevel Pinion Gear

The Input Pinion (PN: 7-211310021, NSN: 1615-01-163-4573), shown in Figure 32, is a gear in the main transmission for AH64 Apache System. CCAD has identified this part as a Critical Parts Demand Item. The proposed repair would be to apply DDM to repair corrosion and micro-wear pitting at bearing journal and lands. Material and part repair testing at bearing contact/ working surface would be required to approve this Non-Critical Safety Item (CSI). DDM represents an alternative repair to chromium electroplating at the seal journal to increase repair damage tolerance limits beyond current repair process limits. Material and part repair testing at bearing contact/working surface would be required or remanufactured by DDM. The Fedlog parts cost is $3,566/ea., and potential savings of $1,212/ea., or $64,273 for the 53 ea. In SAFR has been estimated. Implementation would also provide critical parts support relief and reduced scrap by developing, qualifying, and authorizing a repair using DDM for an area of the gear that no other repair process can achieve.

Figure 32 – Input pinion for AH64 identified by CCAD as a Critical Parts Demand item DDM repair.

9.3 Cooling Fan Shaft

The Cooling Fan Shaft (PN:70361-03014-101, NSN:3040-01-329-6480), shown in Figure 33, is found in the Axial Transmission Oil Cooling Fan for H60 Blackhawk, Pavehawk and Seahawk Helicopter Systems. CCAD has identified this part as a Critical Parts Demand Item. The proposed repair would be to apply DDM to repair corrosion and micro-wear pitting at bearing journal and lands and would require testing at bearing contact/working to approve this Non-Critical Safety Item (CSI). DDM represents an alternative repair to chromium electroplating at

the seal journal to increase repair damage tolerance limits beyond current repair process limits. The SAFR team estimates savings can be obtained if the part can be repaired or remanufactured by DDM. The Fedlog parts cost is $6,383.99.00/ea. Based on the acceptable “Rule of Thumb” repair cost threshold of 66% cost of part ($4,213/ea.) the potential cost savings of $2,169/ea, or $26,330 for the 12ea. In SAFR is estimated.

Figure 33 – Cooling fan shaft for AH64 identified by CCAD as a Critical Parts Demand item DDM repair candidate.

10. INSPECTION AND PREPARATION OF COMPONENTS PRIOR TO EVALUATION

10.1 Cooling Fan Shaft

The Cooling Fan Shaft is composed of Ti-6Al-4V, and no obvious ware was observed on the bearing surface. The components were solvent cleaned prior to laser deposition.

10.2 Input Bevel Pinion Gear

The Input Bevel Pinion Gear is composed of Alloy AMS 6265, which is designed for carburization. Various degrees of ware were observed on the bearing surface. The component represents a carburized surface that was left intact and was solvent cleaned prior to laser deposition.

10.3 T700 Power Turbine Shaft

The T700 Power Turbine Shaft is composed of Inconel Alloy 718. There was no obvious ware found on the bearing surface, however, chromium electroplating was observed by chemical etching found on a sample. The current approved repair method for the part is chromium electroplating. The component was solvent cleaned prior to laser deposition.

11. TECHNICAL FINDINGS

11.1 Cooling Fan Shaft

The technical data for the cooler fan shaft can be found in the Depot Maintenance Work Requirement (DMWR) 1-4140-228, and the fan is shown in Figure 34. The cost of each part is $6,160.55. The DMWR requires that minimum diameter of the Shaft be 1.9685 in, shown in Table 12. Over their lifecycle the cooler fan shaft were showing ware and a reduced diameter, smaller than what was accepted according to its DMWR specifications. Table 13 displays the LENS laser deposition repair parameters as well as the process parameters for the cooler fan shaft.

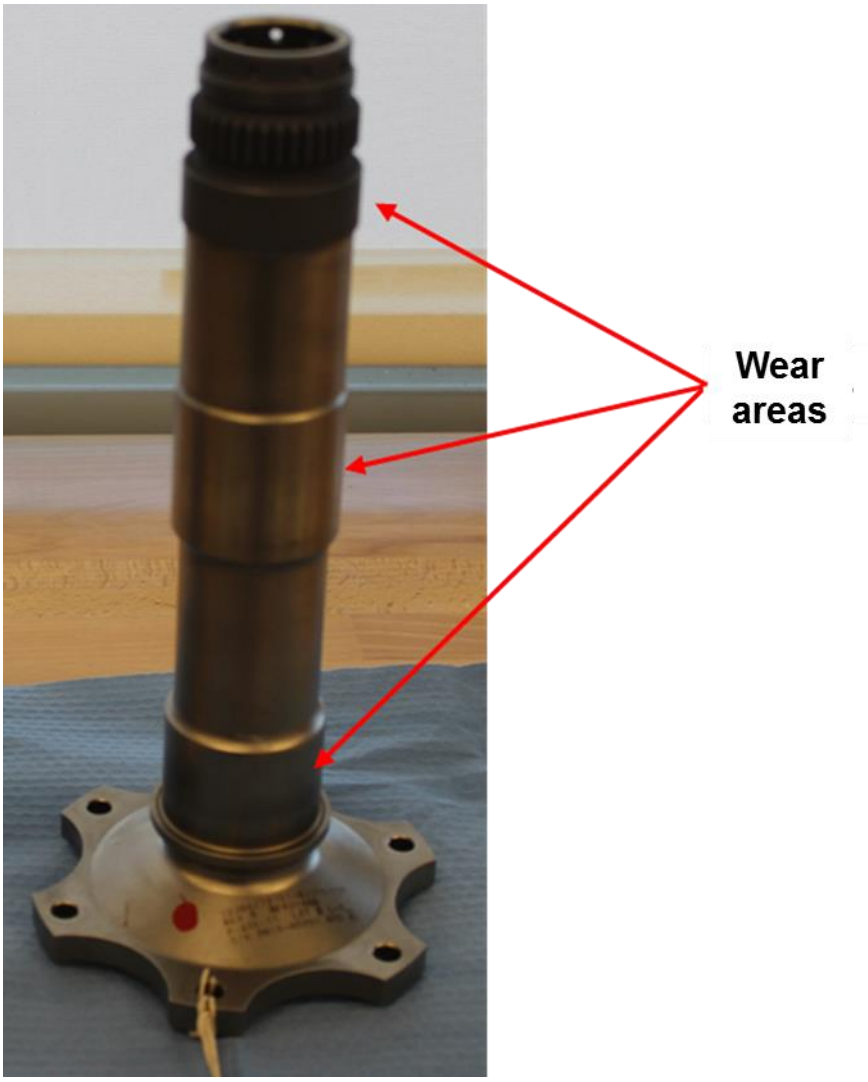

Figure 34 – Cooling fan shaft faults with bearing journal wear.

Table 12 – Cooling fan shaft initial dimensions.

Candidate Serial Number	Measured Journal Diameter, cm (in)
E815-00395	4.99872 (1.9680)
418651	4.99874 (1.9681)
C815-00451	4.99874 (1.9681)

Table 13 – Ti-6Al-4V laser deposition repair parameters for the cooler fan shaft.

	LENS Settings	Process Parameters
Laser Power	9.6 V	415 W
Speed	83333.325 CPS	0.63 m/min. (25 IPM)
Powder Flow Rate	3 RPM	3 GPM (0.007 lb/min.)
Shielding Gas Flow Rate	40 LPM	40 LPM (85 CFH)
Powder Purge Flow Rate	4 LPM	4 LPM (8.5 CFH)
Hatch Spacing	1/3 Overlap	0.9 mm (0.037 in.)
Height Offset	0.365 in.	0.9 cm (0.365 in.)
O_2 Level	< 20 PPM	< 10 PPM
Incident Angle	0° and 15° (15° used for lower bearing surface)	
Deposition Layer Thickness was 0.175 mm (0.007 in.)		

Vickers and Rockwell hardness measurements were taken across the Deposit, HAZ, and Substrate, shown in Table 14. Figure 35 shows where the hardness measurements were taken on the micrograph, and the hardness measurements for each area.

The processing was done on sample cooler fan shaft parts and the following results were obtained for the Shaft properties post deposit. Figure 35 shows macrographic, 36(a), and micrographic pictures of the deposit, 36 (b), and the HAZ, 36 (c). The substrates before and after the deposition occurred were analyzed and the microstructures were observed in Figure 37 and 38. Figure 39 shows the microstructure of the Ti-6Al-4V deposit that is obtained at various cooling rates.

An analysis of the microstructure of the deposit was conducted to ensure that the porosity was not excessive, which is shown in Figure 40. The diameter of representative pores was approximately 25 μm (0.001 inch), and the sum of the diameters of porosity did not exceed 1,000 μm (0.040 inch) in any linear inch of clad. Figures 41-43 show the results of the radiographic-

based tomography for the cooling fan shaft following deposition. Figure 44 shows the result of the post-process machining and dimensional tolerance to ensure that DMWR specifications were met following deposition.

Post process machining and dimensional inspection proved that the repair Cooling Fan Shafts met DMWR dimensional specifications. These specifications were limited to a .001 inch variance from thermal distortion. Figure 45 and Table 15 summarize these results.

Table 14 – Microhardness of cooler fan shaft.

	Vickers	Rockwell C
Clad	379.13	39.7
HAZ	313.25	32.6
Substrate	303.13	31.3

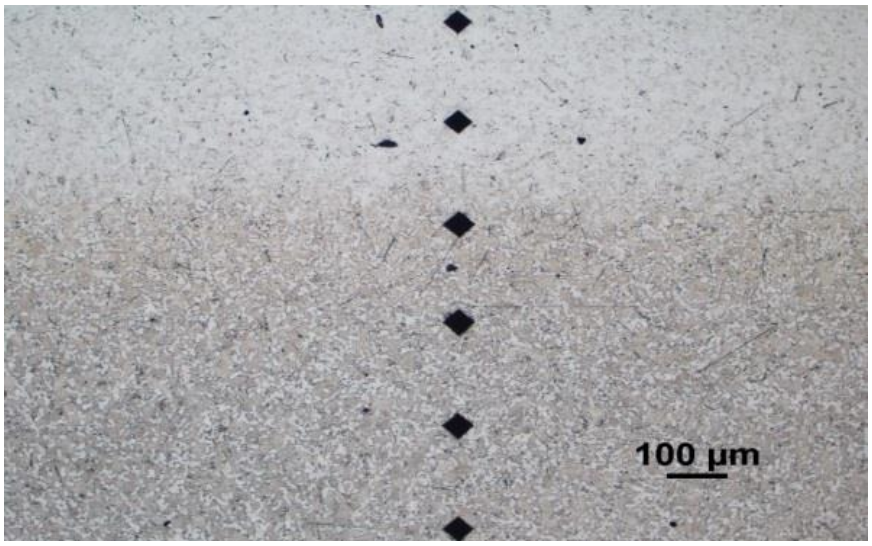

Figure 35 – Microhardness Measurement cooler fan shaft.

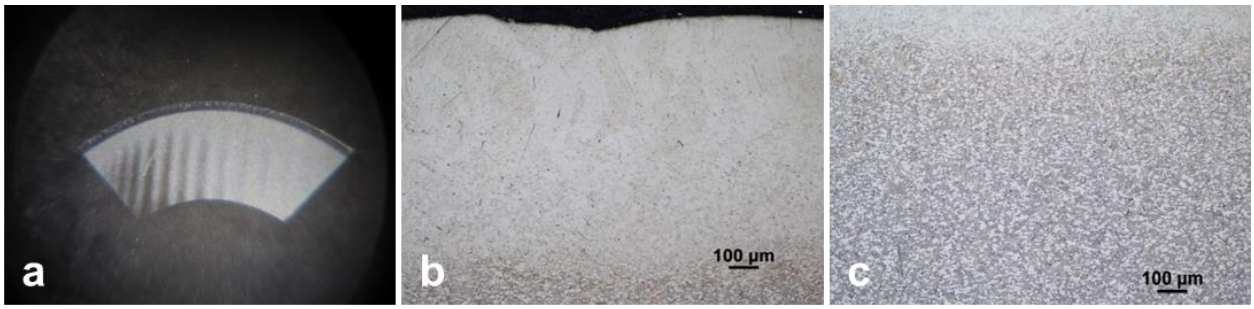

Figure 36 – (a) Macrograph longitudinal section cooling fan shaft. (b) Micrograph deposit and interface cooling fan shaft. (c) Micrograph interface, HAZ, and substrate.

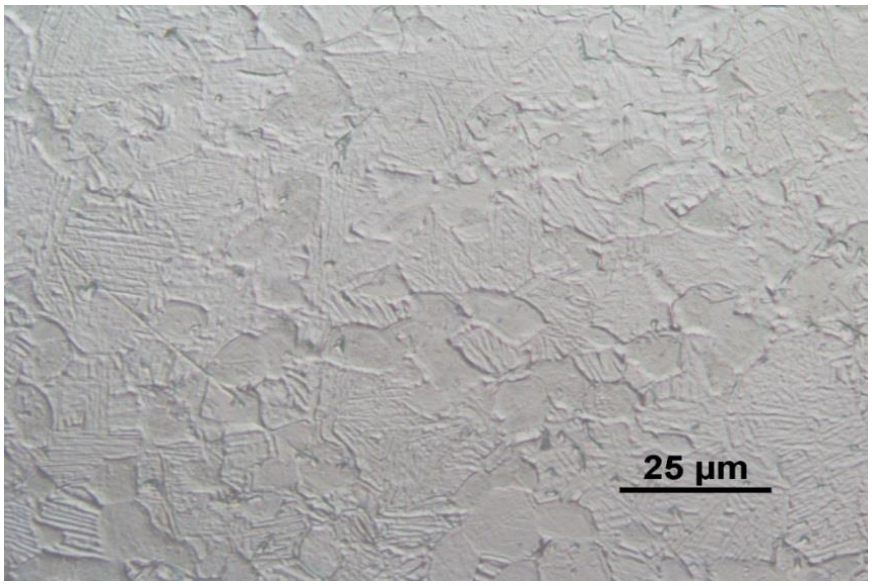

Figure 37 – Micrograph of unaffected Ti-6Al-4V substrate cooler fan shaft.

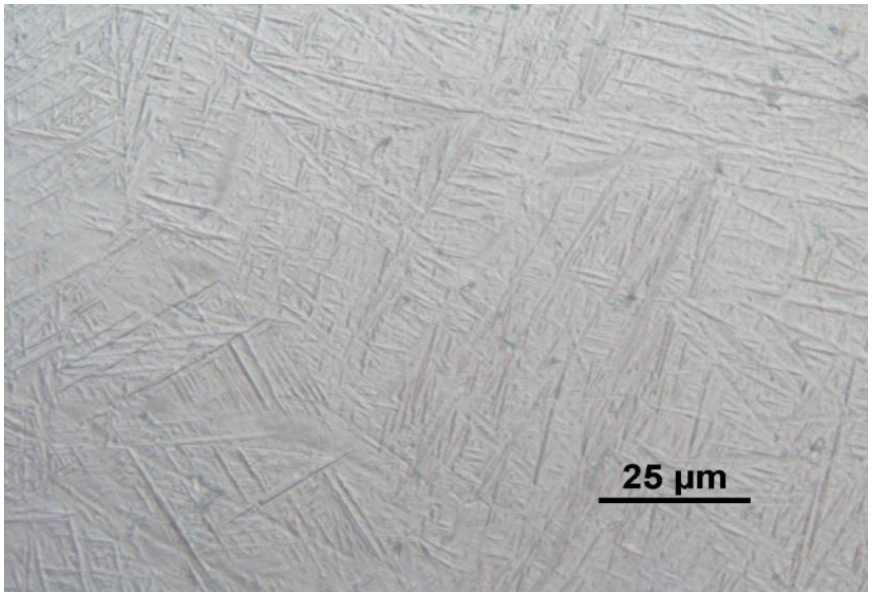

Figure 38 – Micrograph of Ti-6Al-4V deposit cooler fan shaft.

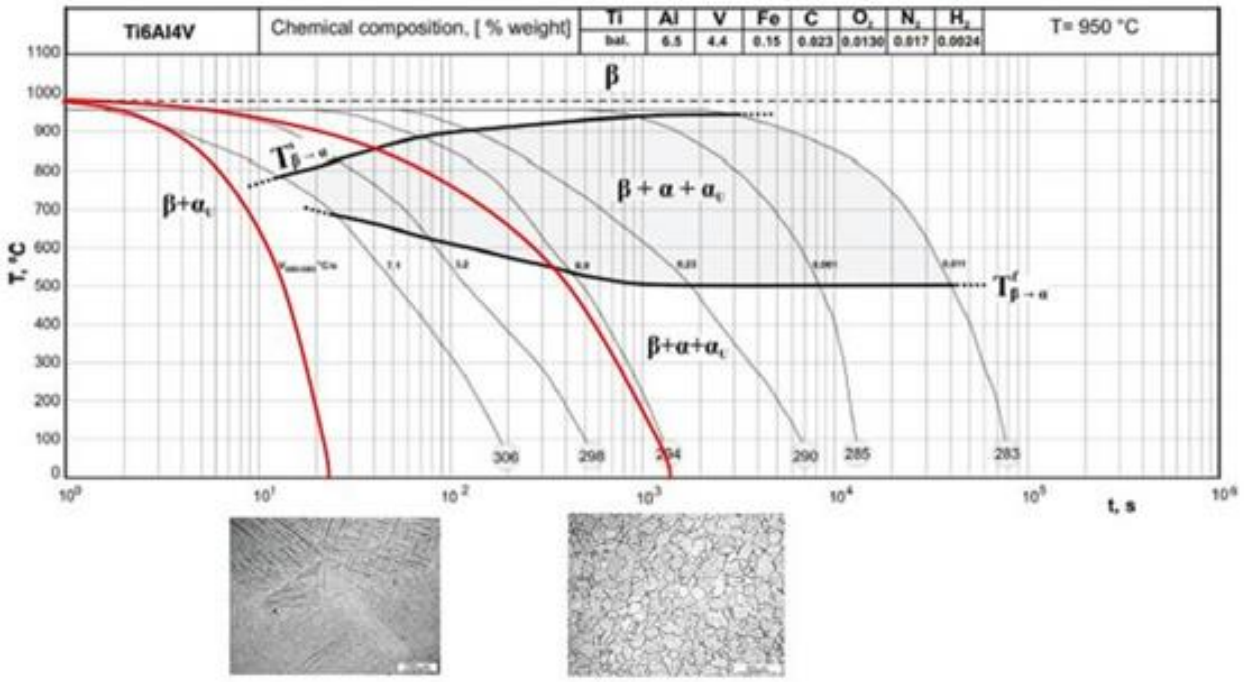

Figure 39 – Analysis of deposition and substrate based on Ti-6Al-4V CCT Diagram.

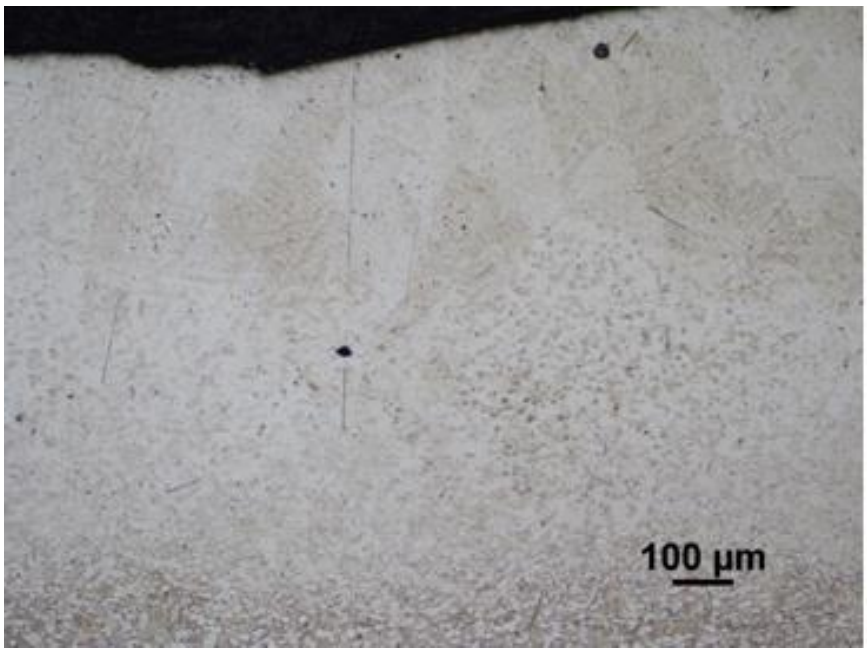

Figure 40 – Micrographic analysis for Microporosity of Ti-6Al-4V deposit.

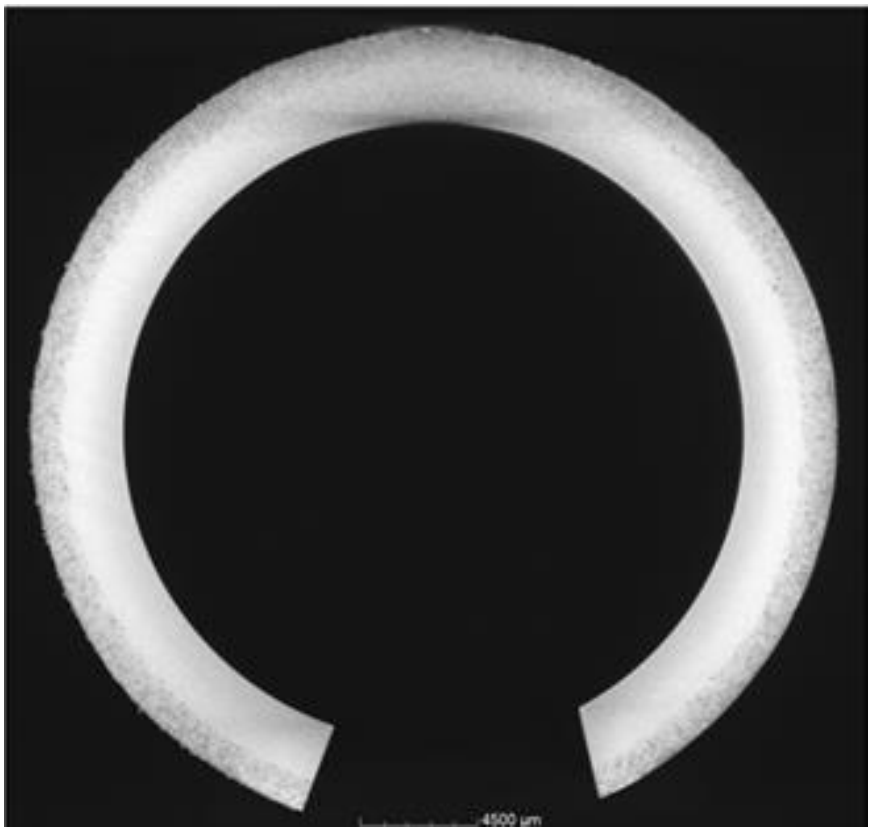

Figure 41 – Radiographic-based tomography of cooler fan shaft.

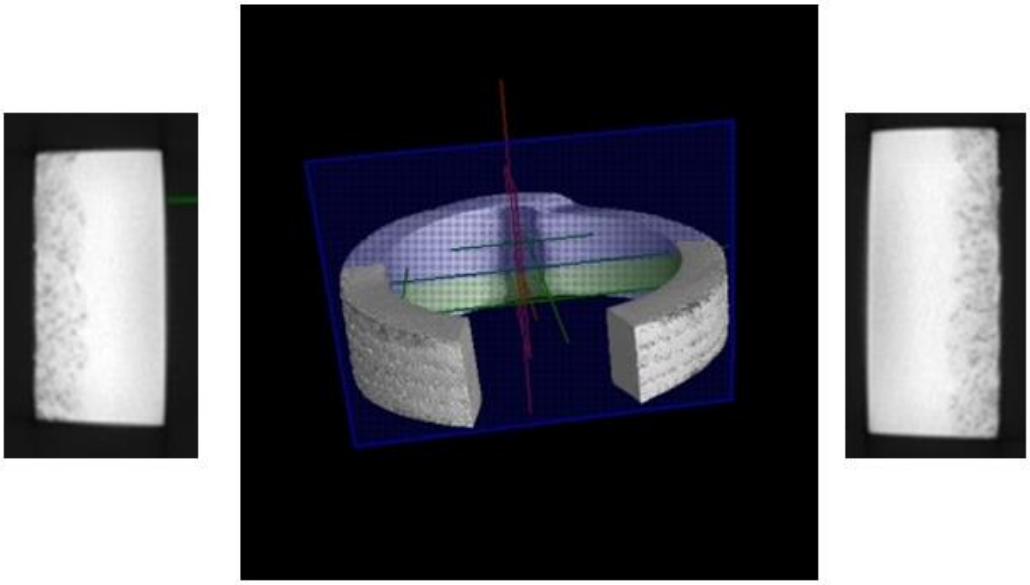

Figure 42 - Radiographic-based tomography of cooler fan shaft.

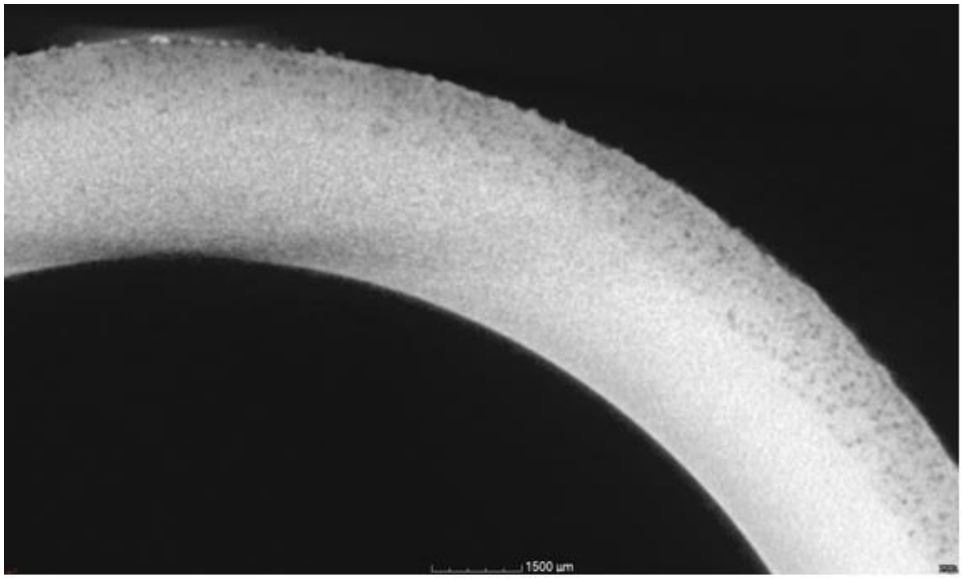

Figure 43 - Radiographic-based tomography of cooler fan shaft.


Figure 44 - Post-process machining and dimensional inspection cooler fan shaft.

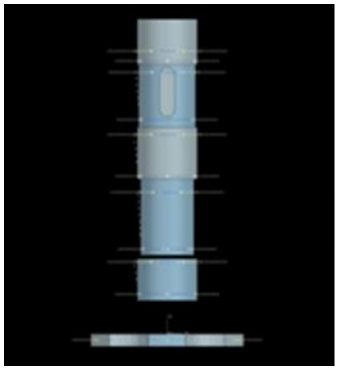

Candidate Serial Number	Measured Journal Diameter, cm (in)
E815-00395	N/A
418651 (Cladded)	5.087874 (2.0031)
C815-00451 (Machined)	4.99999 (1.9685)

Figure 45 – Coordinate measurements of cooling fan shaft after repair.

Table 15 – Coordinate measurements for potential thermal distortion of cooling fan shaft after repair.

Candidate Serial Number	Variance of Journal Diameter Center Before Repair, mm (in)	Variance of Journal Diameter Center After Repair, mm (in)
E815-00395	0.000, -0.0254 (0.000, -0.001)	N/A
418651 (Cladded)	0.000, -0.0254 (0.000, -0.001)	0.000, -0.0254 (0.000, -0.001)
C815-00451 (Machined)	0.000, -0.0254 (0.000, -0.001)	0.000, -0.0254 (0.000, -0.001)

Cost Benefit Analysis Cooling Fan Shaft

The relevant costs for performing Cooling Fan Shafts in house are the onetime non-recurring cost for the fixture, the labor for setup and processing, the cost of the Ti-6Al-4V material, the post machining, and post inspection cost.

There were assumptions that were made during the analysis with respect to the fixture, the setup, processing, machining, post inspection, and material. The Fixture assumptions were that the fixture cost was $1000, and this cost was to be distributed throughout the total # of shafts, there were approximately 100 parts done per year, and processing was done in batches of ten shafts. The labor assumption was that the labor rate was $50/hour. The setup assumptions were that the initial setup of the laser and workspace was one hour, with two people needed to conduct this setup. The purge of the chamber with argon takes four hours, with one person needed for this, and one half hour is needed for final setup and inspection. The processing assumptions are that deposition takes ten minutes per section with each shaft containing three sections; the total processing time for each part includes the deposition time as well as intermittent adjustments to shaft position while switching sections. The total time for one shaft is estimated at one hour. The machining assumptions are that the cost to use the machine is $16.12/hour, and the machining time is approximately one hour per shaft. The post inspection cost assumptions are that the post

inspection includes dimensional inspection, visual inspection, and optional NDE, estimated at one hour per shaft. Lastly, the material assumptions are that powder costs $150/lb, the powder feeder can hold three pounds of powder and one pound is required per shaft, the capture efficiency of the powder is approximately 20%, though one pound of powder is still needed for one shaft, argon gas is needed during the setup process, and a pack of twelve Argon gas tanks is $260, two single tanks are used during the purge process, and every additional tank gives two hours of run time. Table 16 shows the associated costs for repairing each Cooling Fan Shaft based on the previous assumptions. For the first year the cost for repair is $659.75 per part, and in year five that price drops slightly to $651.75.

Table 16 – Cost benefit analysis cooling fan shaft

Capital Cost		Price	Shafts/Year	Year	Price/Part
Fixture Cost Year 1		$ 1,000.00	100	1	$ 10.00
Fixture Cost Year 2		$ -	100	2	$ 5.00
Fixture Cost Year 3		$ -	100	3	$ 3.33
Fixture Cost Year 4		$ -	100	4	$ 2.50
Fixture Cost Year 5		$ -	100	5	$ 2.00
Machine Amortization		Price Per Year	Hours Utilized Per Year	Cost Per Hour	Price/Part
Machine Cost Per Year		$ 200,000.00	1040	$ 192.31	$ 288.46
Labor Cost		Time/Shaft (Hours)	Hourly Labor Rate	Workers	Price/Part
Laser Setup		0.1	$ 50.00	2	$ 10.00
Argon Setup		0.4	$ 50.00	1	$ 20.00
Laser Processing		1	$ 50.00	1	$ 50.00
Post Machining		1	$ 50.00	1	$ 50.00
Post Inspection		1	$ 50.00	1	$ 50.00
					$ 180.00
Machine Cost		Time/Part (Hours)	Hourly Machine Rate	Price/Part	
Post Machine Cost		1	16.12	$ 16.12	
				$ 16.12	
Material Cost		Material/ Part	Material Unit Price	Price/Part	
Titanium Alloy Powder		1	$ 150.00	$ 150.00	
Process Gas		0.7	$ 21.67	$ 15.17	
				$ 165.17	
Total cost per shaft					
* Note the cost decreases with a higher number of parts due to the fixture cost being distributed over a higher number of parts. Assuming 100 shafts/year the shaft price is listed for years 1-5					

Year	Total Cost/ Shaft
1	$ 659.75
2	$ 654.75
3	$ 653.08
4	$ 652.25
5	$ 651.75

Proposed Depot Maintenance Work Requirement for repair of the Cooling Fan Shaft

Based upon the positive results obtained during the evaluation of the Axial Transmission Oil Cooling Fan shaft, a DMWR was prepared by Genesis Engineering that defines the repair process for this components. The proposed DMWR may be found in Appendix D.

11.2 H60 Pinion Gear

The technical data for the H60 Pinion Gear is found in DMWR-1-1615-371. There were multiple areas of faults found on the piece including gear teeth, pitting/scuffing, seal journal wear, and OD & shoulder wear, these faults are shown in Figure 46. The piece is composed of AMS 625 and each part costs $4,447.13. Three components were evaluated initially for laser deposition repair. Table 17 shows the bearing surface diameter for each part upon initial evaluation. Each part had diameters less than 2.299 inches, which was the minimum specification requirement from the DMWR. Table 18 shows the process parameters that were decided upon for laser deposition for the H60 Pinion Gear repair. Powder flow rates in g/min differed among the different material choices but were the same at 1 cm^3/min.

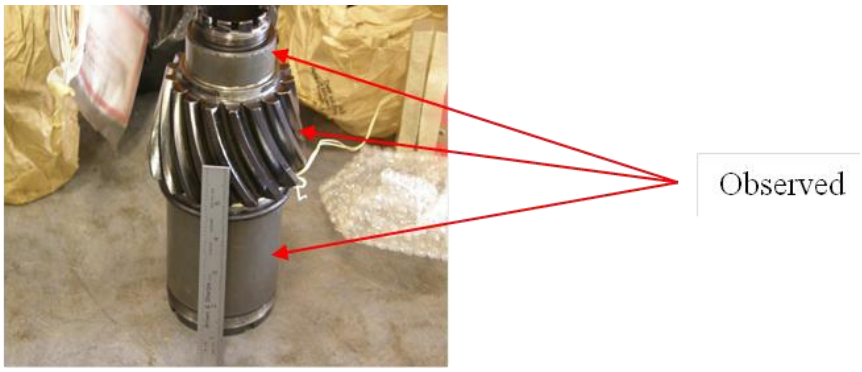

Figure 46 – H60 pinion gear faults.

Table 17 – Initial diameters H60 pinion gear

Candidate Serial Number	Measured Journal Diameter, cm (in)
A319-02156	5.839206 (2.2989)
B319-00443	5.837428 (2.2982)
C319-00496	5.841492 (2.2998)

Table 18 – Laser deposition process parameters for H60 pinion gear.

Laser Power (watts)	Travel Speed (IPM)	Powder Type	Powder Flow Rate (g/min)*	Gas Type	Gas Flow Coaxial Rate (cfh)	Gas Flow Process Rate (cfh)	Gas Flow Trailing Rate (cfh)	Gas Flow Powder Feeder Rate (cfh)	Powder Nozzle Standoff (mm)	Focus Head Standoff (mm)	Spot Size (mm)	Comments
1000	25	SS 431/ 20% TiC	7	Ar	20	20	20	20	10	212	~2.5	0.55 in. helical with 0.05 in.step

Hardness tests were performed using the applicable ASTM-E384 specification with a Leco M-400-G1 hardness tester in the Vickers scale using a 300 g load. The hardness profile of each deposition material on low carbon steel is shown in Figure 47, and the average hardness of the deposit for each sample is shown in Table 19. The hardness profiles indicate that the deposition material hardnesses had been increased by significantly higher TiC concentrations. The hardness also slightly increased, by approximately 25 HV, with multi-layer deposition when compared to the single layers. The localized hardness measurements on the TiC particles were above 2000 HV.

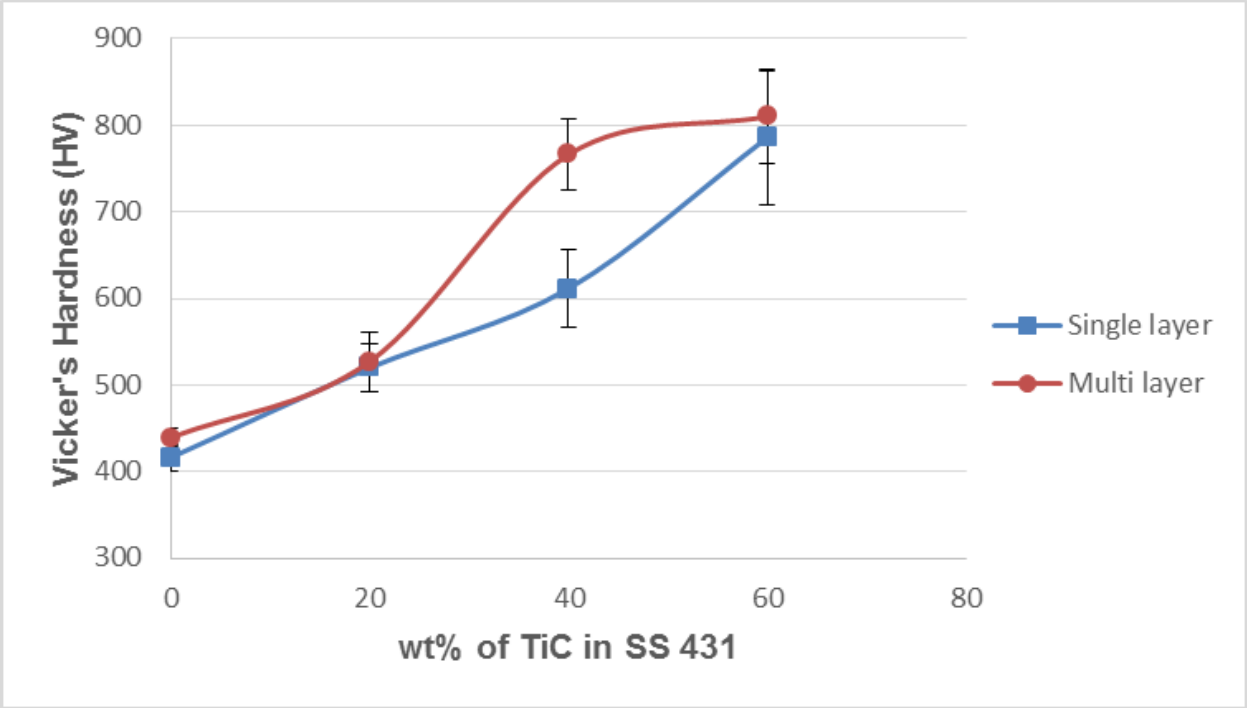

Figure 47 – Hardness of deposits produced using increasing amount of TiC blended in SS 431 powder that had been deposited on low carbon steel.

Table 19 – Vickers hardness of SS 431 and SS 431/TiC composites for single layer and multi-layer depositions.

	SS 431		SS 431/ 20 wt% TiC (28.13 vol% TiC)		SS 431/ 40 wt% TiC (53.07 vol% TiC)		SS 431/ 60 wt% TiC (70.14 vol% TiC)	
Deposit Layers	Single	Multi	Single	Multi	Single	Multi	Single	Multi
Average Vickers Hardness	416	439	520	527	611	766	786	810
Standard Deviation	15.7	10.7	28.5	34.0	45.5	40.3	77.5	54.1

The hardness profiles for the carburized 8620 steel and two selected deposition materials, SS 431/20 TiC and SS 431/40 TiC, are shown in Figure 48. The measured surface hardness of the samples are also shown in Table 20. The hardness profiles indicate that both deposition materials had achieved higher hardnesses than the carburized 8620 steel. The surface hardness of the carburized 8620 steel was 703 HV. The deposition material SS 431/20 TiC exhibited a hardness of approximately 50 HV above the carburized 8620 steel which was seen to be 746 HV. The hardness of the deposition material representing the SS 431/40 TiC was found to exceed the required hardness by over 100 HV.

The microstructural cross-sections of two materials deposited on carburized 8620 steel substrate are shown in Figure 49. The microstructural images indicated that unmelted TiC particles tended to remain at the top of deposit surface. This is believed due to the relatively lower density of TiC particles providing buoyancy within the molten SS 431 pool. Multiple boundary lines also appeared within the microstructure and delineated the multiple tracks. This observation is reinforced in the image of Figure 50. The length of the boundary line increased at higher TiC content. These boundary lines may also indicate cracks that have been backfilled by liquid during the deposition process.

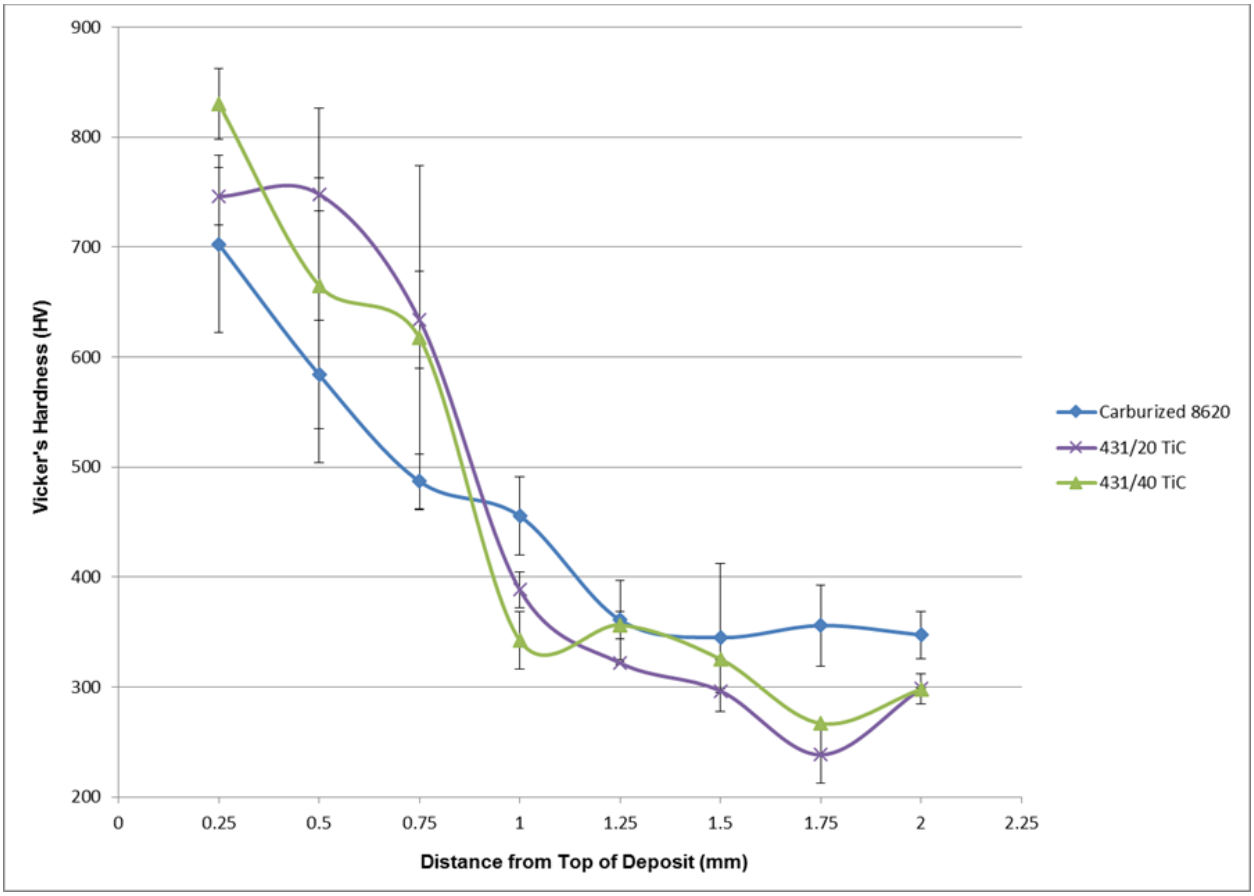

Figure 48 – Hardness profile with four different mixtures of SS 431 and TiC on carburized 8620 steel.

Table 20 – Surface hardness of carburized 8620 steel and two selected deposition materials.

	Carburized 8620 Steel	SS 431/20 TiC	SS 431/40 TiC
Average Vickers Hardness	703	746	830
Standard Deviation	80.5	21.25	142.4

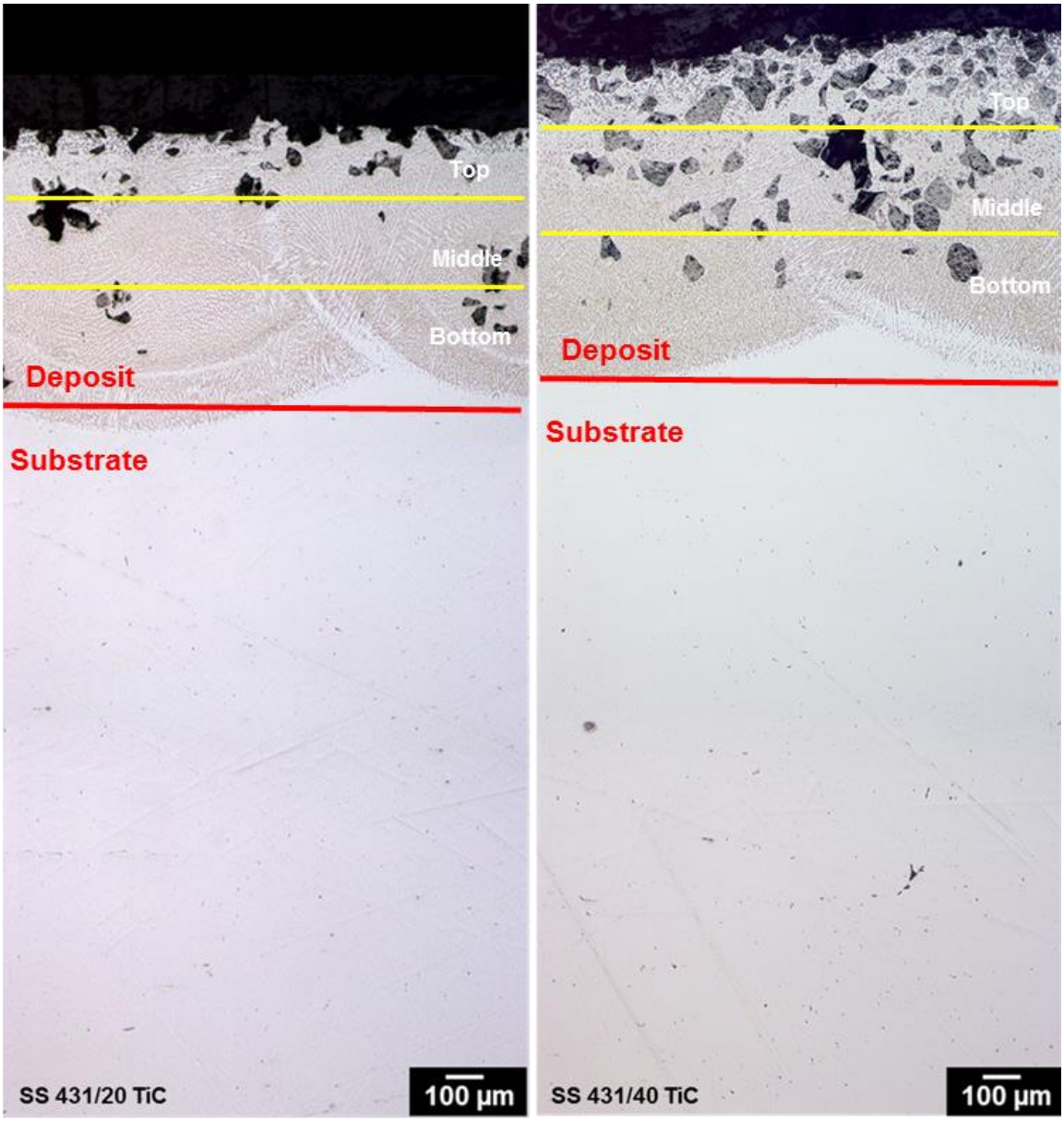

Figure 49 – Microstructure cross-section of each sample with respective deposit, HAZ, and 8620 base material.

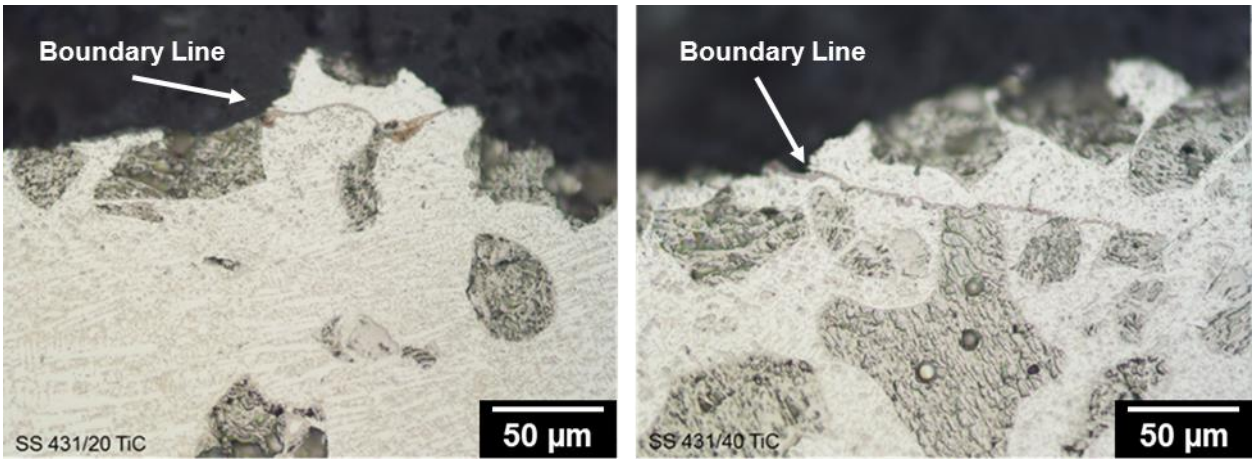

Figure 50 – Boundary lines which appeared in each deposition sample.

.

The micro hardnesses of transverse and longitudinal cross-sections representing the RCF test specimens are shown in Figure 51 and Table 21. Hardness of the HAZ was approximately 290 HV. The non-carburized 8620 steel substrate, representing the carburized surface removed, had a hardness of approximately 320 HV for the transverse and longitudinal cross-sections. However, the deposited material at the transverse cross-section displayed higher hardness of 65 HV. The roller grind surface of the laser deposited RCF specimen had a hardness at 697 HV.

Microstructural examination was conducted on the RCF test specimen and involved preparation of two samples, a transverse cross-section and a longitudinal cross-section. The transverse sample was cut perpendicular to the laser deposition direction, and the microstructure is shown in Figure 52. The longitudinal sample was cut parallel to the laser deposition direction, and microstructural images for the longitudinal sample are shown in Figure 53.

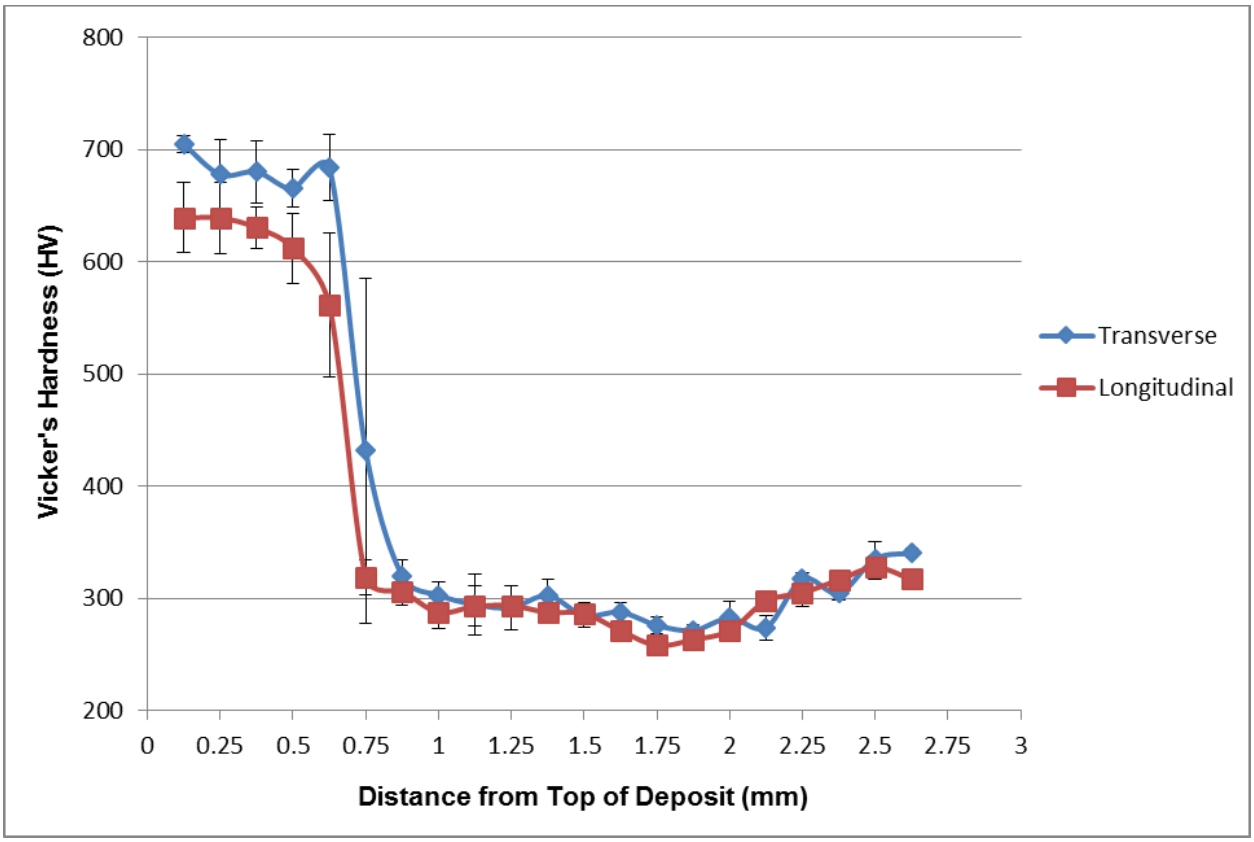

Figure 51 – Hardness profile of SS 431/20 TiC laser deposited on 8620 carburized steel of transverse and longitudinal cross-sections.

Table 21 – Micro hardnesses for SS 431/20 TiC deposit, HAZ, and substrate for the transverse and longitudinal cross-sections.

	SS 431/20 TiC Deposition Materials	HAZ	8620 Steel Substrate
Average Transverse Hardness (HV)	682 (STDEV = 12.8)	290 (STDEV = 13.9)	324 (STDEV = 14.3)
Average Longitudinal Hardness (HV)	616 (STDEV = 29.3)	286 (STDEV = 17.0)	317 (STDEV = 8.0)
Average Surface Hardness (HV)	697 (STDEV = 18.8)	–	–

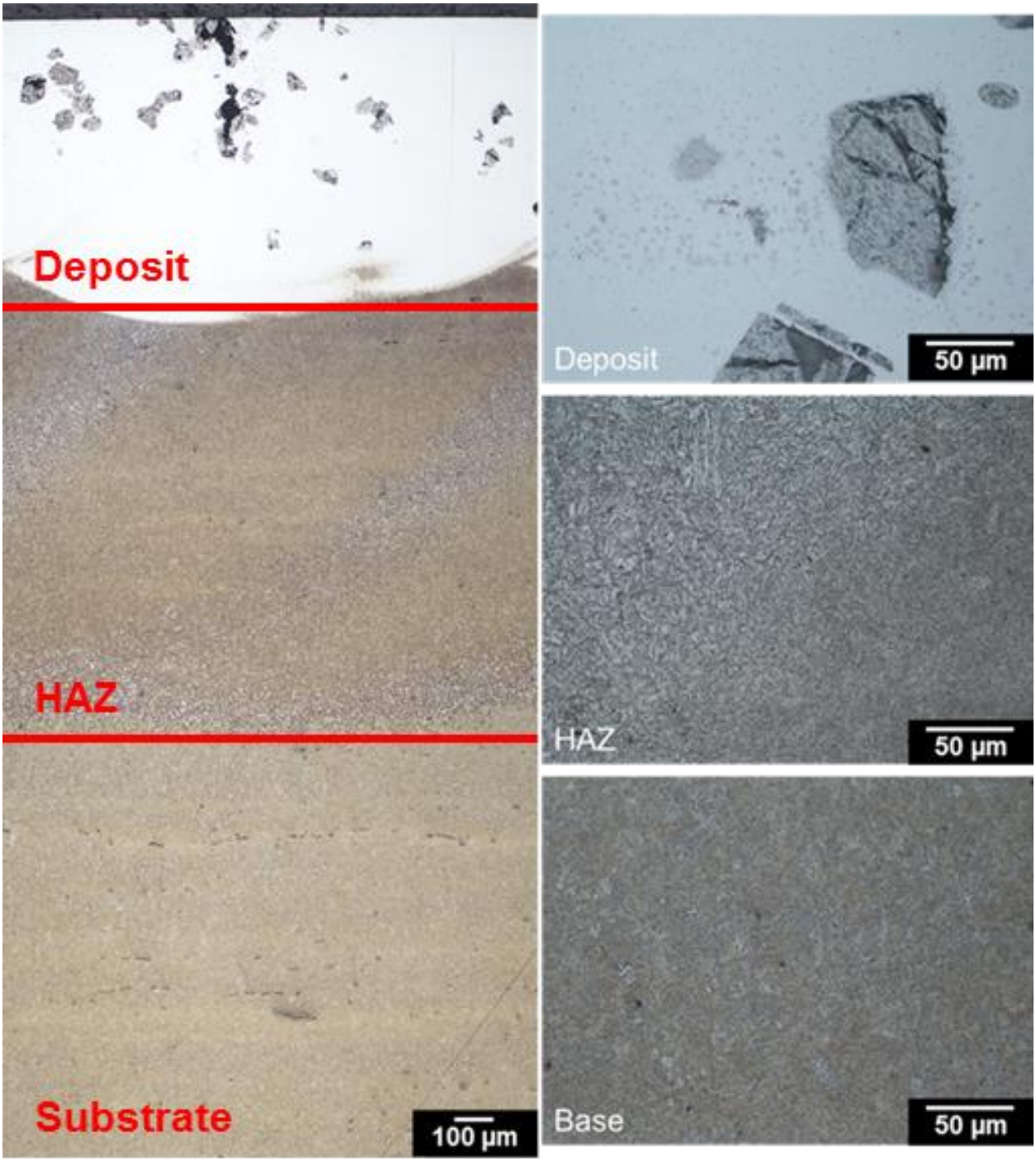

Figure 52 – Microstructures of RCF test specimen with laser deposited SS 431/20 wt% TiC representing transverse cross-section.

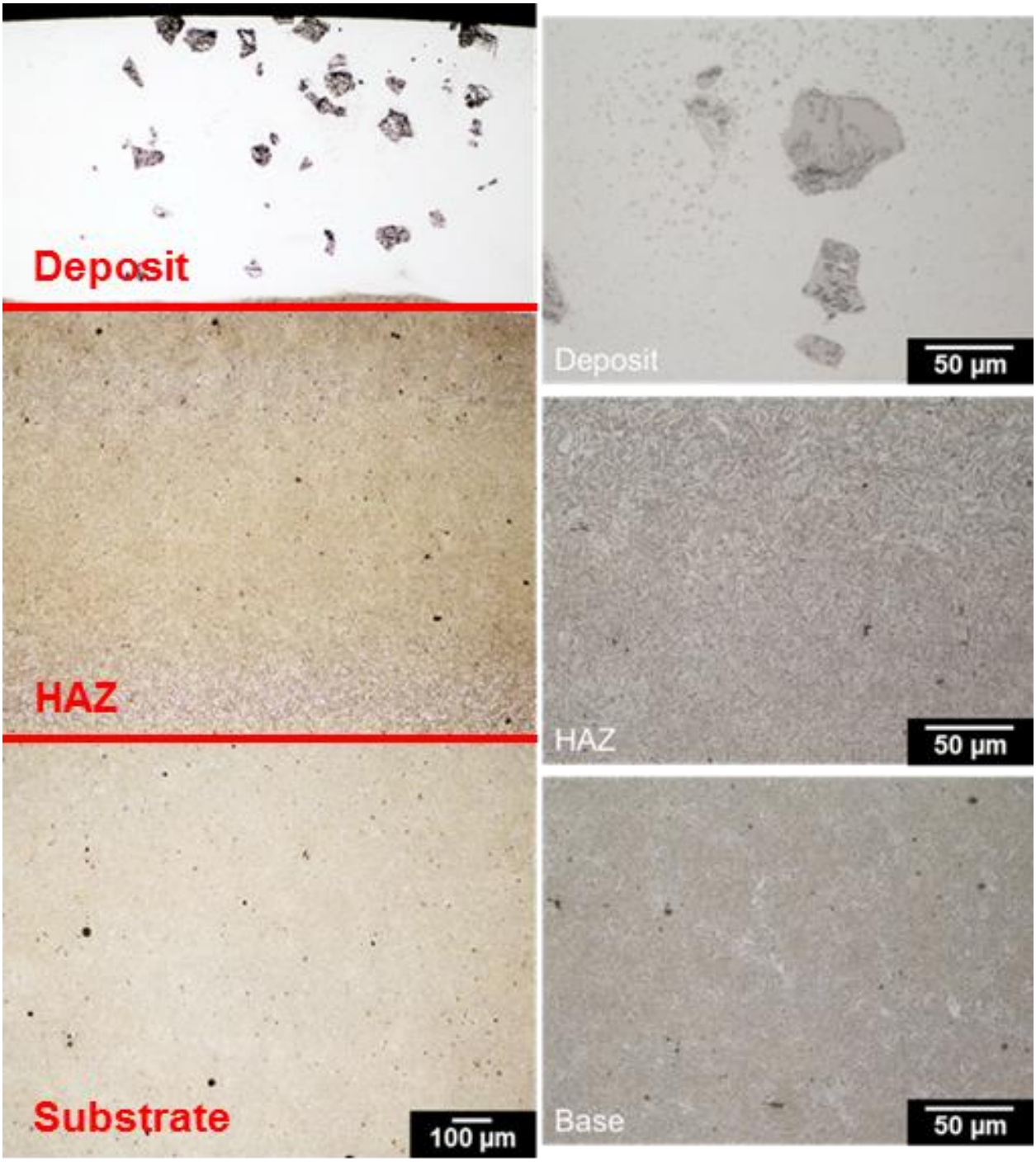

Figure 53 – Microstructures of RCF test specimen with laser deposited SS 431/20 wt% TiC representing longitudinal cross-section.

The cross-section of the SS 431/20 TiC produced for RCF testing was characterized by ESEM and EDS. Figure 54 shows an SEM image of the SS 431/20 TiC that had been deposited. In Figure 54, three locations were chosen for elemental analysis. Location A (white area) represented the SS 431 rich region. Location B (dark dendrite) is believed to be the TiC phase that had precipitated within the SS 431 matrix, and location C represented an unmelted TiC particle. The complete results of the elemental analysis of each region are listed in Table 22.

The SEM image in Figure 55 shows a TiC particle that had been retained within the molten pool, as well as other phases that had been formed during processing. Most notably, the secondary phase apparent at this magnification appears to be dendritic TiC. Figure 55 shows the rich region of individual elements in the composite system. The EDS mapping images also provided evidence that the TiC had dissolved and diffused into SS 431. This is based on the location of titanium (Ti) and iron (Fe) shown in Figure 55. A small amount of vanadium (V), which was observed in the original powder, was also present in the TiC particle. Elemental Ti and V only appeared at unmelted TiC particles and the small dark regions. The elements contained within the SS 431, Fe, Cr, and Ni, remained only in the white areas. The EDS elemental analyses results also showed that the amount of carbon increased in the SS 431 region, as shown in Table 22. The higher carbon within the matrix material would enhance the overall hardness of the matrix. SEM image via back-scattered electrons, Figure 56 and 57 also showed that the TiC particles were dissolved and formed small dendritic constituents near the surface of the TiC particle. The dissolved Ti and C phase that surrounded the original TiC particles are believed to be responsible for the formation of TiC that had reprecipitated during cooling.

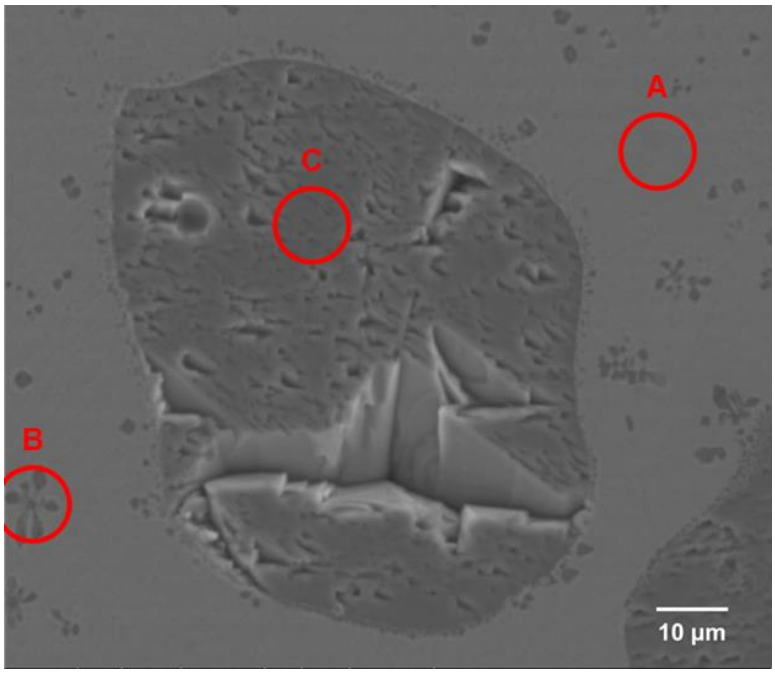

Figure 54 – SEM image of SS 431/20 TiC laser deposited material. Red circles indicate the area characterized by EDS analysis.

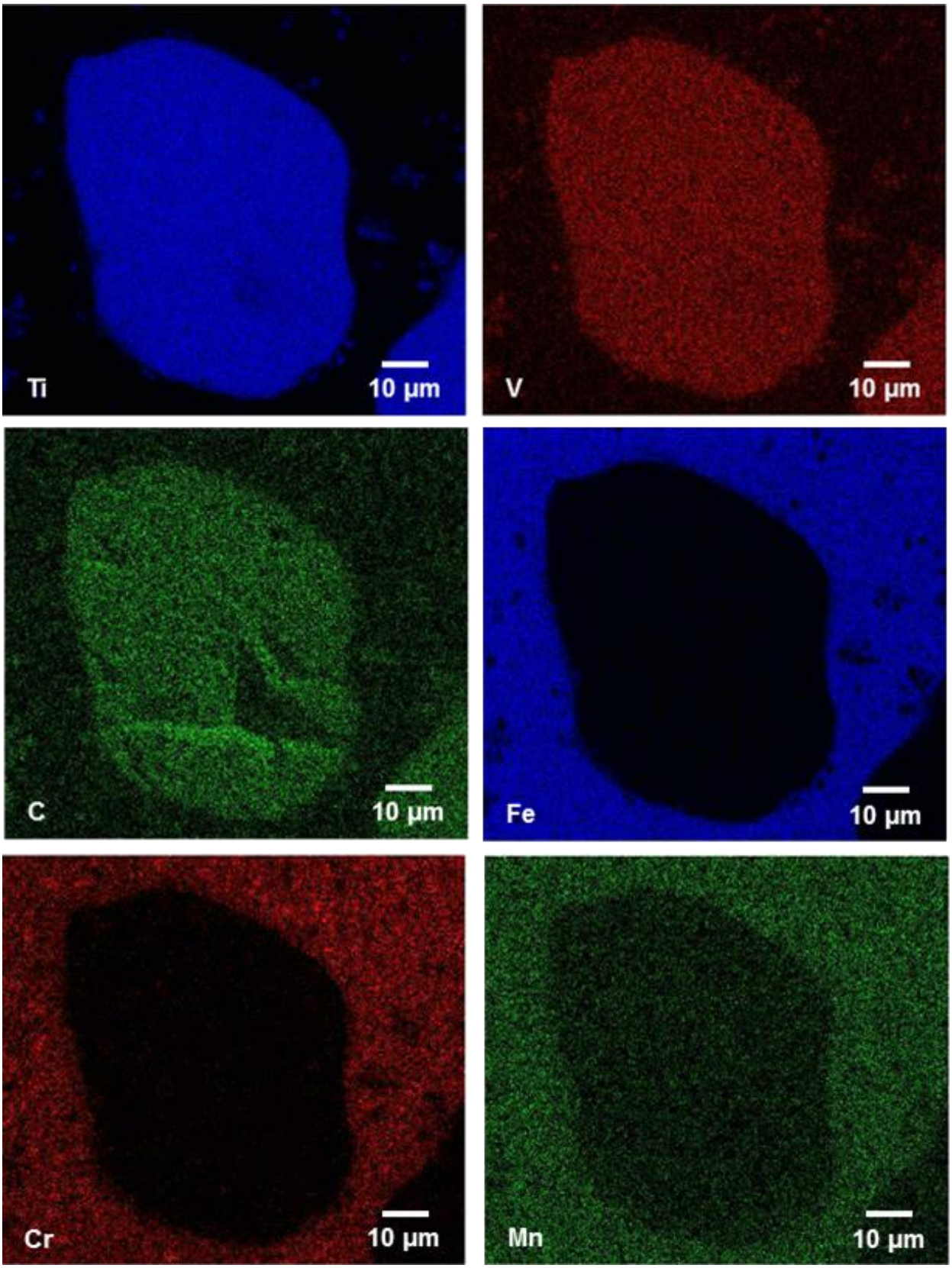

Figure 55 – Images generated by EDS mapping analyzer. Each image shows the respected element located from Figure 52.

Table 22 – EDS elemental analysis results of each region of the RCF testing specimen. The results are also compared to the chemical composition from the reference.

Elements (wt%)	Fe	Cr	Ti	Ni	Mn	V	C	Si	Al	Ca
8620 Base	97.19	0.51	-	0.40	0.67	-	0.88	0.36	-	-
HAZ	96.83	0.59	-	0.47	0.62	-	1.04	0.45	-	-
A. Deposit (White Area)	78.47	10.01	4.58	1.01	0.42	-	3.98	1.26	0.27	-
B. Deposit (Black Dot)	33.76	4.77	47.69	0.37	0.24	0.34	11.51	1.08	-	0.22
C. Deposit (Black Particle)	21.09	2.27	62.26	0.23	-	0.31	13.85	-	-	-
Normalized 8620 steel (ASM Handbook)	96.9-98.02	0.4-0.6	-	0.4-0.7	0.7-0.9	-	0.18-0.23	0.15-0.35	-	-
SS 431	79.17	15.58	-	1.36	0.44	-	2.5	0.4	0.54	-
TiC	-	-	83.81	-	-	0.34	15.85	-	-	-

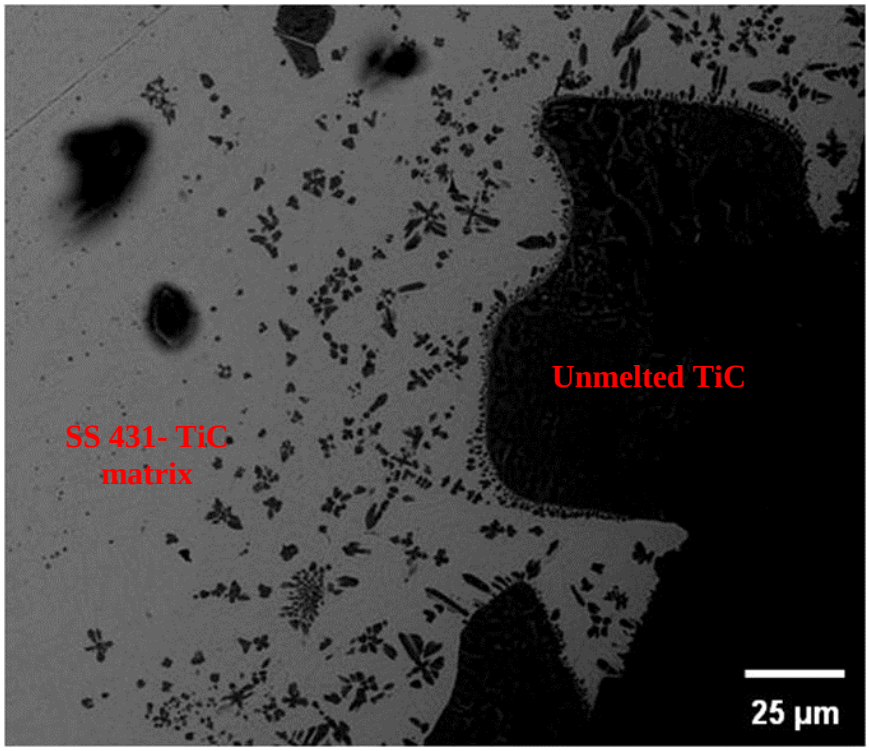

Figure 56 – SEM image showing TiC particles along with precipitates of TiC formed during cooling.

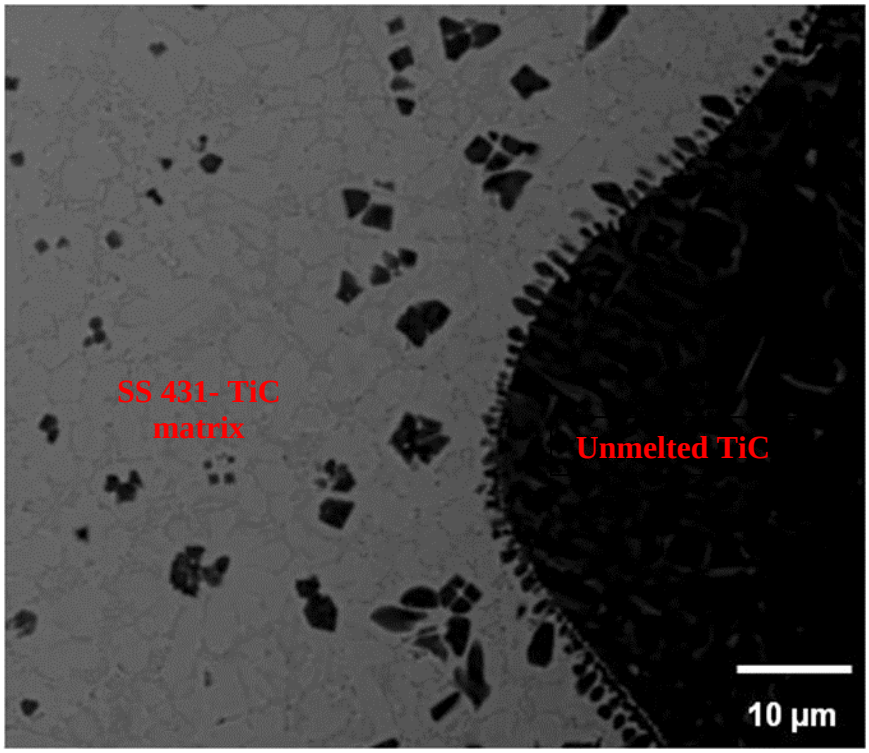

Figure 57 – SEM image showing TiC precipitation.

11.3 Rolling Contact Fatigue Test

The rolling contact fatigue (RCF) test simulates the rolling and sliding action that occurs in a gear mesh. Figure 58 shows a general schematic of the rolling contact fatigue test, and Figure 59 is a picture of the rolling contact fatigue test rig. The specimen and load rollers are cylindrical. The outside diameter of the load roller is crowned to concentrate the load at the center of contact, and eliminate the possibility of concentrated loading at the edge of contact due to misalignment. A normal load is applied by air pressure. Phasing gears, attached to the shafts on which the specimen and load rollers are mounted, control the extent of sliding at the specimen/load roller interface. For this testing, 56 tooth and 16 tooth gear were utilized to cause the load roller surface velocity to be 1.21 times that of the specimen velocity. Tests were conducted at 3000 RPM, and a 2068 MPa (300 ksi) stress load. Complete details of the test are shown in Table 23. [22]

The intent for this evaluation was to compare the performance of the specimens representing the deposited material to prior data representing the 8620 base metal that had been carburized. All tests were conducted in oil heated to 70°C (158°F). Searching tests were conducted with a baseline group of specimens to find loads that resulted in initial surface durability failures.

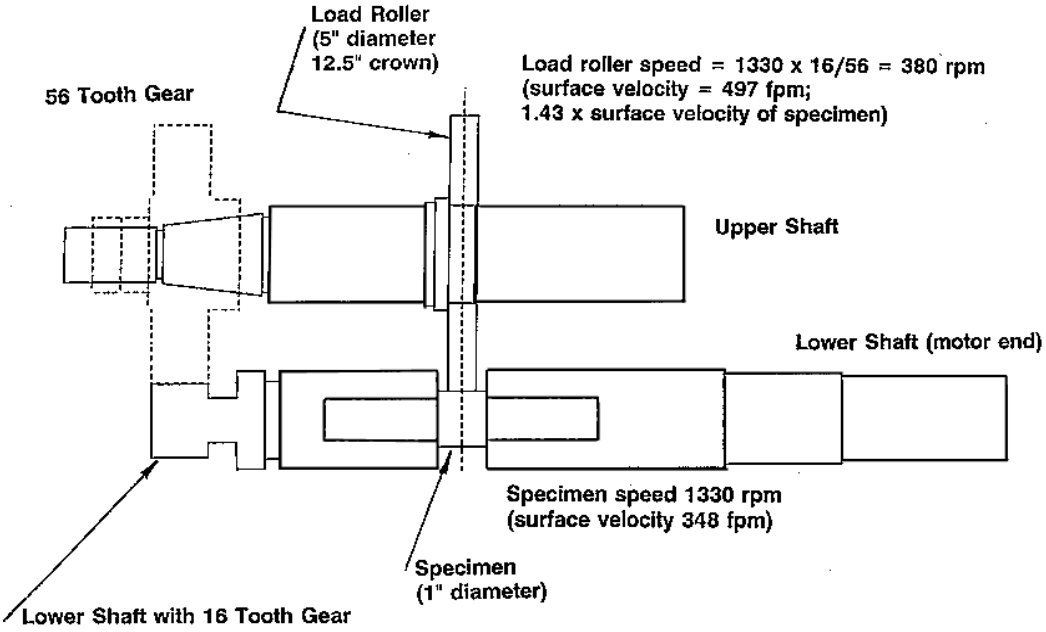

Figure 58 – Schematic of the rolling contact fatigue test. [21]

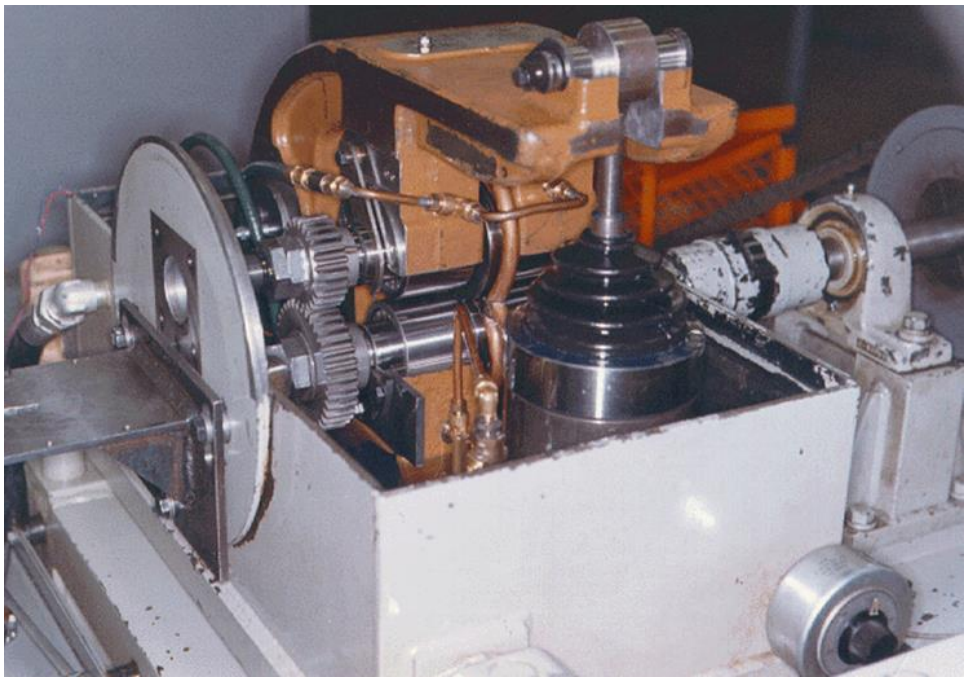

Figure 59 – Photograph of the rolling contact fatigue test at the Drivetrain Technology Center of the Applied Research Laboratory.

Table 23 – Rolling Contact Fatigue Testing condition details. [22]

RPM:	3000 (approximately)
Phasing Gear Set:	16/56 Tooth
Test Plan:	1) Conduct searching tests to find loads to result in 12-15 million cycles to pitting and 30-50 million cycles to pitting. First searching load 350 KSI. 2) Conduct six tests at each load. Use three machines (two at each load on each machine). Work this testing with that for Half Factorial Conditions 1-6, and 8.
Run Out Limit:	100 million cycles
Run-in:	Stabilize at temperature. Roll over by hand with no load on load rod. Run 10 minutes at each of 25%, 50% and 75% contact stress. Reset timer and run 10 minutes at test stress.
Lubricant:	Texaco OEM DEXRON III
Lubricant Temp:	70°C (158°F)
Filter:	10 micron (nominal)
Lubricant Change Interval:	about 1200 hours
Wear Measurement:	Measure diameter of specimen at start of test, at each inspection, and at end of test. **STOP TEST IF WEAR EXCEEDS 0.0015 INCHES DIAMETER REDUCTION.** For long tests with low wear, measure diameter every other inspection.
Special Notes:	Inspect all specimens and load rollers per attached.

11.4 Results of Rolling Contact Fatigue Test

Three specimens representing the SS 431/20 TiC deposited on carburized 8620 steel were tested by rolling contact fatigue at the Gear Research Institute. Test specimens were contacted against a carburized 8620 steel roller. Tests were conducted at 3000 RPM, and a 2068 MPa (300 ksi) bearing load, with lubricant heated to 70°C (158°F). These testing conditions reflected the exact parameters that were used previously during RCF testing of carburized 8620 steel.

Comparable testing results are shown in Table 24. The results of the SS 431/20 TiC samples showed an average of 98.8 hours of lifetime (17,300,000 cycles), and all specimens failed with surface scuffing on both the specimen and roller. The surface scuffing failure of the SS 431/20 TiC specimen is shown in Figure 60. Surface scuffing occurs when both surfaces of the test specimen and test roller exhibit wear. This condition is shown as Figure 61 and results in an increased surface contact area during RCF testing. The increased contact area reduces the stress load on the test specimen, and affects both the RCF test result and service life of the test specimen. Test 3, which represented the SS 431/20 TiC specimen, failed with surface pitting, which is illustrated in Figure 62. The surface pitting failure is usually caused by internal voids or cracks within the test specimen. Figure 62 appears to indicate that the pitting occurred at the interface of the deposited material and the 8620 steel substrate. This could be due to lack of fusion occurring at the deposit and substrate interface during the laser deposition process.

A Weibull plot representing the SS 431/20 TiC specimens and the prior results for the carburized 8620 steel specimens tested under rolling contact fatigue is shown in Figure 63. The SS 431/20 TiC specimens have a R^2 value at 0.96 and the Weibull equation is show in Equation 5. The carburized 8620 steel specimens have a R^2 value at 0.97 and the Weibull equation is show as Equation 6.

$$y = 4.9772x - 23.727 \quad \text{Eq. (5)}$$

$$y = 2.8317x - 14.612 \quad \text{Eq. (6)}$$

The high Weibull modulus reflected in the 431/20 TiC material had the similar wear failure time from surface scuffing. The carburized 8620 steel failed at the middle of the contact region after more than 150 hours, averaging 27,000,000 cycles. Figure 64 is a photograph of the carburized 8620 steel specimen, representing the surface pitting failure and without surface scuffing.

The surface scuffing occurred on both the SS 431/20 TiC specimen and the carburized 8620 steel roller; this is believed due to the extreme high hardness of the unmelted TiC particles on the surface of the specimens. Surface finish measurement were also conducted on the RCF testing rollers and SS 431/20 TiC specimens. Figure 65 represents the surface finish of carburized 8620 steel roller for RCF Test 2 and shows a relatively smooth curved surface of the testing roller. As the roller was worn, the measured curve became uneven, which is shown as Figure 66. The SS 431/20 TiC specimen from Test 2 also exhibited a worn surface due to surface scuffing, and this is illustrated in Figure 67.

There are several explanations for the surface scuffing observed on the specimen and roller. Because the SS 431-TiC composite structure is softer than the undissolved TiC particles, the SS 431 matrix material could experience local wear causing detachment of the TiC particles which remained on the uneven surface of RCF specimen. The high hardness of the TiC particles would promote wear on the surface of the carburized steel roller. Another explanation is that the granular morphology of the TiC particles promoted wear on both the test specimen and the roller. Detailed results of the surface roughness for the RCF test specimen are shown in next section, "Results of Tribology Analysis".

Table 24 – Rolling contact fatigue testing of SS 431/20 TiC and reference carburized 8620 steel.

Test #	Substrate	Coating	Load (N)	Speed (RPM)	Lifetime (Hours)	Cycles ($x10^6$)	Observation
SS 431/20 TiC Deposited on Carburized 8620 Steel							
1	8620	SS 431/20 TiC	5720	2915	96.2	16.83	Wear Failure, Surface scuffing on both specimen and roller
2	8620	SS 431/20 TiC	5720	2915	80.6	14.10	Wear Failure, Surface scuffing on both specimen and roller
3	8620	SS 431/20 TiC	5720	2915	119.7	20.94	Surface Origin Pitting, Surface scuffing on both specimen and roller
				Average	98.8	17.29	
Carburized 8620 Steel							
1	8620	8620	5556	2922	135.4	23.74	Surface Origin Pitting
2	8620	8620	5556	2922	188.1	32.98	Surface Origin Pitting
3	8620	8620	5556	2919	84.2	14.75	Surface Origin Pitting
4	8620	8620	5556	2925	207.9	36.49	Surface Origin Pitting
				Average	153.9	26.99	

Figure 60 – RCF test results showing scuffing surface on the SS 431/20 TiC.

Figure 61 – RCF test results showing scuffing surface on the carburized 8620 steel roller.

Figure 62 – RCF test results showing surface pitting on the SS 431/20 TiC specimen.

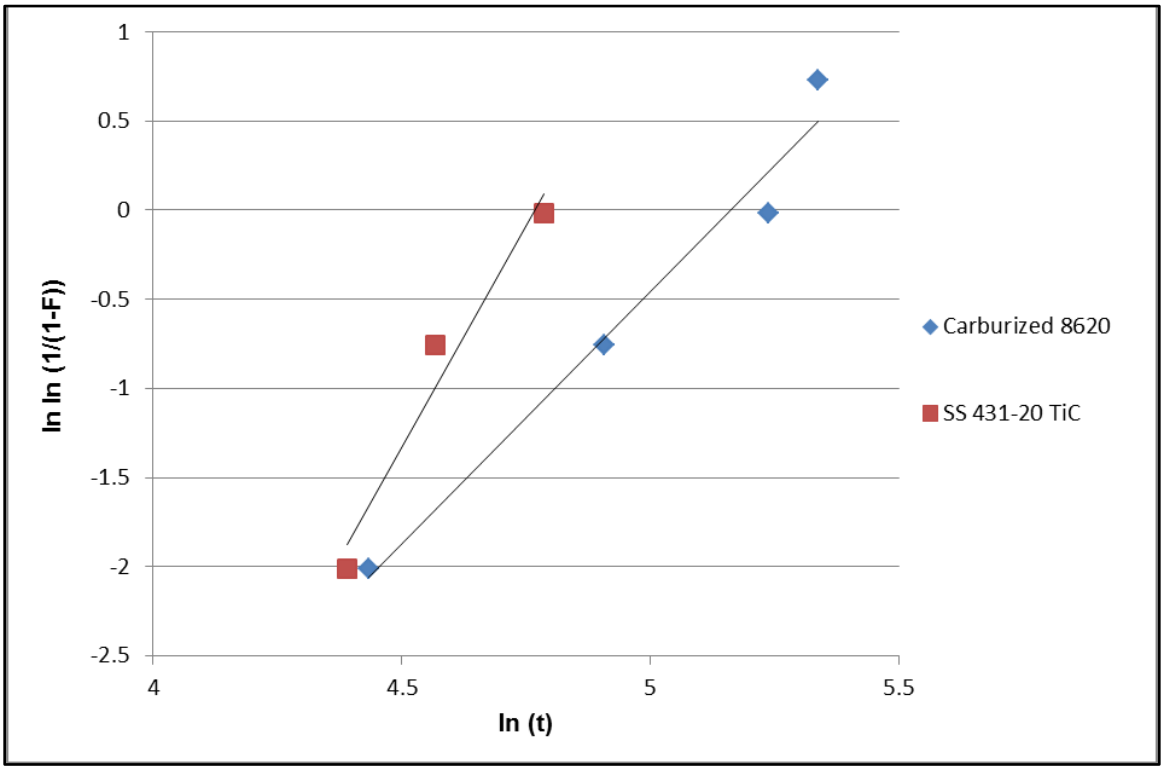

Figure 63 – Weibull plot of rolling contact fatigue life time for the carburized 8620 steel and laser deposited SS 431/20 TiC.

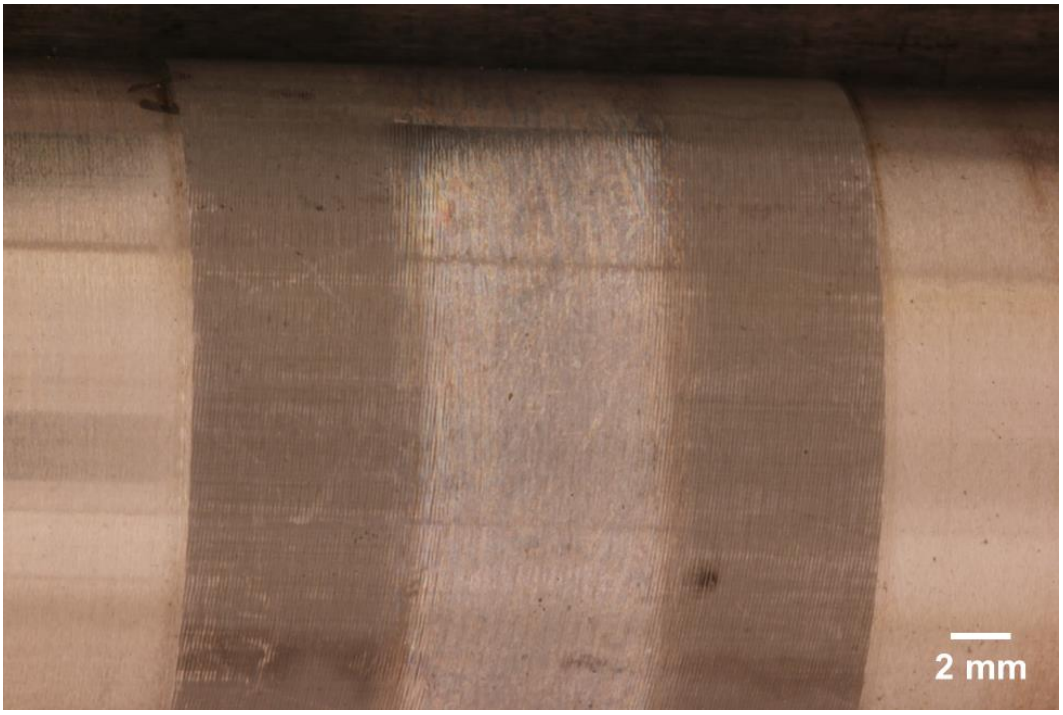

Figure 64 – RCF results of the carburized 8620 steel specimen without scuffing surface.

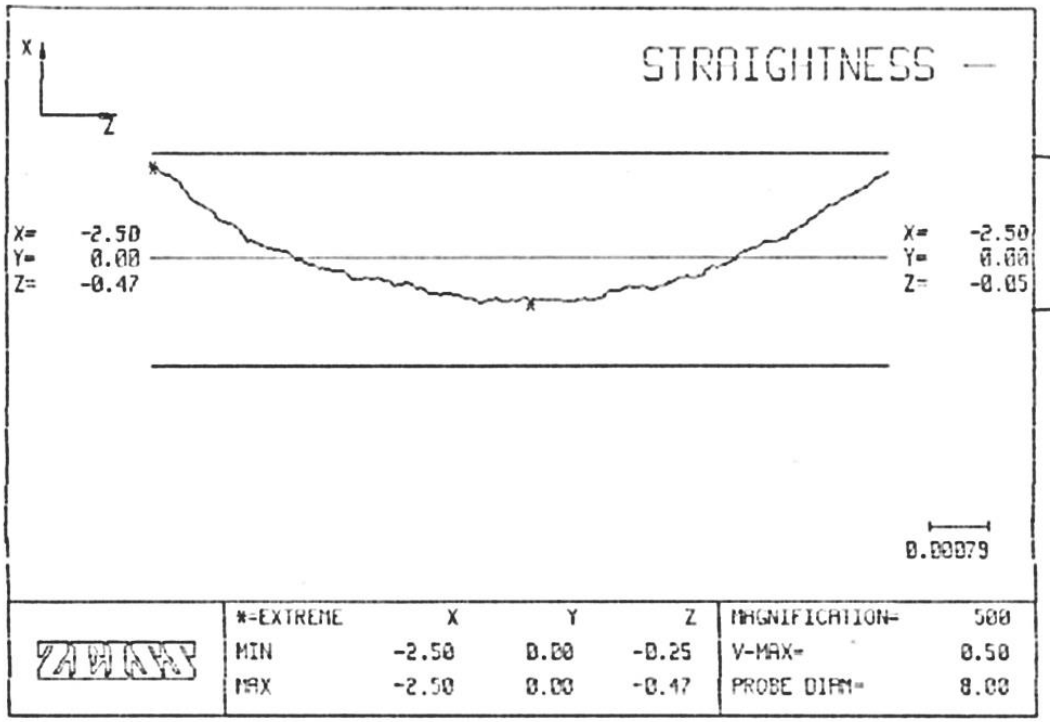

Figure 65 – Tribology analysis results of carburized 8620 steel roller before RCF testing.

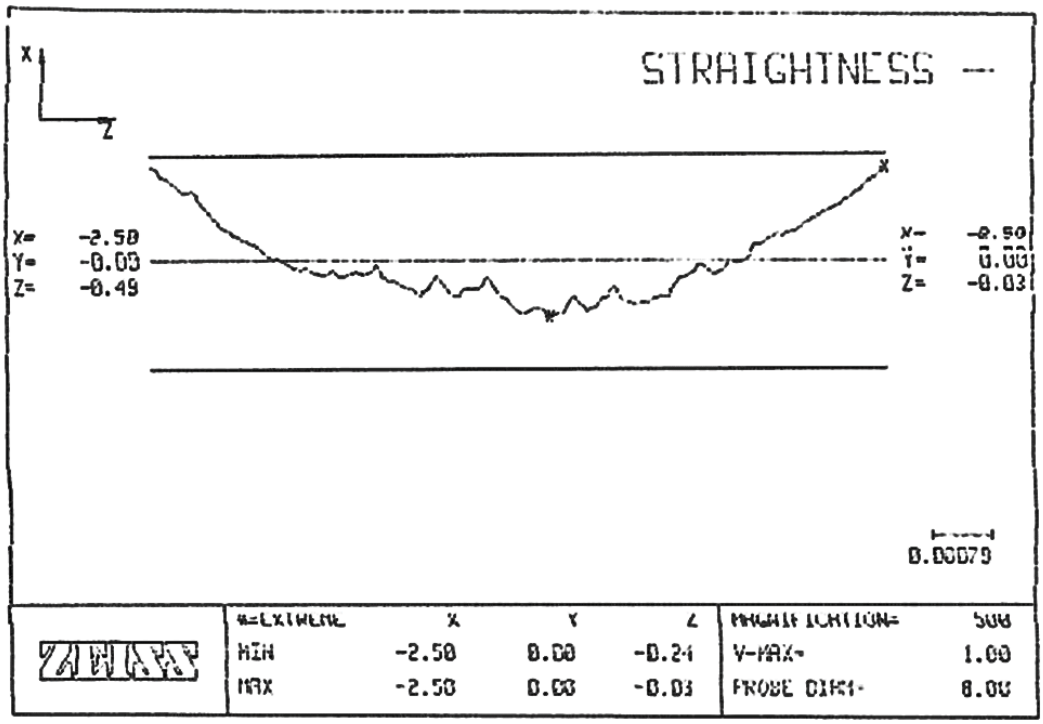

Figure 66 – Tribology analysis results of carburized 8620 steel roller after RCF testing.

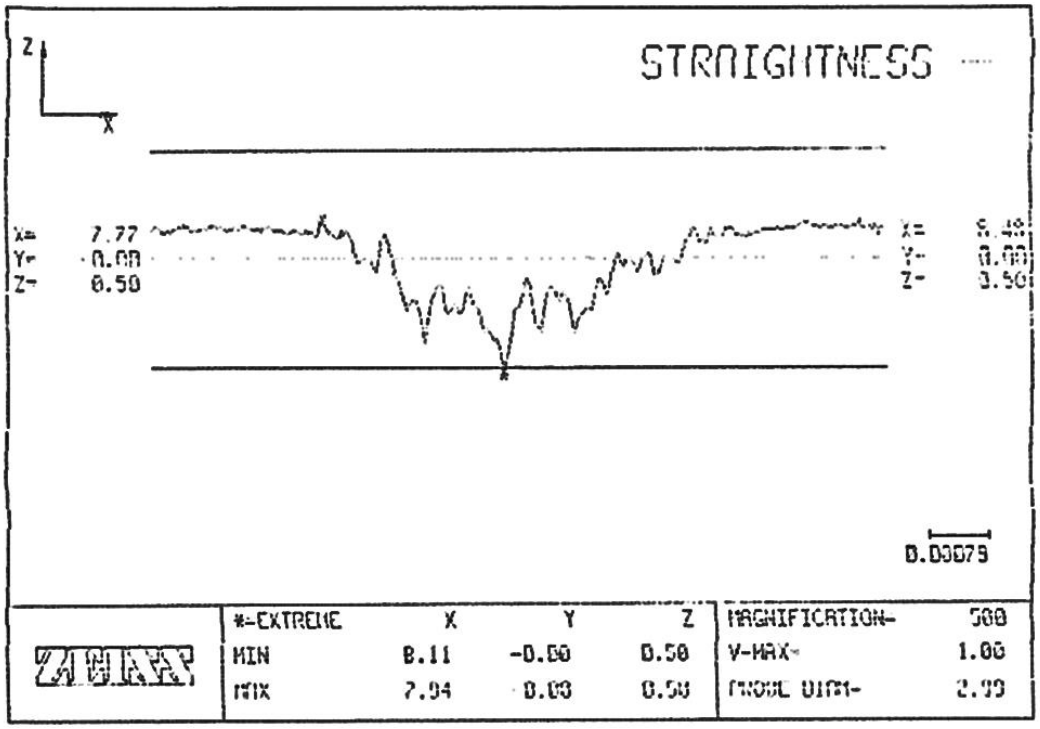

Figure 67 – Tribology analysis results of SS 431/20 TiC deposit material after RCF testing.

11.5 T700 Power Shaft Assembly

The technical data for the T700 power shaft assembly can be found in DMWR 1-2840-248, shown in Figure 68. The material is composed of Inconel 718®, and the faults found upon initial evaluation were bumper land heat discoloration, bumper land rubs, fretting, and wear on Dia G, K, and bumper lands. The cost of each part is $16,677 each and the objectives for the program were to replace the chrome plating repair, and lower the repair cost and TAT.

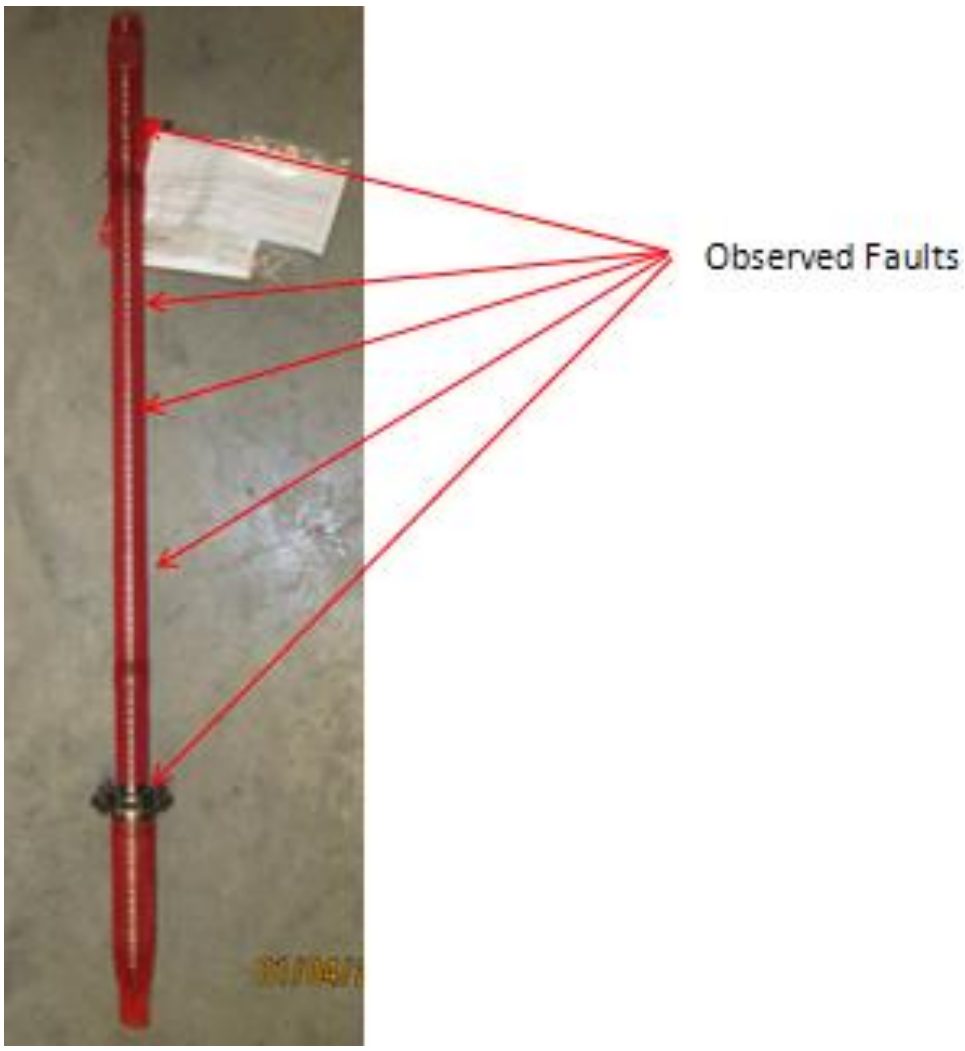

Figure 68 – T700 power shaft assembly initial faults.

The production for Inconel 718® specimens are shown in Figure 69. The Inconel 718® turbine shaft was laser deposited with powder materials of Inconel 718®, SS 431, SS 431/20 TiC, and SS 431/40TiC. The process parameters that were utilized were the same parameters that were developed during process development. The powder flow rate was adjusted base on material densities, which provided the same volumetric flow rate of material at 1.0 cm^3/min. The four laser deposited samples were roller ground to match the surface finish requirement at Quala-Die, Inc., Figure 70 shows the finished samples.

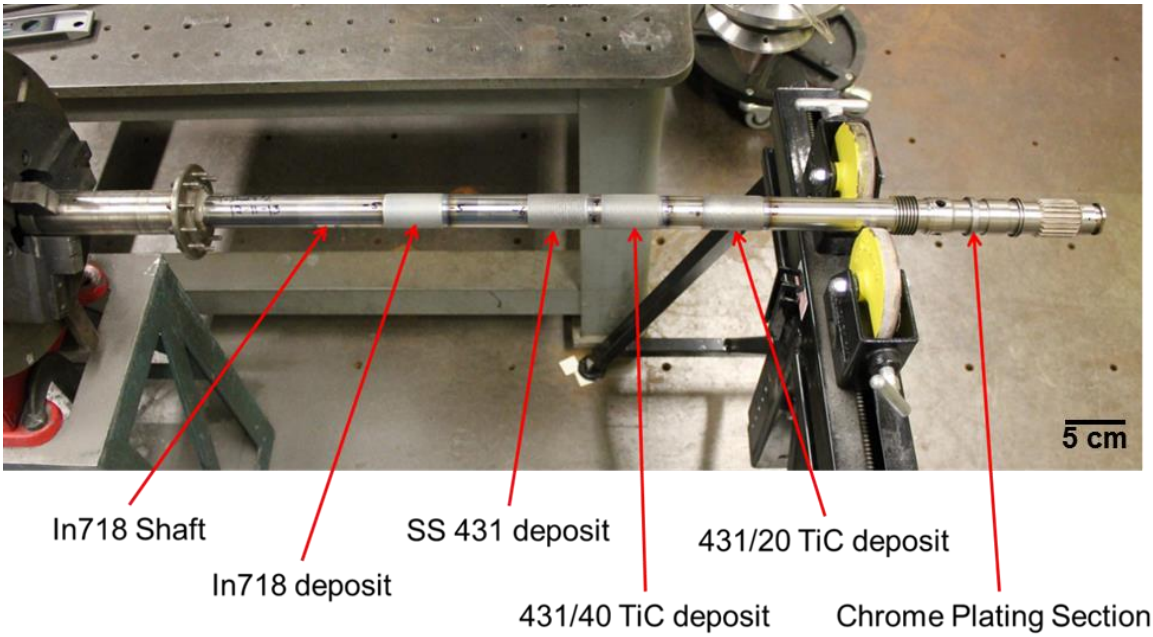

Figure 69 – Inconel power shaft showing laser deposition with selected materials.

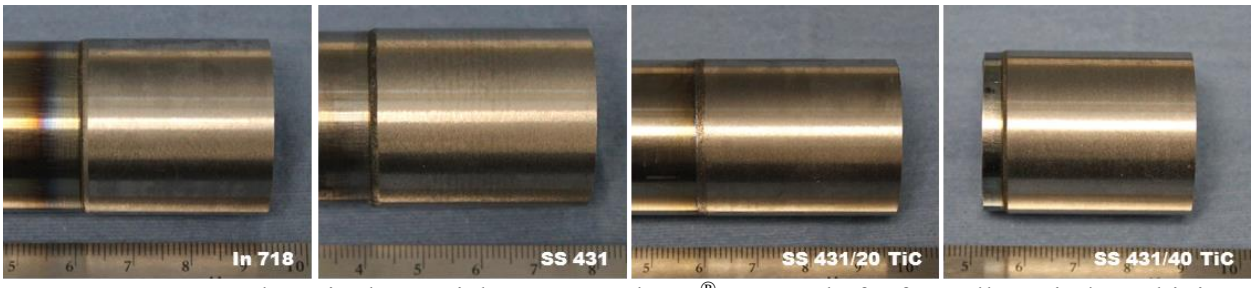

Figure 70 – Laser deposited materials on Inconel 718® power shaft after roller grind machining (scale in cm).

The chrome plated section, shown in Figure 71, gives the T700 Power Shaft increased hardness at that end. The average Vickers hardness measurement for the chrome plated section was 743 HV. Figure 70 also shows the chrome plated section of the shaft, a micrograph of the chromium electroplating on the Inconel 718® substrate, and the interface between the chromium and Inconel 718® substrate. Figure 72 shows the metallurgical analysis of the deposition material for the Inconel 718® power shaft.

The micro hardness profiles for the deposition materials and the substrate for the Inconel 718® shaft are shown in Figure 73, and the surface hardness of the samples are shown in Table 25. The original Inconel 718® shaft had an average hardness at 442 HV, and the chromium electroplated surface of the shaft had a hardness of 711 HV. All of the deposited materials on Inconel 718® exhibited lower hardness of 400 HV than the chromium electroplated surface. It is believed that dilution of the nickel base material into the deposit was responsible for the lower hardness values. Reducing heat input during the deposition process could possibly minimize the dilution and SS 431 and/or SS 431 with TiC, which could result in higher concentration of the deposition material chemistry and increased hardness for multiple layers.

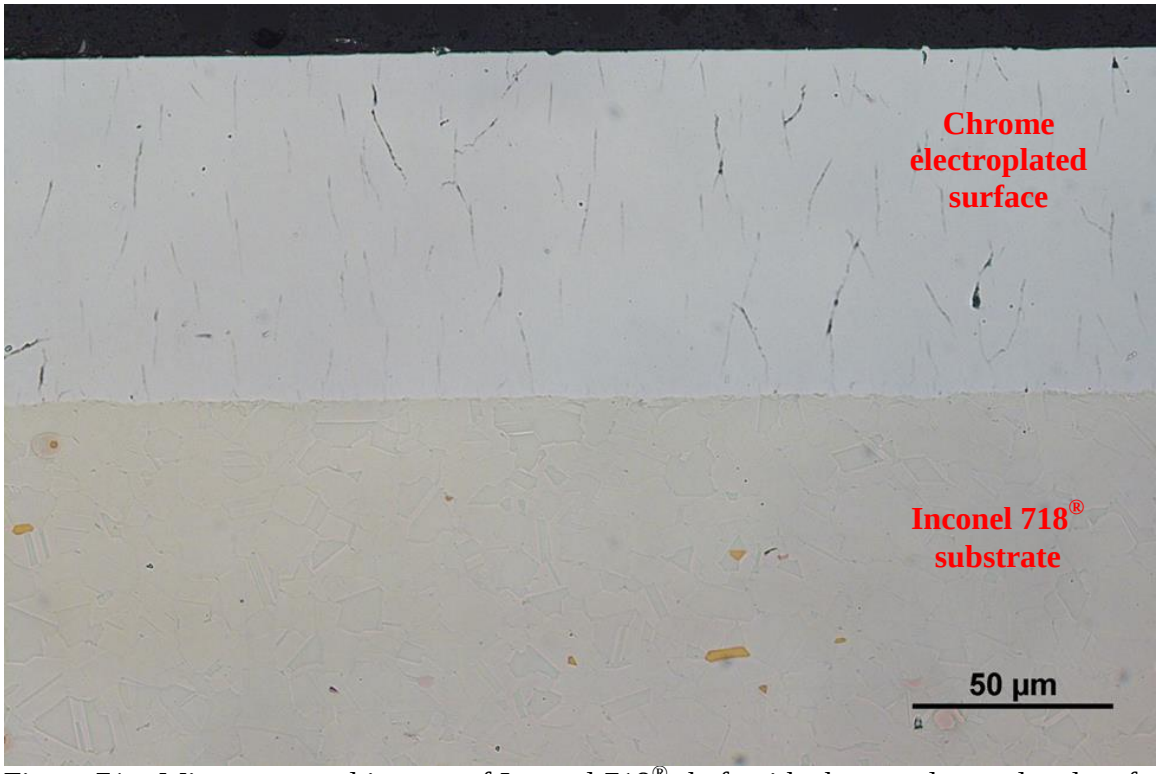

Figure 71 – Microstructural images of Inconel 718® shaft with chrome electroplated surface.

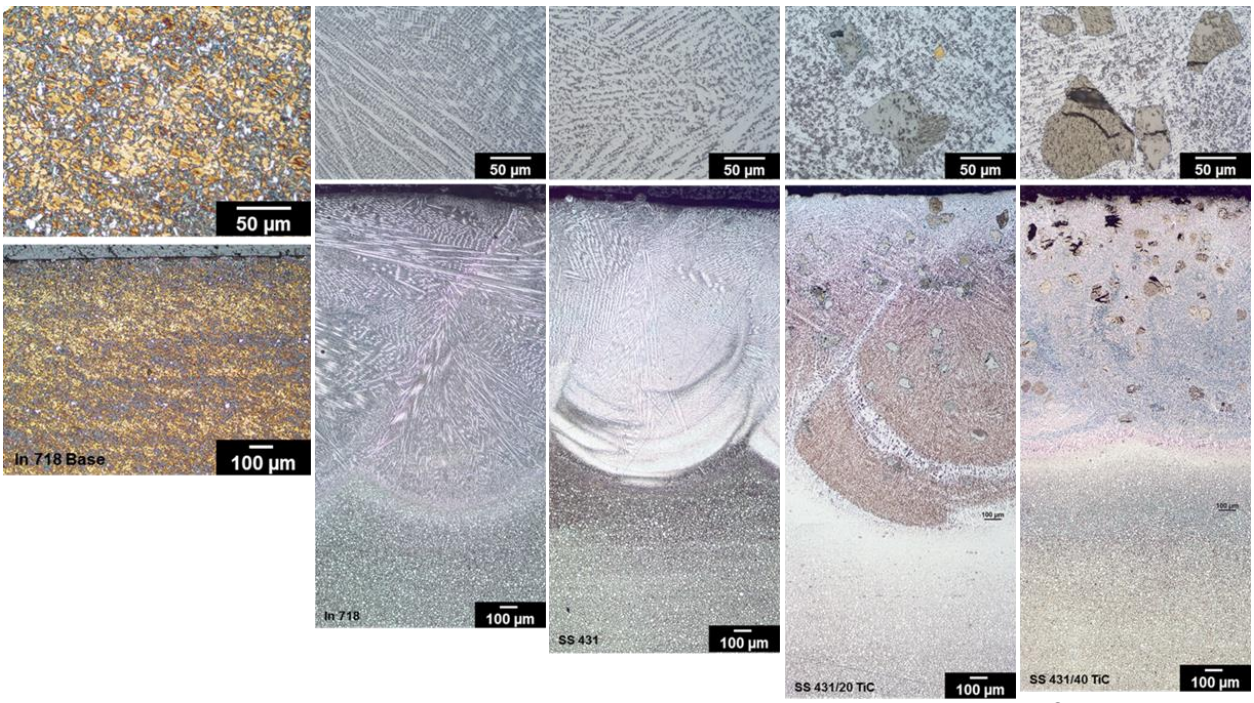

Figure 72 – Metallurgical analysis of the deposition material for the Inconel 718® power shaft.

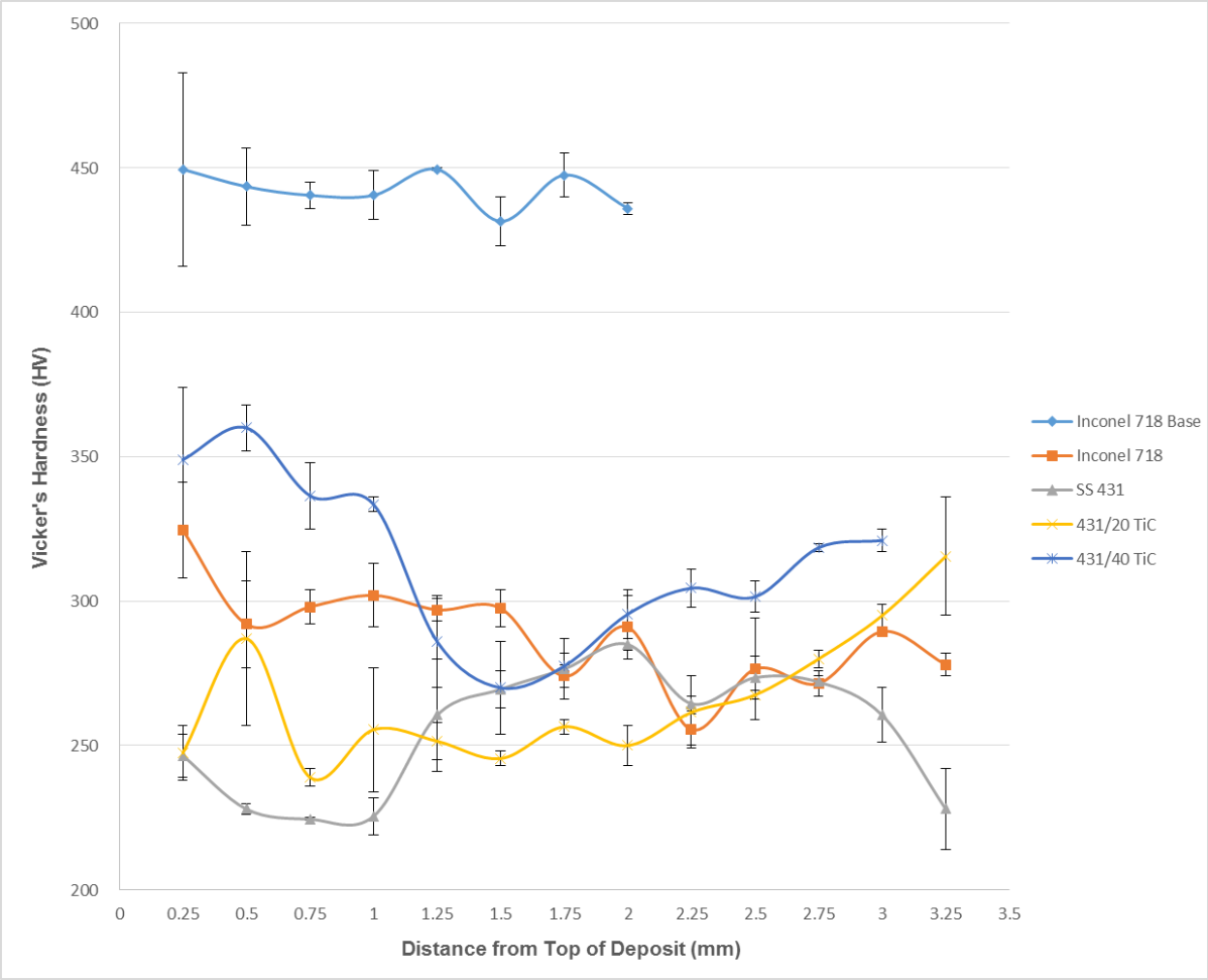

Figure 73 – Hardness of Inconel 718® shaft with deposited materials.

Table 25 – Micro hardnesses of Inconel 718® shaft with deposition materials.

	Inconel 718® Shaft	Inconel 718® Deposit	SS 431 Deposit	SS 431/20 TiC Deposit	SS 431/40 TiC Deposit	Chrome Electroplated
Average Vickers Hardness	442	304	231	257	345	711
Standard Deviation	6.07	12.29	8.97	18.14	10.55	21.47

11.6 Tribology Analysis

A Zygo NewView 7300 optical profilometer at the Materials Characterization Laboratory was used for measuring surface roughness. Zygo optical profilometer is a non - contact profilometer which measures light reflection from the surface of the test samples. A beam from the instrument is split into two paths by a beam splitter. One path lights onto the sample surface, and the other lights to a reference mirror. Reflections from both paths of light projected onto a detector. The different wavelengths of light occur due to height variances from the test sample and reference surfaces. The software package, MetroPro, measures the height difference from bright and dark bands, and generates a surface measurement 3D map along with surface roughness measurement. [26,27] The complete results of the tribology analysis results which generated by Metro are included in Appendix E.

The surface roughness was measured with both the carburized 8620 steel RCF specimen and the laser deposited SS 431/20 TiC RCF specimen. Measurement was also conducted on the Inconel 718® shaft and the four materials that had been laser deposited onto the shaft: Inconel 718®, SS 431, SS 431/20 TiC, and SS 431/40TiC.

The results of the surface roughness measurements on the carburized 8620 steel RCF specimen and the laser deposited SS 431/20 TiC RCF specimen are shown in Table 26. Individual surface roughness maps are also shown in Figures 74 to 76. The roughness measurements showed the surface of the SS 431/20 TiC deposit could meet the smoothness requirement dictated by the application for a bearing surface. However, Figure 76 represents a portion of the surface area of the SS 431/20 TiC deposit that exhibits pores on the surface, with resulted in a slightly rougher surface than the results from Figure 75. The microstructural SEM image representing the cross-section is shown in Figures 77 and 78. Both microstructure and SEM images show the pores may be related to ejection of the original TiC particles. This is believed to be caused by removal of the TiC particles during yielding of the adjacent matrix material during cyclic loading of the roller grinding process. The morphology of the TiC particles could contribute to the uneven surface on the SS 431/20 TiC deposit and the surface scuffing during RCF testing.

The Inconel 718® shaft and the four different laser deposited materials on the Inconel 718® shaft were also analyzed using the Zygo optical profilometer for surface roughness. The results for Inconel 718® samples are shown in Table 27, individual surface roughness maps are also shown in Figures 79 to 83. The Ra values for all of the deposit materials are larger than that defined for the application. The results also indicated a much rougher surface was produced with the deposited materials than the carburized 8620 steel. This data are shown in Table 20. It is believed that the surface roughness obtained after machining was related to the hardness of materials. The softer materials were more easily scratched by small particles that were removed during machining and resulted in a rougher surface finish. The hardness of the Inconel 718® and the deposited materials on the Inconel 718® shaft were much softer than the carburized 8620 steel and the SS 431/20 TiC deposited on the carburized 8620 steel. The comparison of surface roughness with the respected hardness results are shown in Table 25. This data shows a correlation between higher hardness and lower Ra value, or a smoother surface.

Table 26 – Surface roughness of the RCF test specimens.

	Baseline Carburized 8620 Steel	SS 431/20 TiC on Carburized 8620 Steel	SS 431/20 TiC on Carburized 8620 Steel (with defects)
Avg. Ra (μm)	0.848	0.171	0.193
Areal Ra (μm)	0.856	0.183	0.193

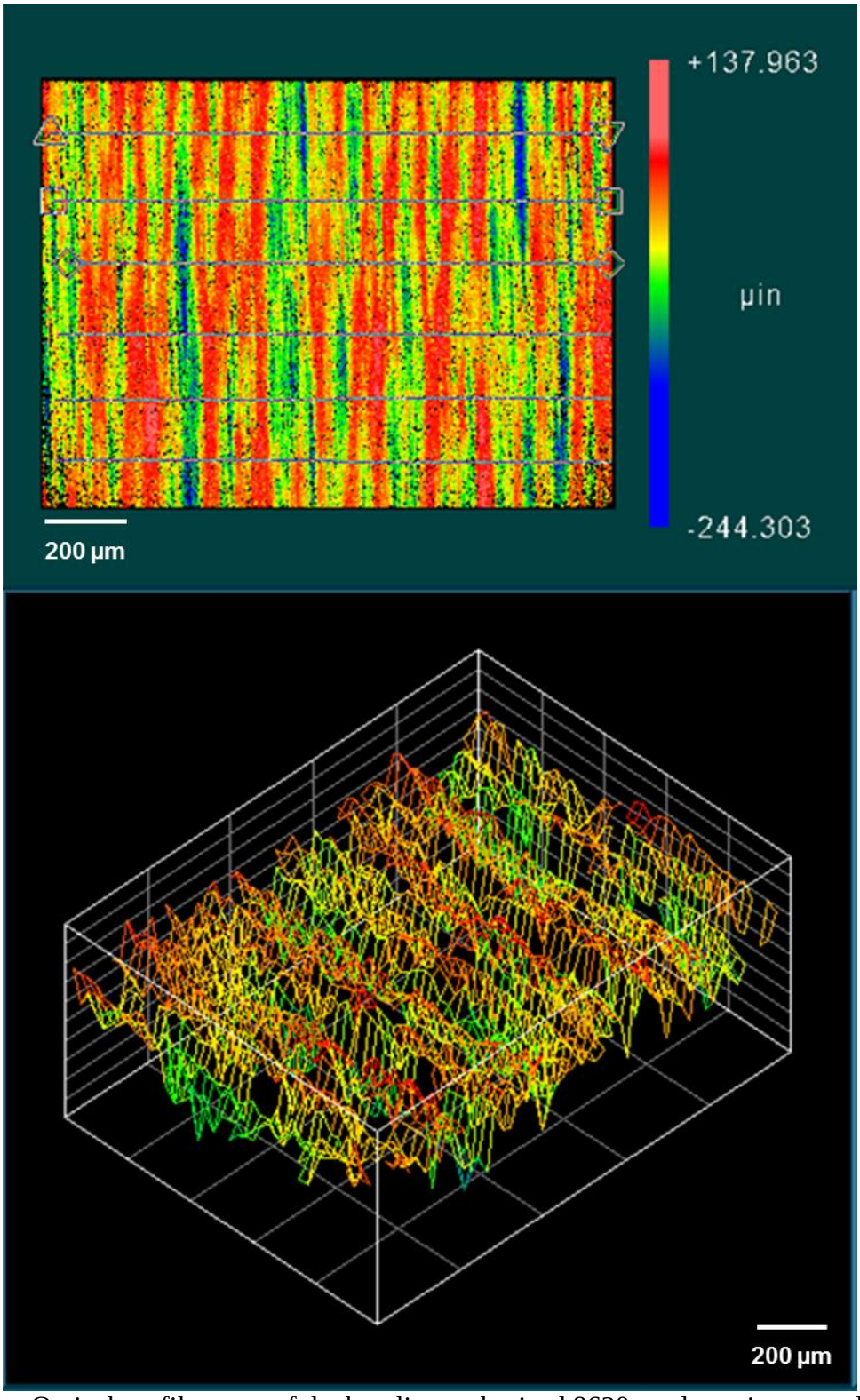

Figure 74 – Optical profilometry of the baseline carburized 8620 steel specimen used in the RCF test.

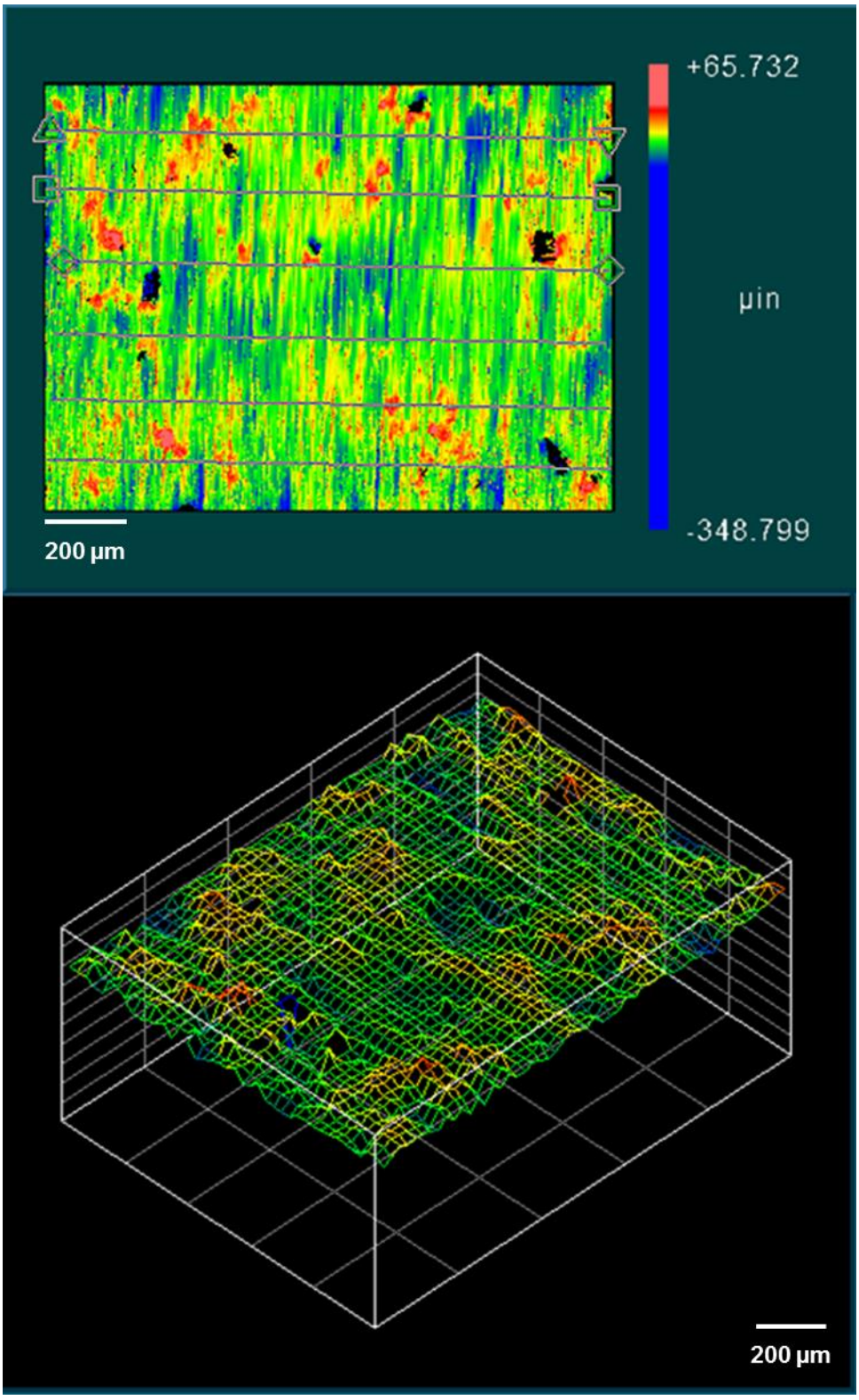

Figure 75 – Optical profilometry of the SS 431/20 TiC RCF test specimen, at the surface without defects.

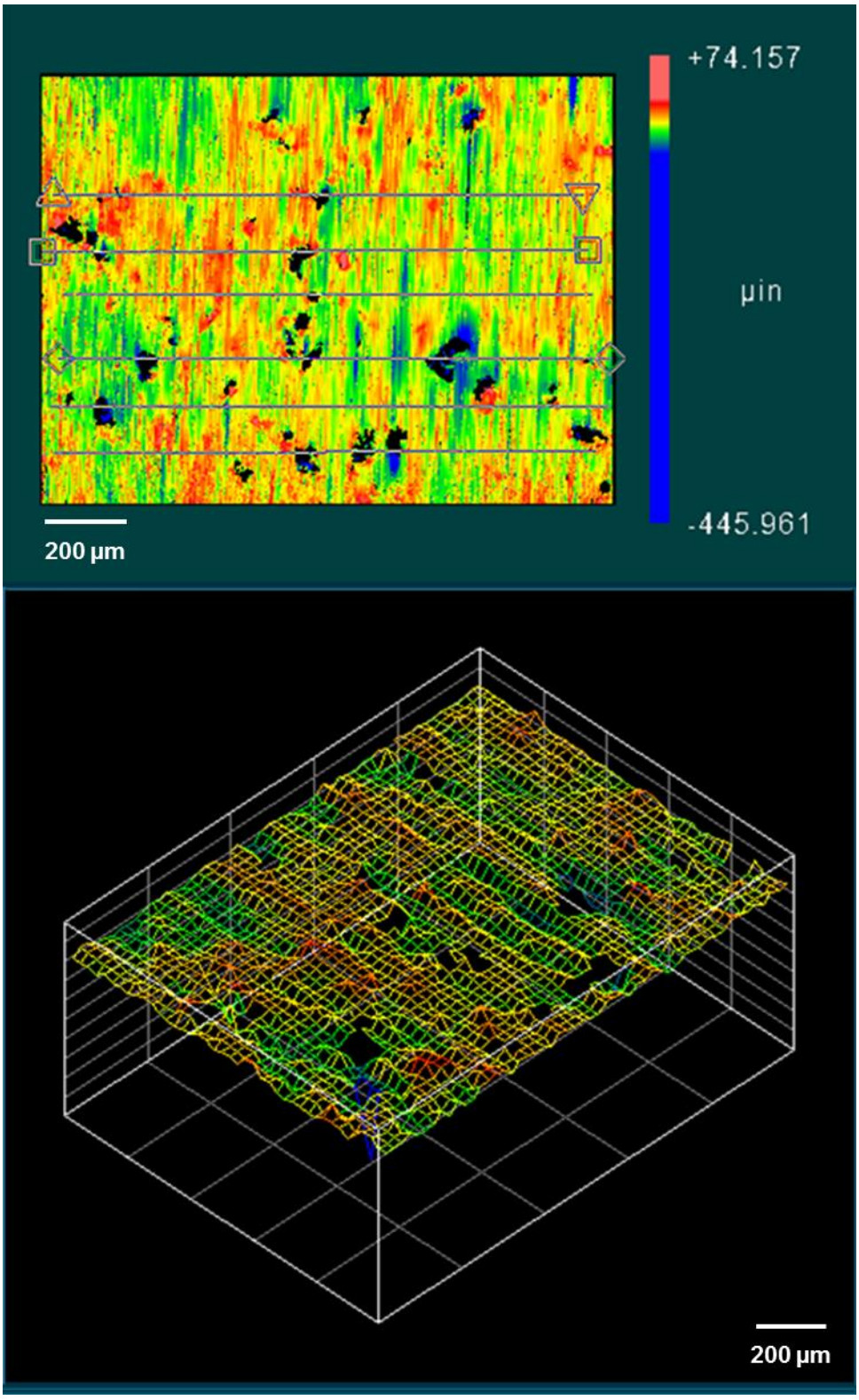

Figure 76 – Optical profilometry of the SS 431/20 TiC RCF test specimen, at the surface with defects.

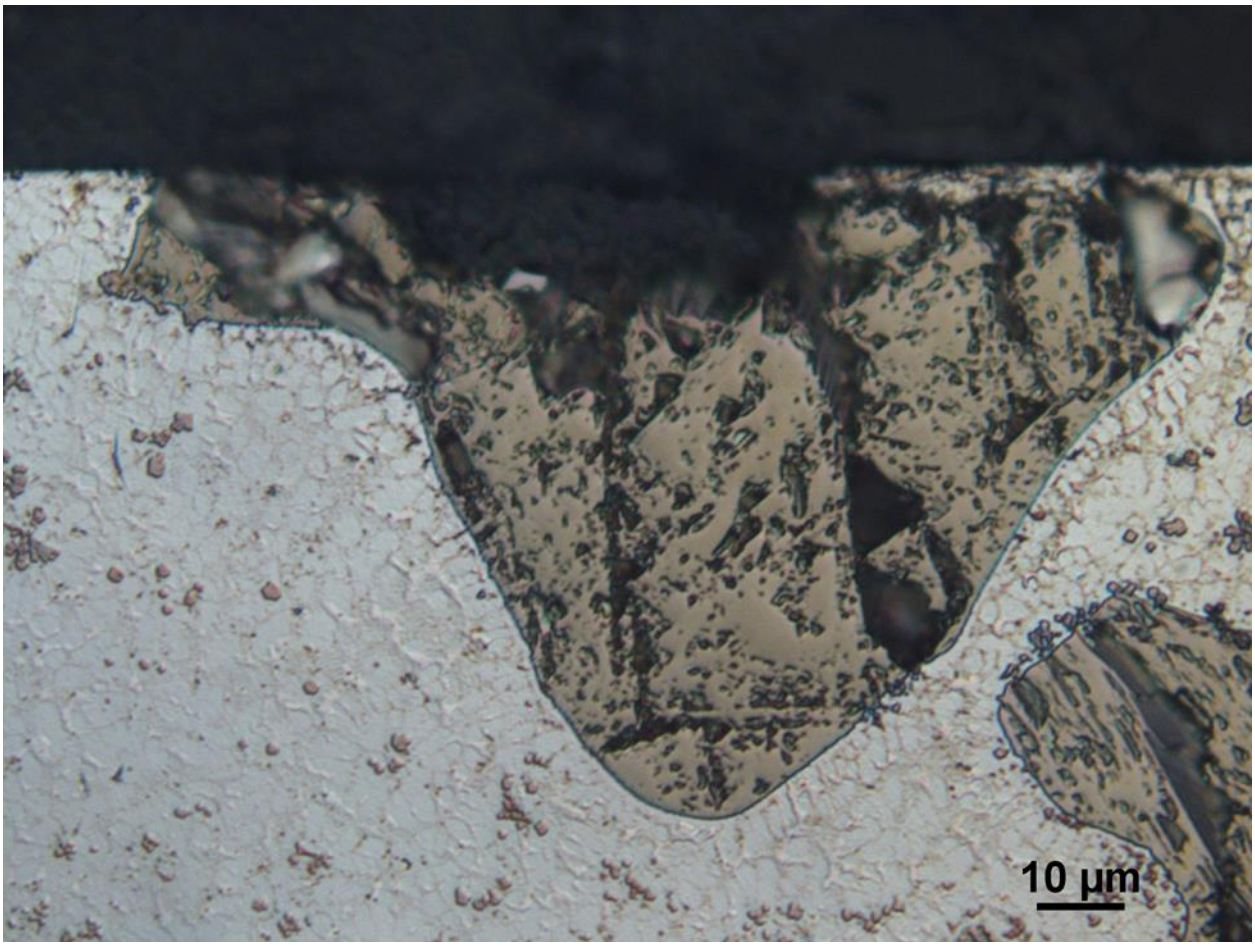

Figure 77 – Microstructural image showing the voids on the surface of RCF specimen.

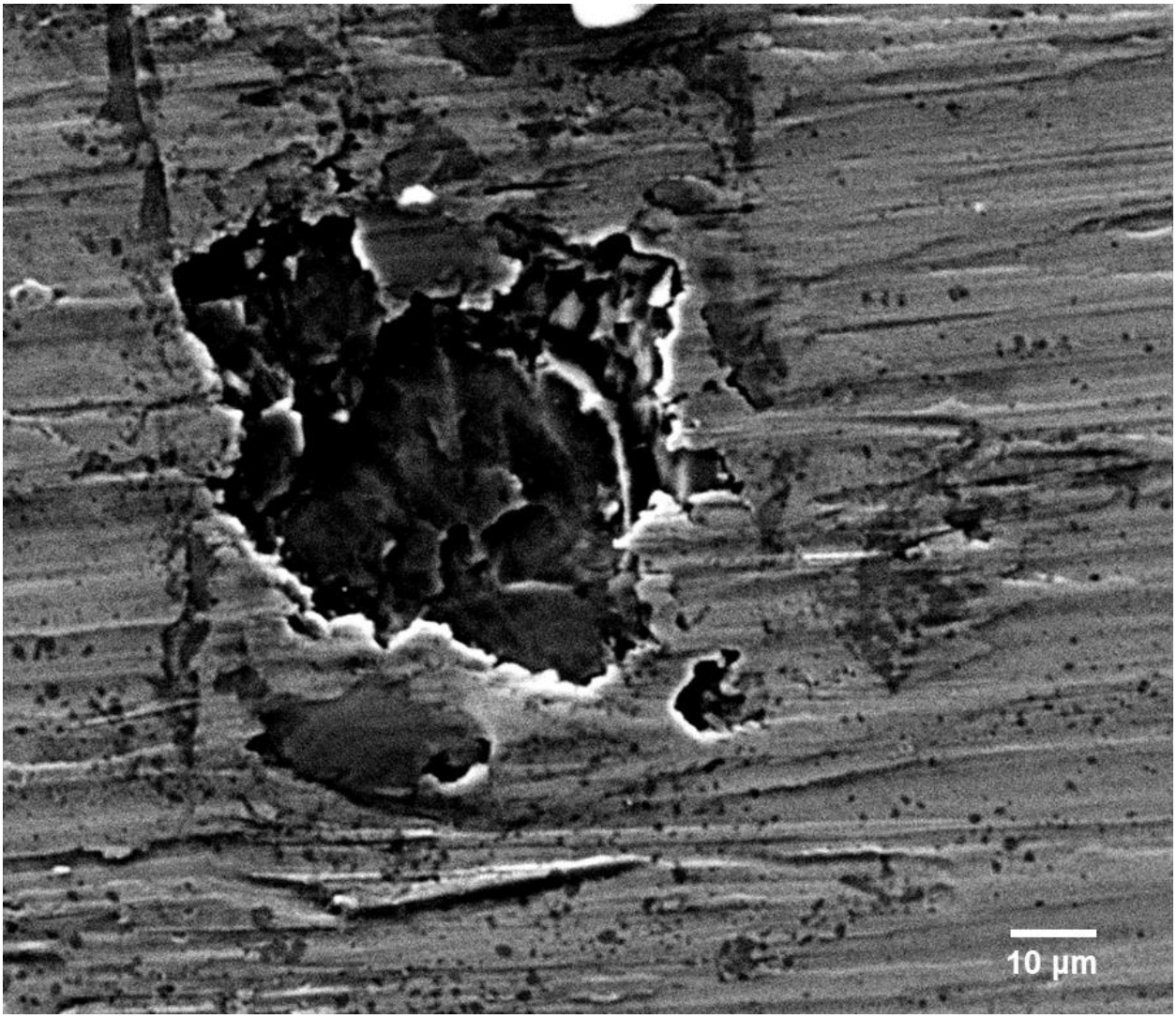

Figure 78 – SEM image shows the voids on the surface of RCF specimen.

Table 27 – Surface roughness of baseline material and laser deposited materials for power shaft.

	Baseline Inconel 718®	Inconel 718® on Inconel 718®	SS 431 on Inconel 718®	SS 431/20 TiC on Inconel 718®	SS 431/40 TiC on Inconel 718®
Avg. Ra (µm.)	0.833	0.889	1.46	1.12	0.843
Areal Ra (µm.)	0.965	0.912	1.46	1.12	0.841

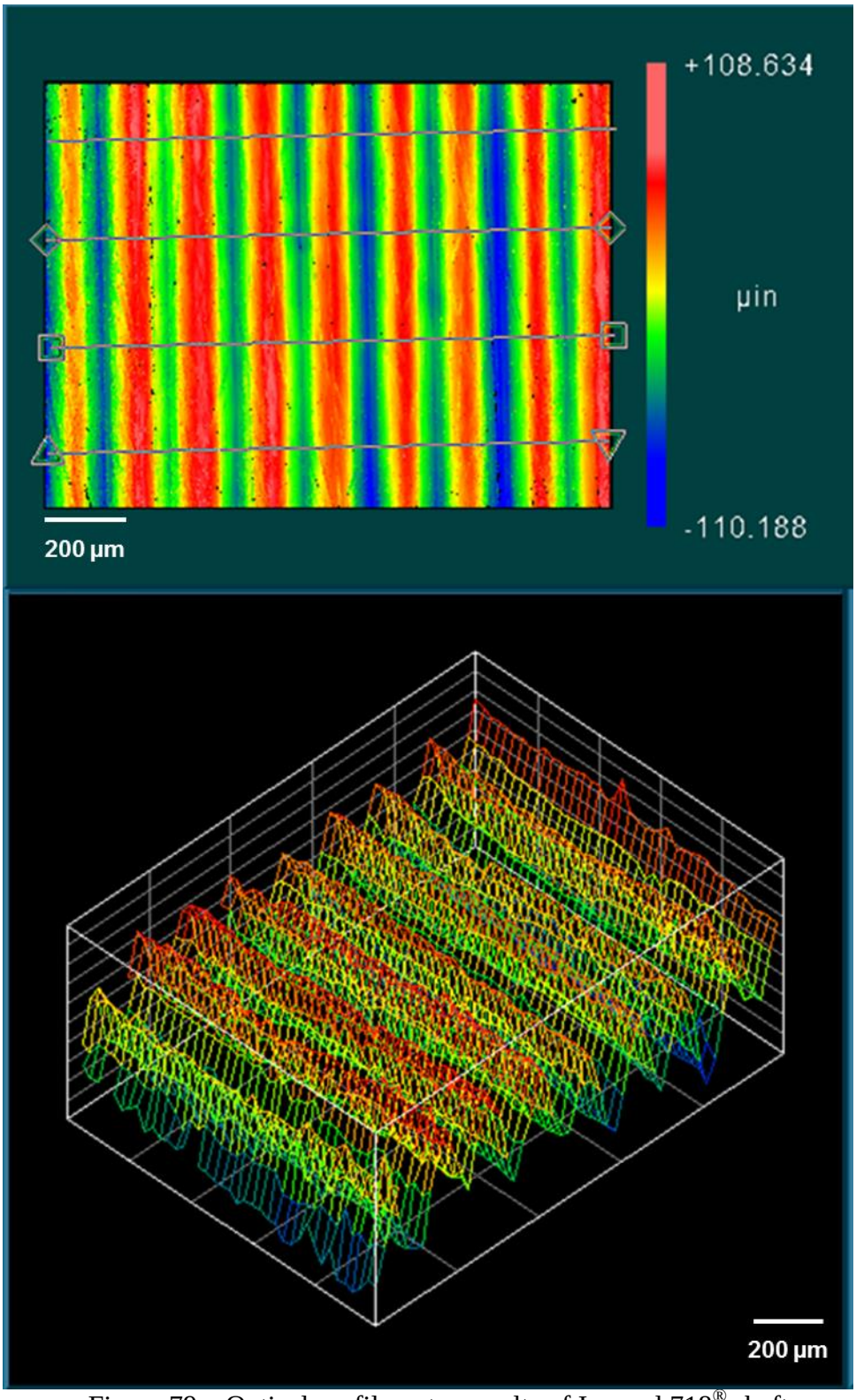

Figure 79 – Optical profilometry results of Inconel 718® shaft.

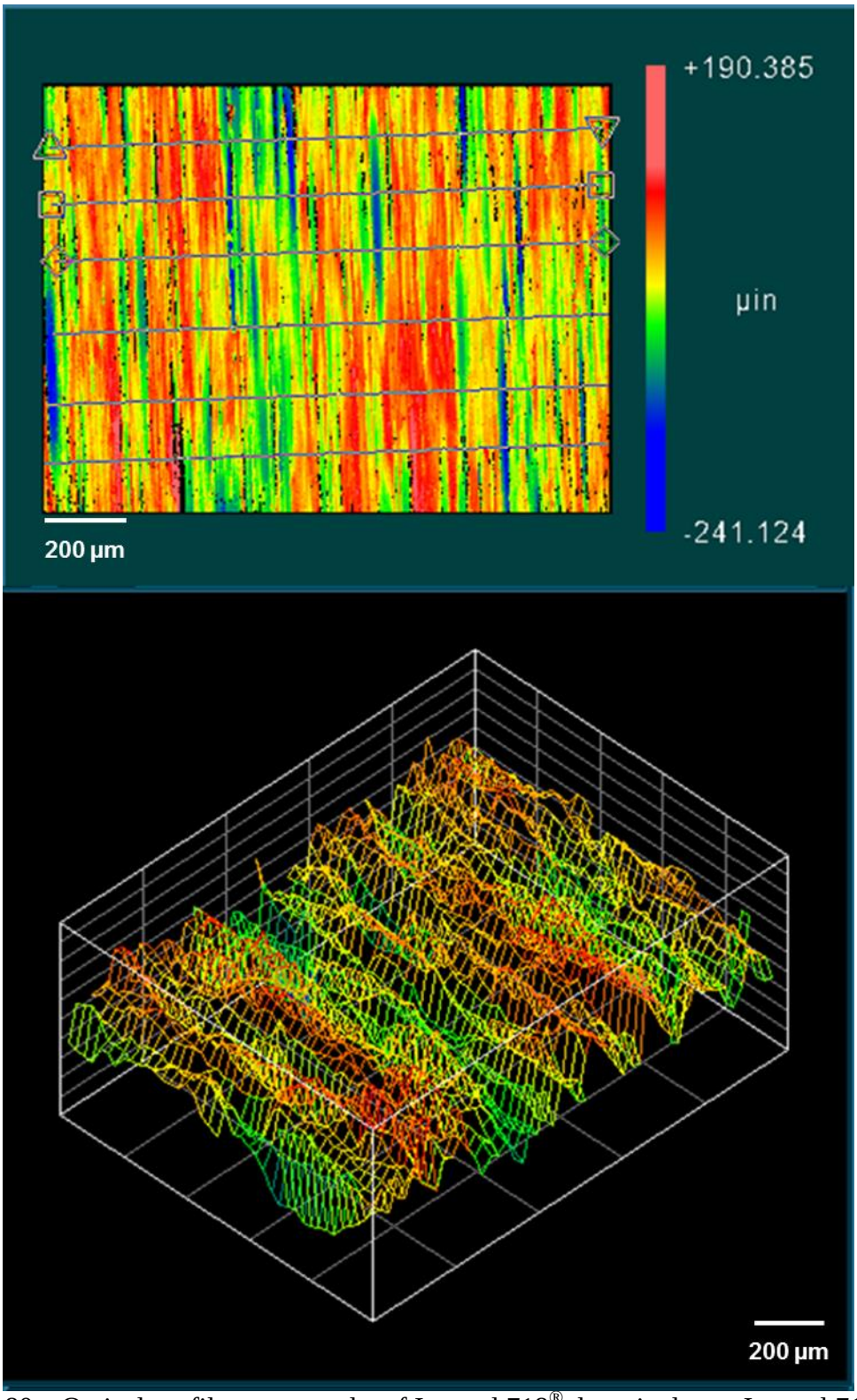

Figure 80 – Optical profilometry results of Inconel 718® deposited onto Inconel 718® shaft.

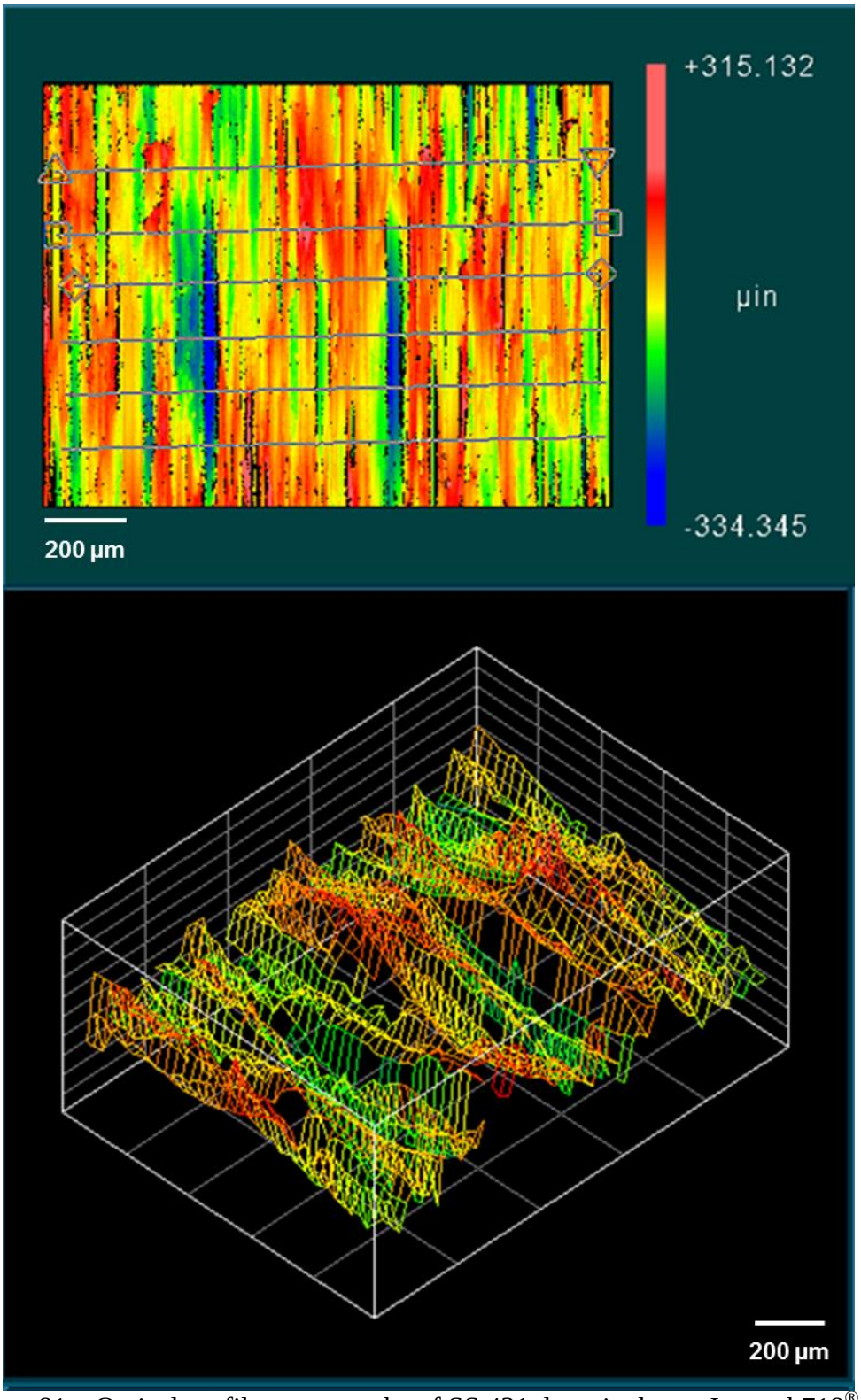

Figure 81 – Optical profilometry results of SS 431 deposited onto Inconel 718® shaft.

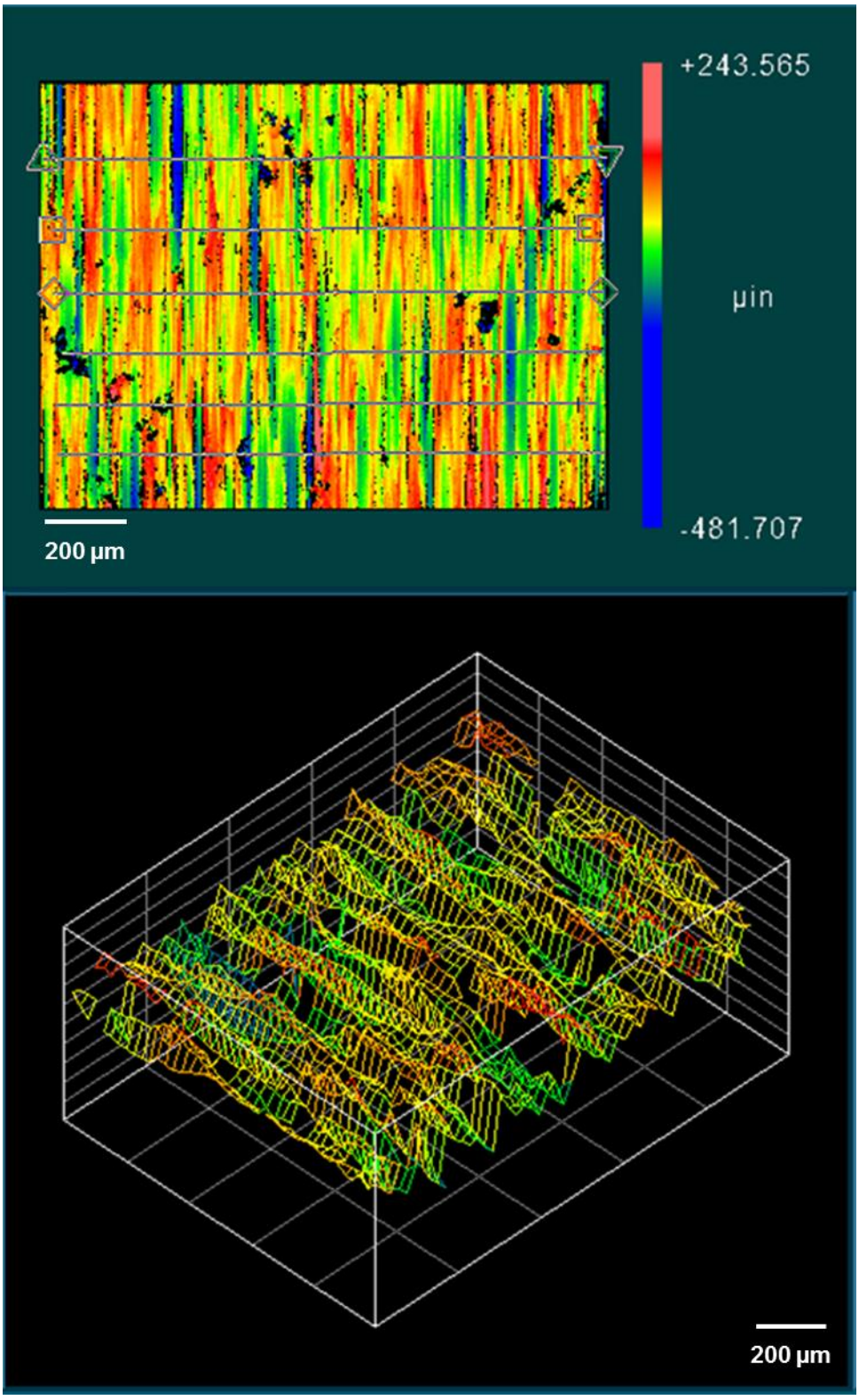

Figure 82 – Optical profilometry results of SS 431/20 TiC deposited onto Inconel 718® shaft.

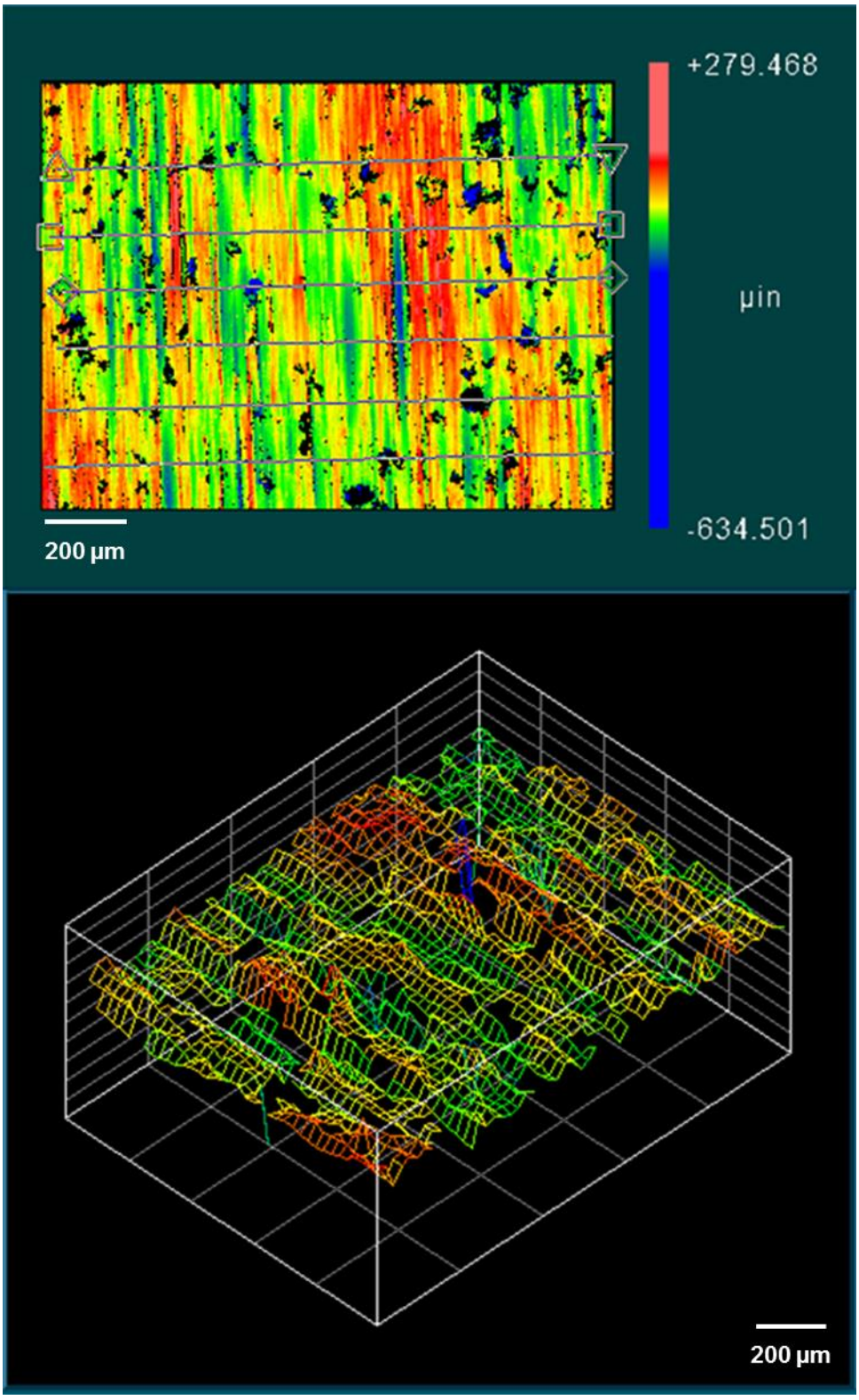

Figure 83 – Optical profilometry results of SS 431/40 TiC deposited onto Inconel 718® shaft.

12. SUMMARY OF KEY FINDINGS

Laser deposition processes for repairing components representing Ti-6Al-4V alloy, 8620 steel having a carburized surface, and Inconel 718® having chromium electroplated surface were evaluated. The objective was to establish processing parameters and deposition materials that could emulate the characteristics of the various surfaces for use as a repair process. Actual parts representing engine drive train components were utilized for these evaluations, and the areas for repair primarily represented bearing surfaces. Evaluations were conducted with deposition materials representing Inconel 718®, martensitic SS 431, and martensitic SS 431 with TiC to form a metal matrix composite system. All deposition materials were used in powder form, and the evaluations included detailed characterization of the deposits produced from these materials on Ti-6Al-4V, 8620 steel, and Inconel 718®. The conclusions that may be drawn from this research are shown below.

- A laser-based repair process was developed for repairing a Ti-6Al-4V cooling fan shaft using Ti-6Al-4V alloy for deposition. The process was able to produce a high quality repair surface having hardness slightly higher than the original material. The hardness of the laser deposit was measured to be 380 VHN; whereas, the hardness of the original material was 300 VHN. The slightly higher hardness of the deposit was attributed to the formation of α', a martensitic structure, during rapid cooling. Dimensional measurements performed after the repair process showed no discernible distortion associated with the laser repair. There was very minor microporosity observed within the deposit, which were approximately 25 mm (0.001 inch) in diameter. The results of the evaluation indicated that the Ti-6Al-4V cooling fan shaft may be repaired using the laser deposition process, and a Depot Maintenance Work Requirement (DMWR) for the repair process was prepared. An economic analysis of the process also indicated that the laser-based repair process could be implemented at an approximate cost of $660 per shaft.

- Laser deposition of a SS 431-TiC composite material was successfully conducted for use in repairing carburized surfaces on 8620 steel and chromium electroplating surfaces on Inconel 718®. Evaluations were conducted with deposition materials representing Inconel 718®, martensitic SS 431, and SS 431 with TiC to form a metal matrix composite system. All materials were used in powder form, and the evaluations included detailed characterization of the deposits produced from these materials on 8620 steel or Inconel 718®.

- The use of the martensitic SS 431 with TiC as a powder blend for laser deposition was found to be applicable for the repair of 8620 carburized surfaces. Details results of this evaluation indicated:

    - microstructural analysis determined that the single layer deposition provided good deposition quality. However, multiple layer depositions with above 20 wt% of TiC concentration resulted in the generation of surface cracks. Microstructural analysis also indicated that the unmelted TiC particles tended to remain near the top of deposit surface due to buoyancy of the lower density of TiC particles when compared to the molten SS 431 melt pool,

- micro hardness testing of the laser deposits indicated that the deposition material provided higher hardness with increased TiC content in the SS 431 matrix. Results also showed that multiple layer deposition had higher hardness than single layer deposition due to decrease substrate dilution in the upper layer,

- micro hardness testing also indicated that the hardness of the SS 431/20 TiC deposited on the carburized 8620 steel matched the hardness of the carburized 8620 steel. Micro hardness of the deposited materials was found to be exhibit an area average Vickers hardness of 750 HV,

- laser deposition of a SS 431-20 TiC powder blend was evaluated using the rolling contact fatigue test, and the results of these tests indicated that the laser deposit exhibited slightly greater wear than the carburized surface under the same conditions,

- rolling contact fatigue testing of the composite SS 431/20 TiC deposit displayed significant surface scuffing. It is believed that this was due to the extremely high hardness of the unmelted TiC particles that were ejected from the surface of specimens, which began to wear the surface of the carburized steel roller,

- SEM images showed that some of the TiC particles dissolved and the Ti and C were reprecipitated in the SS 431 matrix. Chemical analysis by EDS further supported this conclusion, and

- surface roughness of specimens must have a Ra value less than 0.81 μm. Tribology analysis after roller grind machining indicated that surface roughness of the laser deposited SS 431/20 TiC composite can be achieved with Ra = 0.19 μm.

- Inconel 718® powder, martensitic-grade SS 431, and the martensitic SS powder blended with TiC were evaluated as deposition materials for use in repairing the surface of the Inconel 718® having a chromium electroplated surface. The results of this investigation were:

  - micro hardness testing found the chromium electroplated surface exhibited an average Vickers hardness of 700 HV. None of the selected deposition materials deposited on the Inconel 718® matched the hardness of the chromium electroplated surface. The hardnesses measured for these specimens were: Inconel 718® deposit HV_{ave} = 300, SS 431 deposit HV_{ave} = 230, SS 431/20 TiC deposit HV_{ave} = 260, and SS 431/20 TiC deposit HV_{ave} = 350, and

  - tribology analysis found the laser deposited materials on the Inconel 718® shaft have higher Ra value than 0.81 μm: Inconel 718® deposit Ra = 0.89, SS 431 deposit Ra = 1.46, SS 431/20 TiC deposit Ra = 1.12, and SS 431/20 TiC deposit Ra = 0.84.

13. RECOMMENDATIONS

- Conduct full qualification trials for laser-based deposition repair of the Ti-6Al-4V on the Ti-6Al-4V AH64 cooling fan shaft.
- Continue characterization of SS 431 with 20% (wt.) TiC deposits for use in repairing carburized surfaces. This should be conducted under direct comparison of the 8620 steel that had been carburized and the 8620 steel repaired using SS 431/20 TiC under rolling contact only.
- Evaluate low heat input laser repair of Inconel 718® components with potential alternate deposition materials. This should also include additional characterization upon successful identification of material and processing conditions that meet Inconel 718® and chromium electroplated hardness requirements.

REFERENCES

[1] Optomec, "Optomec Presents Final Report on LENS Phase II at 2006 CTMA Symposium in Williamsburg, Virginia," *http://www.optomec.com/site/archived_news/news9* 2006.

[2] S. J. Tuppen, P. E. Daum, M. J. Rawson, K. A. Lucas, W. J. Brindley, in Cost Effective Manufacture via Net-Shape Processing. (RTO, Neuilly-sur-Seine, France, 2006), vol. RTO-MP-AVT-139, pp. p. 2-1, 2-26.

[3] B. Slaughter. (Additive Manufacturing Consortium Kick-off Meeting, Edison Welding Institute, 2010).

[4] K. T. Slattery, paper presented at the 2nd SAlAS Symposium, Stellenbosch, South Africa, 14-16 September 2008.

[5] J. Franklin, paper presented at the American Helicopter Society 66th Annual Forum, Phoenix, Arizona, May 11 - 13 2010.

[6] E. Fodran. (Additive Manufacturing Consortium Kick-off Meeting, Edison Welding Institute, 2010).

[7] C. English. (Additive Manufacturing Consortium Kick-off Meeting, Edison Welding Institute, 2010).

[8] C. A. Brice. (Additive Manufacturing Consortium Kick-off Meeting, Edison Welding Institute, 2010).

[9] W. E. Frazier, *Advanced Materials and Processes* 166, 43 (2008).

[10] W. E. Frazier. (Solomons, Maryland, 2010).

[11] "Titanium Alloy Direct Deposited Products 6Al - 4V Annealed" Tech. Report No. AMS 4999A (SAE International, 2010).

[12]"AISI 8620", Alloy Digest, Engineering Alloys Digest, Inc. Upper Montclair, New Jersey, ASM International (2002)

[13]"ASM Handbook Volume 9 - Metallography and Microstructures". Materials Park, Ohio: ASM International, p. 671 (2004).

[14] S. S. Kiparisov, V. K. Narva, S. Ya. Kolupaeva, "Dependence of the Properties of Titanium Carbide – Steel Materials Upon the Composition of the Titanium Carbide", Moscow Institute of Steel and Alloys. Translated from Poroshkovaya Metallurgiya, No. 7 (151), pp.41-44, (1975)

[15] J. R. Davis, "Nickel, cobalt, and their alloys", Materials Park, Ohio: ASM International, p. 33 (2000).

[16]"Allvac 718", Alloy Digest, Engineering Alloys Digest, Inc. Upper Montclair, New Jersey, ASM International (2002)

[17]"Allvac 718-HS 718-DA", Alloy Digest, Engineering Alloys Digest, Inc. Upper Montclair, New Jersey, ASM International (2006)

[18] R. Boyer, G. Welsch, and E. W. Collings, "Materials Properties Handbook: Titanium Alloys", ASM International, Materials Park, OH (1994)

[19] R. P. Martukanitz, and S. S. Babu, "Development of Advanced Wear and Corrosion Resistant Systems through Laser Surface Modification and Materials Simulation", Final Report on Research Conducted Through a Cooperative Agreement under Instrument Number DE-FC07-02ID14247, Department of Energy Report (2003)

[20] M. Hillert, "Phase Equilibria, Phase Diagrams and Phase Transformations – Their Thermodynamic Basis", 2nd edition, Cambridge University Press (2008)

[21] D. R. McPherson and S. B. Rao, "Mechanical Testing of Gears, Mechanical Testing and Evaluation", Vol 8, ASM Handbook, ASM International (2000)

[22] D. R. McPherson, "The Effect of Lubricant Viscosity, Surface Roughness, and Rolling and Sliding Velocities on EHD Film Thickness and Pitting Fatigue", Gear Research Institute at PSU-ARL (2002)

[23] F. Lia, S. Kelly, R. P. Martukanitz. "Evaluation and Characterization of Materials and Processing Conditions for Establishing a Laser-Based Repair Process for Aerospace Gears". A Thesis in Department of Material Science and Engineering at Pennsylvanian State University. (2012)

[24]"ASTM E384 – 11", West Conshohocken, PA: ASM International (2012)

[25]"ASTM E140 – 12b", West Conshohocken, PA: ASM International (2013)

[26] D. Balasenthil, "ME-255: Principles of Tribology - Surface Properties - Measurement Techniques Profilometer", Dept. of Mechanical Engineering, IISc

[27] M. Visscher, C. P. Hendriks, K. G. Struik, "Optical profilometry and its application to mechanically inaccessible surfaces Part II: Application to elastomer/glass contacts", Precision Engineering, Vol. 16 No 3 (1994)

ACKNOWLEDGEMENTS

The Applied Research Laboratory, the Pennsylvania State University, would like to acknowledge the following organizations and individuals in assisting and supporting the execution of these activities:

ARDEC Benet Laboratories:

- Eric Brown

Corpus Christi Army Depot:

- Mark Velazquez

AMRDEC Aviation Engineering Directorate - Huntsville:

- Ben Plummer
- James Metzger

Genesis Engineering Activities:

- Stan Spielvogel
- Rich Huber

CIMP-3D Activities:

- Ken Meinert
- Abdalla Nassar
- Jay Tressler
- Aaron Isaacson
- Fred Lia
- Matt Osborn (summer intern from UTEP)

APPENDIX A – HARDNESS CONVERSION CHART

TABLE 1 Approximate Hardness Conversion Numbers for Non-Austenitic Steels (Rockwell C Hardness Range)[A, B]

Rockwell C Hardness Number 150 kgf (HRC)	Vickers Hardness Number (HV)	Brinell Hardness Number[C]		Knoop Hardness, Number 500-gf and Over (HK)	Rockwell Hardness Number		Rockwell Superficial Hardness Number			Scleroscope Hardness Number[D]	Rockwell C Hardness Number 150 kgf (HRC)
		10-mm Standard Ball, 3000-kgf (HBS)	10-mm Carbide Ball, 3000-kgf (HBW)		A Scale, 60-kgf (HRA)	D Scale, 100-kgf (HRD)	15-N Scale, 15-kgf (HR 15-N)	30-N Scale, 30-kgf (HR 30-N)	45-N Scale, 45-kgf (HR 45-N)		
68	940	...	...	920	85.6	76.9	93.2	84.4	75.4	97.3	68
67	900	...	...	895	85.0	76.1	92.9	83.6	74.2	95.0	67
66	865	...	...	870	84.5	75.4	92.5	82.8	73.3	92.7	66
65	832	...	(739)	846	83.9	74.5	92.2	81.9	72.0	90.6	65
64	800	...	(722)	822	83.4	73.8	91.8	81.1	71.0	88.5	64
63	772	...	(705)	799	82.8	73.0	91.4	80.1	69.9	86.5	63
62	746	...	(688)	776	82.3	72.2	91.1	79.3	68.8	84.5	62
61	720	...	(670)	754	81.8	71.5	90.7	78.4	67.7	82.6	61
60	697	...	(654)	732	81.2	70.7	90.2	77.5	66.6	80.8	60
59	674	...	634	710	80.7	69.9	89.8	76.6	65.5	79.0	59
58	653	...	615	690	80.1	69.2	89.3	75.7	64.3	77.3	58
57	633	...	595	670	79.6	68.5	88.9	74.8	63.2	75.6	57
56	613	...	577	650	79.0	67.7	88.3	73.9	62.0	74.0	56
55	595	...	560	630	78.5	66.9	87.9	73.0	60.9	72.4	55
54	577	...	543	612	78.0	66.1	87.4	72.0	59.8	70.9	54
53	560	...	525	594	77.4	65.4	86.9	71.2	58.6	69.4	53
52	544	(500)	512	576	76.8	64.6	86.4	70.2	57.4	67.9	52
51	528	(487)	496	558	76.3	63.8	85.9	69.4	56.1	66.5	51
50	513	(475)	481	542	75.9	63.1	85.5	68.5	55.0	65.1	50
49	498	(464)	469	526	75.2	62.1	85.0	67.6	53.8	63.7	49
48	484	451	455	510	74.7	61.4	84.5	66.7	52.5	62.4	48
47	471	442	443	495	74.1	60.8	83.9	65.8	51.4	61.1	47
46	458	432	432	480	73.6	60.0	83.5	64.8	50.3	59.8	46
45	446	421	421	466	73.1	59.2	83.0	64.0	49.0	58.5	45
44	434	409	409	452	72.5	58.5	82.5	63.1	47.8	57.3	44
43	423	400	400	438	72.0	57.7	82.0	62.2	46.7	56.1	43
42	412	390	390	426	71.5	56.9	81.5	61.3	45.5	54.9	42
41	402	381	381	414	70.9	56.2	80.9	60.4	44.3	53.7	41
40	392	371	371	402	70.4	55.4	80.4	59.5	43.1	52.6	40
39	382	362	362	391	69.9	54.6	79.9	58.6	41.9	51.5	39
38	372	353	353	380	69.4	53.8	79.4	57.7	40.8	50.4	38
37	363	344	344	370	68.9	53.1	78.8	56.8	39.6	49.3	37
36	354	336	336	360	68.4	52.3	78.3	55.9	38.4	48.2	36
35	345	327	327	351	67.9	51.5	77.7	55.0	37.2	47.1	35
34	336	319	319	342	67.4	50.8	77.2	54.2	36.1	46.1	34
33	327	311	311	334	66.8	50.0	76.6	53.3	34.9	45.1	33
32	318	301	301	326	66.3	49.2	76.1	52.1	33.7	44.1	32
31	310	294	294	318	65.8	48.4	75.6	51.3	32.5	43.1	31
30	302	286	286	311	65.3	47.7	75.0	50.4	31.3	42.2	30
29	294	279	279	304	64.8	47.0	74.5	49.5	30.1	41.3	29
28	286	271	271	297	64.3	46.1	73.9	48.6	28.9	40.4	28
27	279	264	264	290	63.8	45.2	73.3	47.7	27.8	39.5	27
26	272	258	258	284	63.3	44.6	72.8	46.8	26.7	38.7	26
25	266	253	253	278	62.8	43.8	72.2	45.9	25.5	37.8	25
24	260	247	247	272	62.4	43.1	71.6	45.0	24.3	37.0	24
23	254	243	243	266	62.0	42.1	71.0	44.0	23.1	36.3	23
22	248	237	237	261	61.5	41.6	70.5	43.2	22.0	35.5	22
21	243	231	231	256	61.0	40.9	69.9	42.3	20.7	34.8	21
20	238	226	226	251	60.5	40.1	69.4	41.5	19.6	34.2	20

[A] In the table headings, *force* refers to total test forces.
[B] Annex A1 contains equations converting determined hardness scale numbers to Rockwell C hardness numbers for non-austenitic steels. Refer to 1.12 before using conversion equations.
[C] The Brinell hardness numbers in parentheses are outside the range recommended for Brinell hardness testing in 8.1 of Test Method E10.
[D] These Scleroscope hardness conversions are based on Vickers—Scleroscope hardness relationships developed from Vickers hardness data provided by the National Bureau of Standards for 13 steel reference blocks, Scleroscope hardness values obtained on these blocks by the Shore Instrument and Mfg. Co., Inc., the Roll Manufacturers Institute, and members of this institute, and also on hardness conversions previously published by the American Society for Metals and the Roll Manufacturers Institute.

APPENDIX B – VICKERS HARDNESS RESULTS

Vickers Hardness for Material Selection

Materials	**SS 431**		**SS 431/20 TiC**		**SS 431/40 TiC**		**SS 431/60 TiC**	
Layer	Single	Multi	Single	Multi	Single	Multi	Single	Multi
Hardness Measurement (HV)	421	424	520	541	586	752	699	859
	401	438	545	530	608	697	832	755
	444	433	470	555	550	816	852	820
	413	454	514	461	626	789	862	741
	402	448	550	548	687	777	685	876
Average (HV)	416.2	439.4	519.8	527	611.4	766.2	786	810.2
Standard Deviation	15.74	10.65	28.50	34.02	45.51	40.27	77.48	54.12

Vickers Hardness for Process Development

Carburized 8620		.50 mm from top	.25 mm from top	.50 mm from top	.25 mm from top	Avg.	STDEV
	0.25		783		622	702.50	80.50
	0.5	633		535		584.00	49.00
	0.75		462		512	487.00	25.00
	1	420		491		455.50	35.50
	1.25		325		397	361.00	36.00
	1.5	278		412		345.00	67.00
	1.75		319		393	356.00	37.00
	2	326		369		347.50	21.50
431/20 TiC		.50 mm from top	.25 mm from top	.50 mm from top	.25 mm from top	Avg.	STDEV
	0.25		772		720	746.00	26.00
	0.5	733		763		748.00	15.00
	0.75		590		678	634.00	44.00
	1	405		372		388.50	16.50
	1.25		323		321	322.00	1.00
	1.5	295		298		296.50	1.50
	1.75		213		264	238.50	25.50
	2	285		312		298.50	13.50
431/40 TiC		.50 mm from top	.25 mm from top	.50 mm from top	.25 mm from top	Avg.	STDEV
	0.25		862		798	830.00	32.00
	0.5	826		504		665.00	161.00
	0.75		461		774	617.50	156.50
	1	316		369		342.50	26.50
	1.25		344		369	356.50	12.50
	1.5	325		326		325.50	0.50
	1.75		267		267	267.00	0
	2	299		297		298.00	1.00

Vickers Hardness for Transverse RCF Test Specimen

Transverse		.125 mm from top	.25 mm from top	.125 mm from top	.25 mm from top	.125 mm from top	.25 mm from top	.125 mm from top	.25 mm from top	Avg.	STDEV
	0.125	717		699		699		704		704.75	7.36
	0.25		639		692		661		720	678.00	30.70
	0.375	725		655		680		661		680.25	27.44
	0.5		655		694		655		657	665.25	16.62
	0.625	735		666		664		671		684.00	29.56
	0.75		697		356		351		322	431.50	153.84
	0.875	325		341		305		309		320.00	14.25
	1		303		318		306		285	303.00	11.81
	1.125	281		321		257		319		294.50	26.88
	1.25		310		285		262		310	291.75	19.98
	1.375	304		325		287		294		302.50	14.33
	1.5		278		288		301		272	284.75	10.99
	1.625	303		283		282		283		287.75	8.81
	1.75		270		288		277		269	276.00	7.58
	1.875	279		272		266		269		271.50	4.82
	2		271		307		274		278	282.50	14.36
	2.125	259		281		269		287		274.00	10.82
	2.25		312		320		313		324	317.25	4.97
	2.375	314		302		306		297		304.75	6.22
	2.5		358		341		317		325	335.25	15.72
	2.625	339		341		335		347		340.50	4.33

Vickers Hardness for Longitudinal RCF Test Specimen

Longitudinal		.125 mm from top	.25 mm from top	.125 mm from top	.25 mm from top	.125 mm from top	.25 mm from top	.125 mm from top	.25 mm from top	Avg.	STDEV
	0.125	594		633		680		650		639.25	31.08
	0.25		602		620		687		648	639.25	32.07
	0.375	616		614		661		631		630.50	18.79
	0.5		590		575		655		628	612.00	31.46
	0.625	581		561		462		641		561.25	64.42
	0.75		302		308		342		322	318.50	15.39
	0.875	293		311		296		325		306.25	12.79
	1		278		283		277		312	287.50	14.33
	1.125	293		293		268		318		293.00	17.68
	1.25		299		302		280		293	293.50	8.44
	1.375	283		293		292		282		287.50	5.02
	1.5		288		285		287		286	286.50	1.12
	1.625	272		263		275		275		271.25	4.92
	1.75		249		257		266		260	258.00	6.12
	1.875	263		252		275		263		263.25	8.14
	2		272		265		275		273	271.25	3.77
	2.125	295		290		305		301		297.75	5.72
	2.25		306		290		300		324	305.00	12.37
	2.375	312		312		320		322		316.50	4.56
	2.5		328		345		319		319	327.75	10.62
	2.625	313		304		323		328		317.00	9.25

Surface Hardness on SS 431/20 TiC RCF Specimen

	HRC	Vickers Hardness (HV)
Surface Hardness	60	697
	61	720
	59	674
Average	60	697
Standard Deviation	0.82	18.78

Vickers Hardness for Inconel 718® Shaft and Deposited Materials

Inconel 718 Base		.25 mm from top	.50 mm from top	.25 mm from top	.50 mm from top		Avg.	STDEV
	0.25	416		483			449.50	33.50
	0.5		457		430		443.50	13.50
	0.75	445		436			440.50	4.50
	1		432		449		440.50	8.50
	1.25	450		449			449.50	0.50
	1.5		440		423		431.50	8.50
	1.75	455		440			447.50	7.50
	2		434		438		436.00	2.00
Inconel 718		.25 mm from top	.50 mm from top	.25 mm from top	.50 mm from top		Avg.	STD
	0.25	308		341			324.50	16.50
	0.5		307		277		292.00	15.00
	0.75	304		292			298.00	6.00
	1		291		313		302.00	11.00
	1.25	301		293			297.00	4.00
	1.5		304		291		297.50	6.50
	1.75	270		278			274.00	4.00
	2		280		302		291.00	11.00
	2.25	261		250			255.50	5.50
	2.5		259		294		276.50	17.50
	2.75	276		267			271.50	4.50
	3		289		290		289.50	0.50
	3.25	274		282			278.00	4.00
SS 431		.25 mm from top	.50 mm from top	.25 mm from top	.50 mm from top		Avg.	STD
	0.25	254		239			246.50	7.50
	0.5		230		226		228.00	2.00
	0.75	224		225			224.50	0.50
	1		219		232		225.50	6.50
	1.25	241		280			260.50	19.50
	1.5		276		263		269.50	6.50
	1.75	287		266			276.50	10.50
	2		287		283		285.00	2.00
	2.25	267		262			264.50	2.50
	2.5		266		281		273.50	7.50
	2.75	270		274			272.00	2.00
	3		251		270		260.50	9.50
	3.25	242		214			228.00	14.00
431/20 TiC		.25 mm from top	.50 mm from top	.25 mm from top	.50 mm from top		Avg.	STD
	0.25	238		257			247.50	9.50
	0.5		257		317		287.00	30.00
	0.75	236		242			239.00	3.00
	1		234		277		255.50	21.50
	1.25	245		258			251.50	6.50
	1.5		243		248		245.50	2.50
	1.75	259		254			256.50	2.50
	2		243		257		250.00	7.00
	2.25	274		249			261.50	12.50
	2.5		269		266		267.50	1.50
	2.75	277		283			280.00	3.00
	3		299		291		295.00	4.00
	3.25	336		295			315.50	20.50
431/40 TiC		.25 mm from top	.50 mm from top	.25 mm from top	.50 mm from top		Avg.	STD
	0.25	374		324			349.00	25.00
	0.5		368		352		360.00	8.00
	0.75	325		348			336.50	11.50
	1		336		331		333.50	2.50
	1.25	302		270			286.00	16.00
	1.5		254		286		270.00	16.00
	1.75	282		273			277.50	4.50
	2		287		304		295.50	8.50
	2.25	298		311			304.50	6.50
	2.5		296		307		301.50	5.50
	2.75	317		320			318.50	1.50
	3		325		317		321.00	4.00

Vickers Hardness for Chrome Electroplated Surface on Inconel 718® Shaft

Chrome Electroplated	Vickers Hardness (HV)
	692
	690
	725
	746
	702
Average	711
Standard Deviation	21.47

APPENDIX C – LASER DEPOSTION PROCESS PARAMETERS

	Laser Power (watts)	Travel Speed (IPM)	Powder Type	Powder Flow Rate (g/min)	Gas Type	Gas Flow Coaxial Rate (cfh)	Gas Flow Process Rate (cfh)	Gas Flow Trailing Rate (cfh)	Powder Nozzle Standoff (mm)	Spot Size (mm)	Comments
Material Selection	2000	25	431		Ar	20	20		10	4	1 rev on gullco, 2" DIA. PIPE
	2000	25	431/ 20% TiC		Ar	20	20		10	4	1 rev on gullco
	2000	25	431/ 40% TiC		Ar	20	20		10	4	1 rev on gullco
	2000	25	431		Ar	20	20	30	10	4	candy stripe,step over .075 "., 2nd layer over last .5 ", z up .035", cool down between layers, with trailing shield
	2000	25	431/ 20% TiC		Ar	20	20	30	10	4	candy stripe,step over .075 "., 2nd layer over last .5 ", z up .035", cool down between layers, with trailing shield
	2000	25	431/ 60% TiC		Ar	20	20	30	10	4	candy stripe,step over .075 "., 2nd layer over last .5 ", z up .035", cool down between layers, with trailing shield
	2000	25	431/ 40% TiC		Ar	20	20	30	10	4	candy stripe,step over .075 "., 2nd layer over last .5 ", z up .035", cool down between layers, with trailing shield
Process Development	1000	25	431/ 20% TiC		Ar	20	20	20	10	2.5	candy stripe, step .050", 1.35" length
	1000	25	431/ 40% TiC		Ar	20	20	20	10	2.5	candy stripe, step .050", 1.35" length
RCF Shaft-1	1000	25	431/ 20% TiC		Ar	20	20	20	10	2.5	candy stripe, step .050", 1.35" length
RCF Shaft-2	1000	25	431/ 20% TiC		Ar	20	20	20	10	2.5	candy stripe, step .050", 1.35" length
RCF Shaft-3	1000	25	431/ 20% TiC		Ar	20	20	20	10	2.5	candy stripe, step .050", 1.35" length
RCF Shaft-4	1000	25	431/ 20% TiC		Ar	20	20	20	10	2.5	candy stripe, step .050", 1.35" length

APPENDIX D – DMWR FOR REPAIR OF CRITICAL COMPONENTS

OVERHAUL REPAIR PROCEDURE **DMWR 1-4140-228**

ITEM: SHAFT **PART NO. 70361-03014-101**

A. **EQUIPMENT** OD/ID Grinding machine

LENS Industrial Additive Manufacturing System

B. **MATERIAL** Ti-6V-4V ELI grade by Phelly Materials

C. **FLUORESCENT PENETRANT INSPECTION**

Inspect per **ASTM-E1417**. No fractures or cracks allowed. Part is a Critical Safety Item (CSI). Refer to DMWR 1-4140-228 Overhaul Inspection procedure item no. **4** reference letter **C**.

D. **PROCESS**

PRE-MACHINE REPAIR AREA:

Grind journal diameter to **1.9550-1.9590** inch. Refer to DMWR 1-4140-228 Overhaul Repair procedure for **figure 1.**
NOTE: use a **Silicon carbide** grinding wheel.

E. **FLUORESCENT PENETRANT INSPECTION**

Inspect per **ASTM-E1417**. No fractures or cracks allowed. Part is a Critical Safety Item (CSI). Refer to DMWR 1-4140-228 Overhaul Inspection procedure item no. **4** reference letter **C**.

F. **POWDER APPLICATION**
DDM process the repair area per the parameters listed below.
Refer to DMWR 1-4140-228 Overhaul Repair procedure for **figure 1.**

NOTE: Mask areas surrounding the repair area to prevent straying of powder.

MACHINE PARAMETERS AND MEDIA SPECIFICATIONS:

Media Properties

Type of Powder:	Ti-6V-4V ELI grade (Grade 23) by Phelly Materials or equivalent
Powder Size:	-100/+325 mesh (50 – 150 µm)

Laser

Wave Length:	1070 nm
Spot Size:	2 mm diameters
Average Power:	500 W
Shield Gas:	Ar
Shield Gas Velocity:	30 L/min

Powder Feeder

Type of Nozzle:	Coaxial
Powder Feed Rate:	3 g/min (~3 RPM)
Inert/Carrier Gas:	Ar
Inert/Carrier Gas Flow Rate:	4 L/min

G. FIINISH MACHINE REPAIR AREA

Final grind journal diameter to **1.9685-1.9690** inch. Refer to DMWR 1-4140-228 Overhaul Repair procedure for **figure 1.** Maintain runout requirements. Refer to DMWR 1-4140-228 Overhaul Inspection procedure item no. **6** reference letter **E.**
NOTE: use a **Silicon carbide** grinding wheel.

H. CLEAN PART

Clean part post repair per Paragraph 3-10.

I. STRESS RELIEF

Stress relief part in air furnace at 1100°F for 4 hours and furnace cool. Reapply dry film lubricant per paragraph 3-12.10.

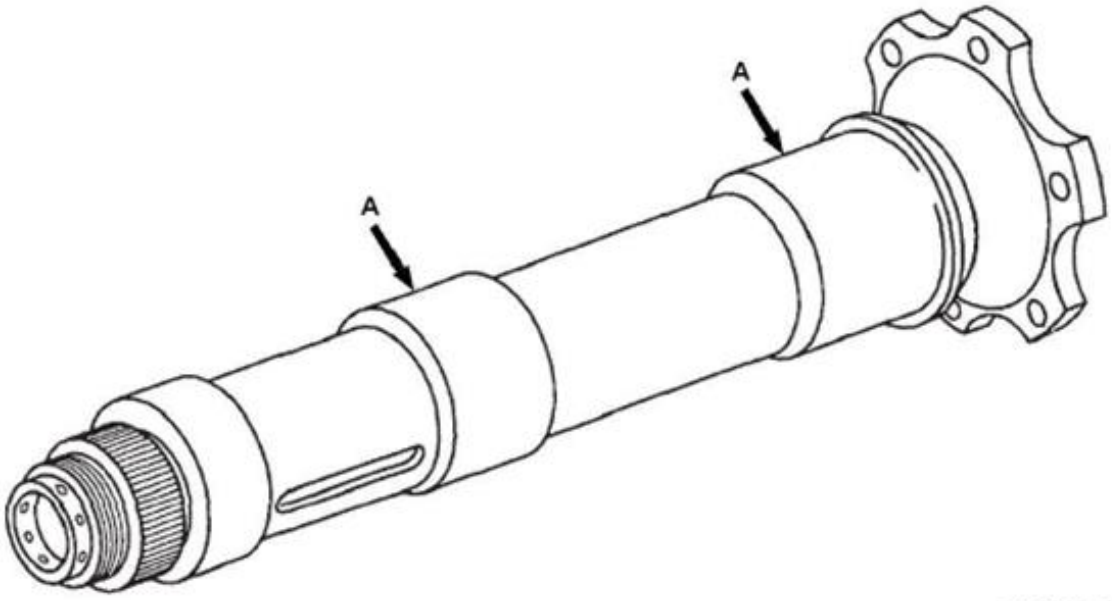

FIGURE 1

APPENDIX E – OPTICAL PROFILOMETRY DATA

Carburized 8620 Steel

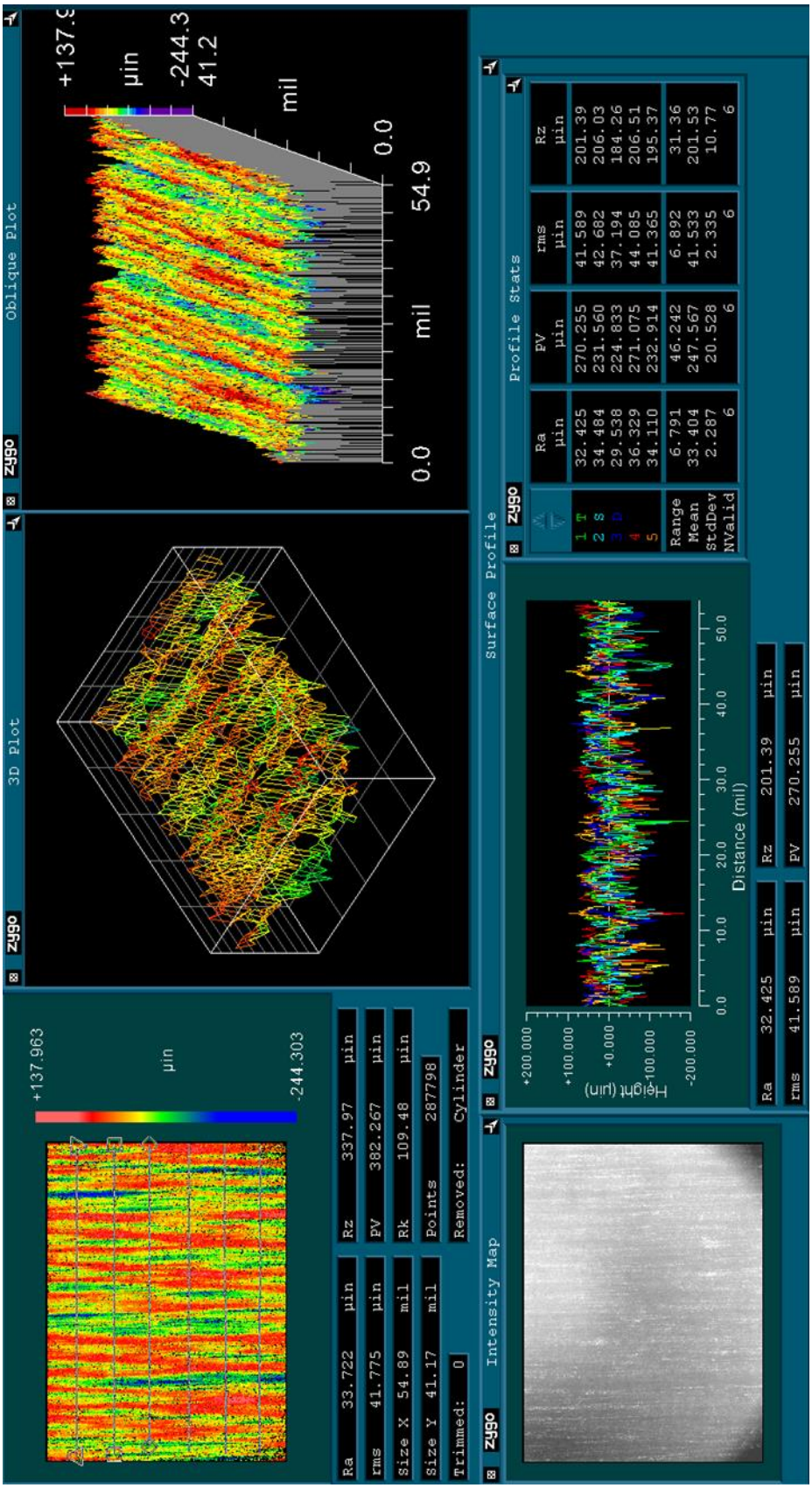

SS 431/20 TiC Laser Deposited on Carburized 8620 Steel

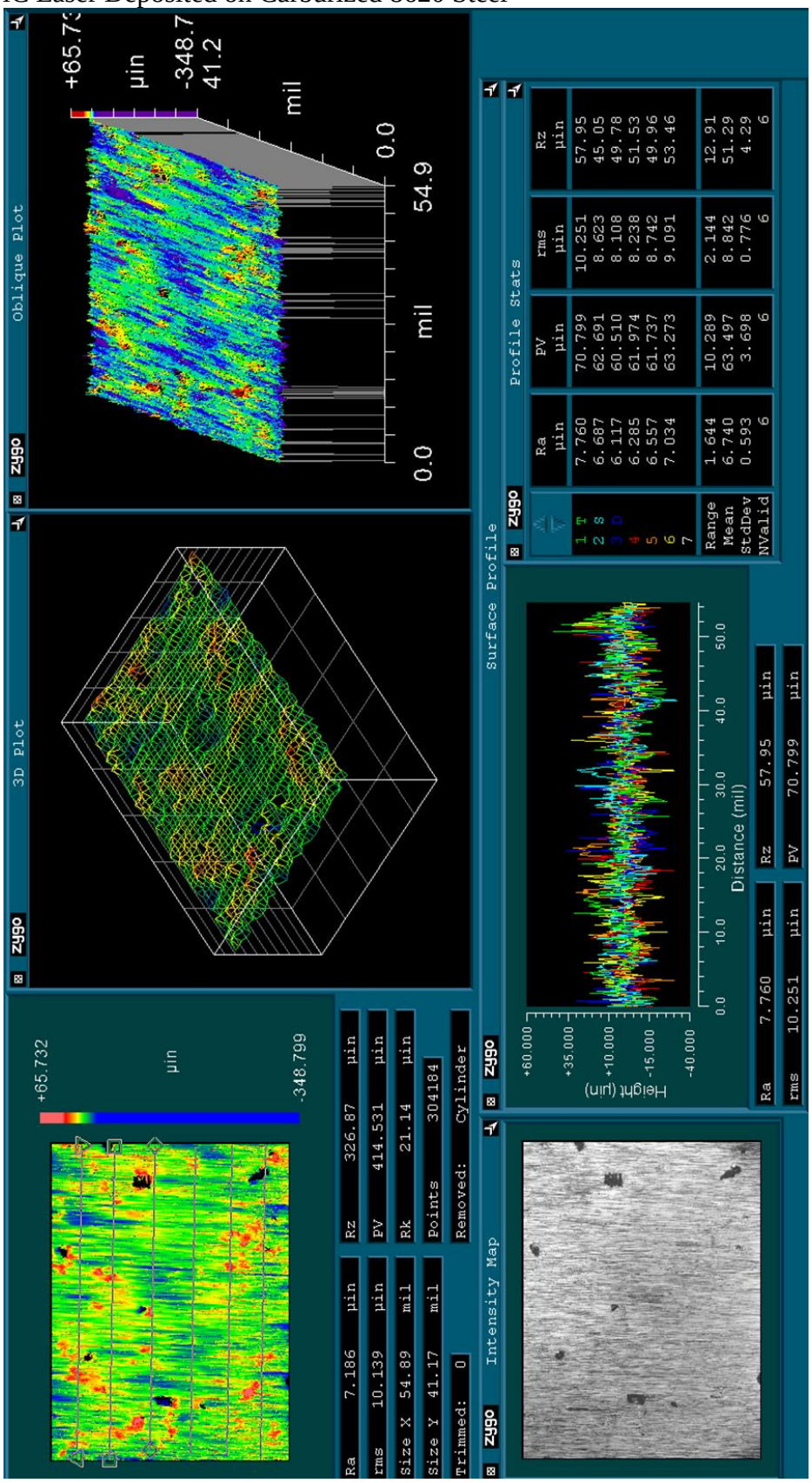

SS 431/20 TiC Laser Deposited on Carburized 8620 Steel, Pores

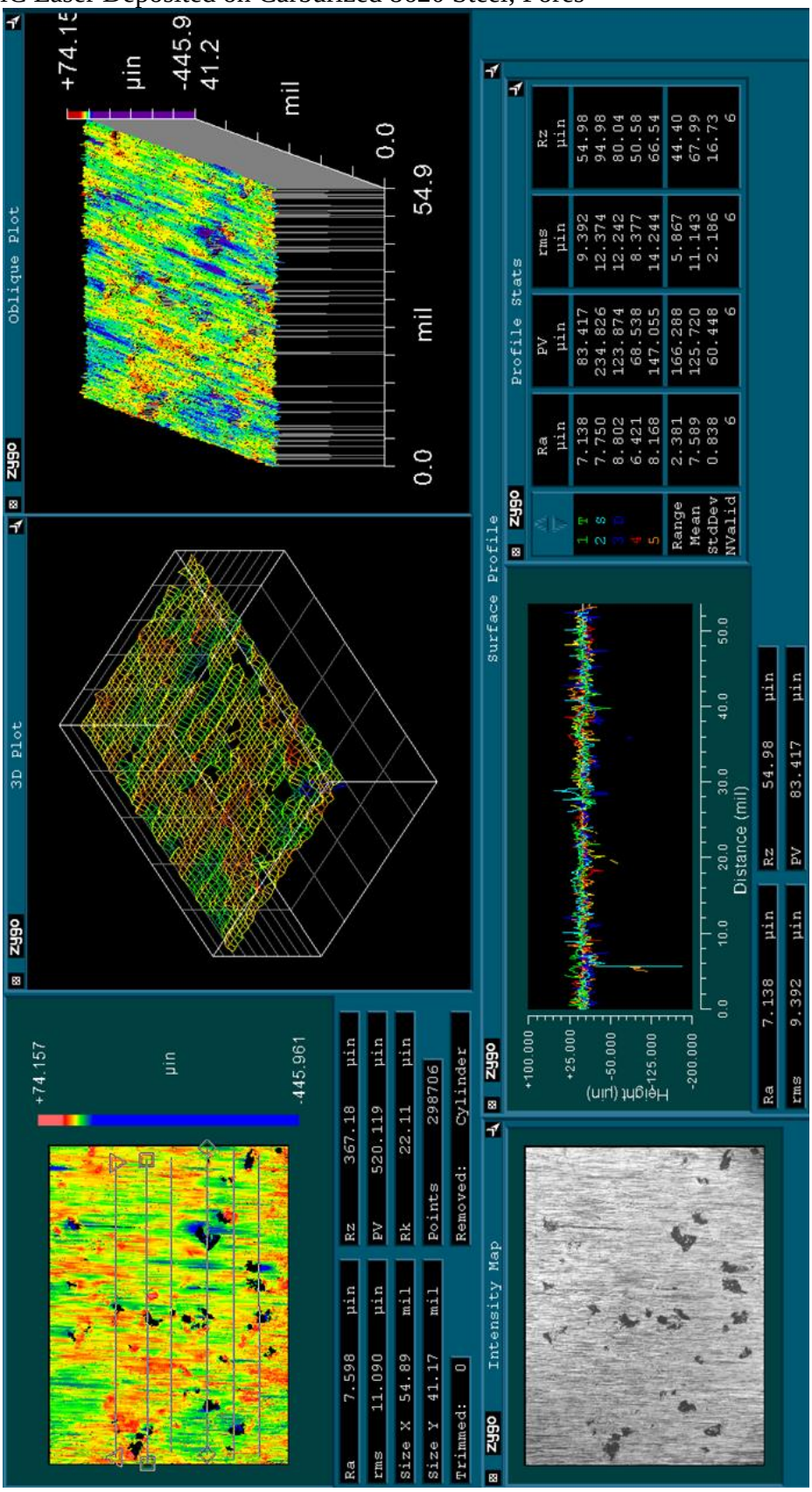

Inconel 718® Shaft

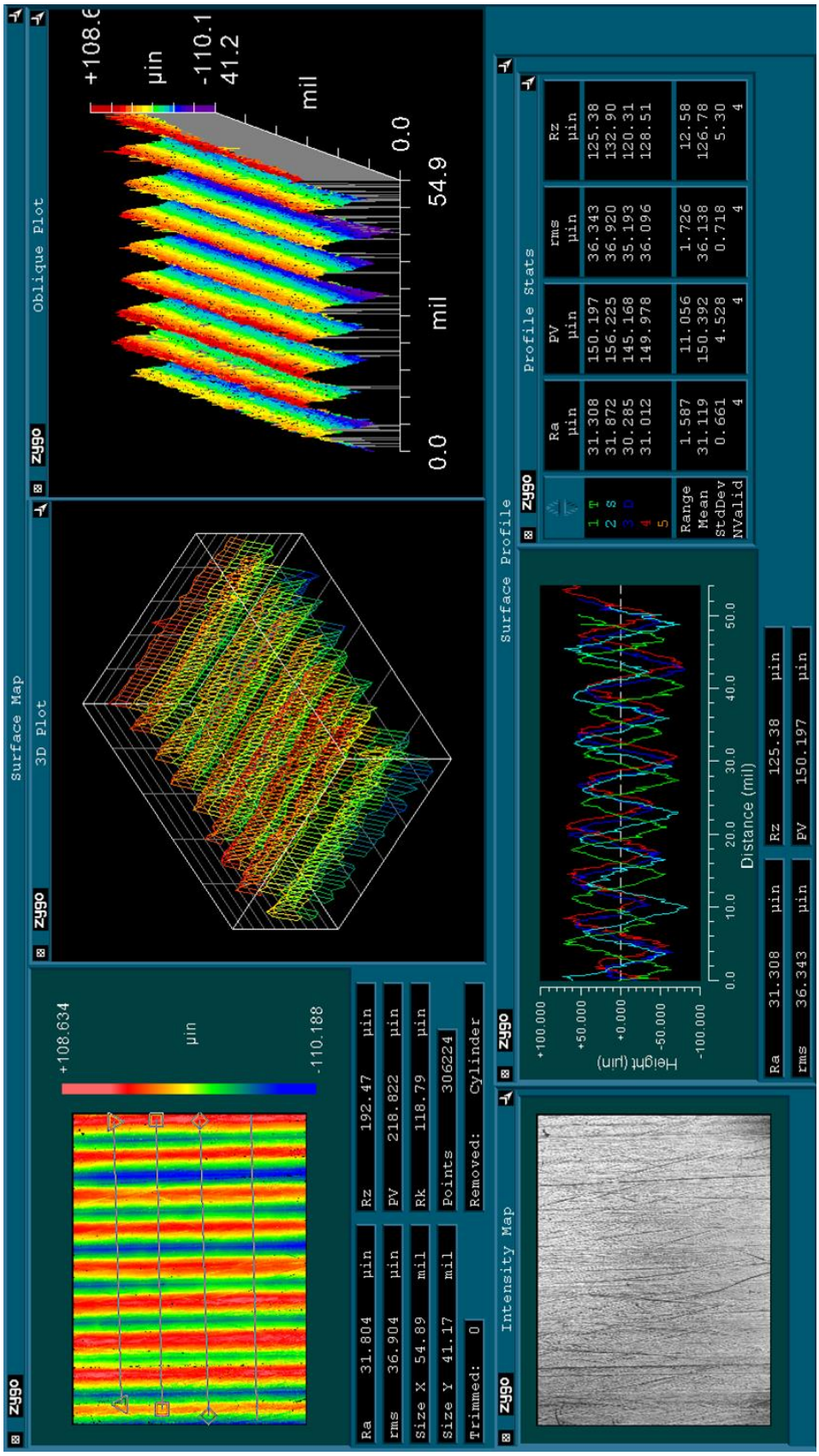

Inconel 718® laser Deposited on Inconel 718® Shaft

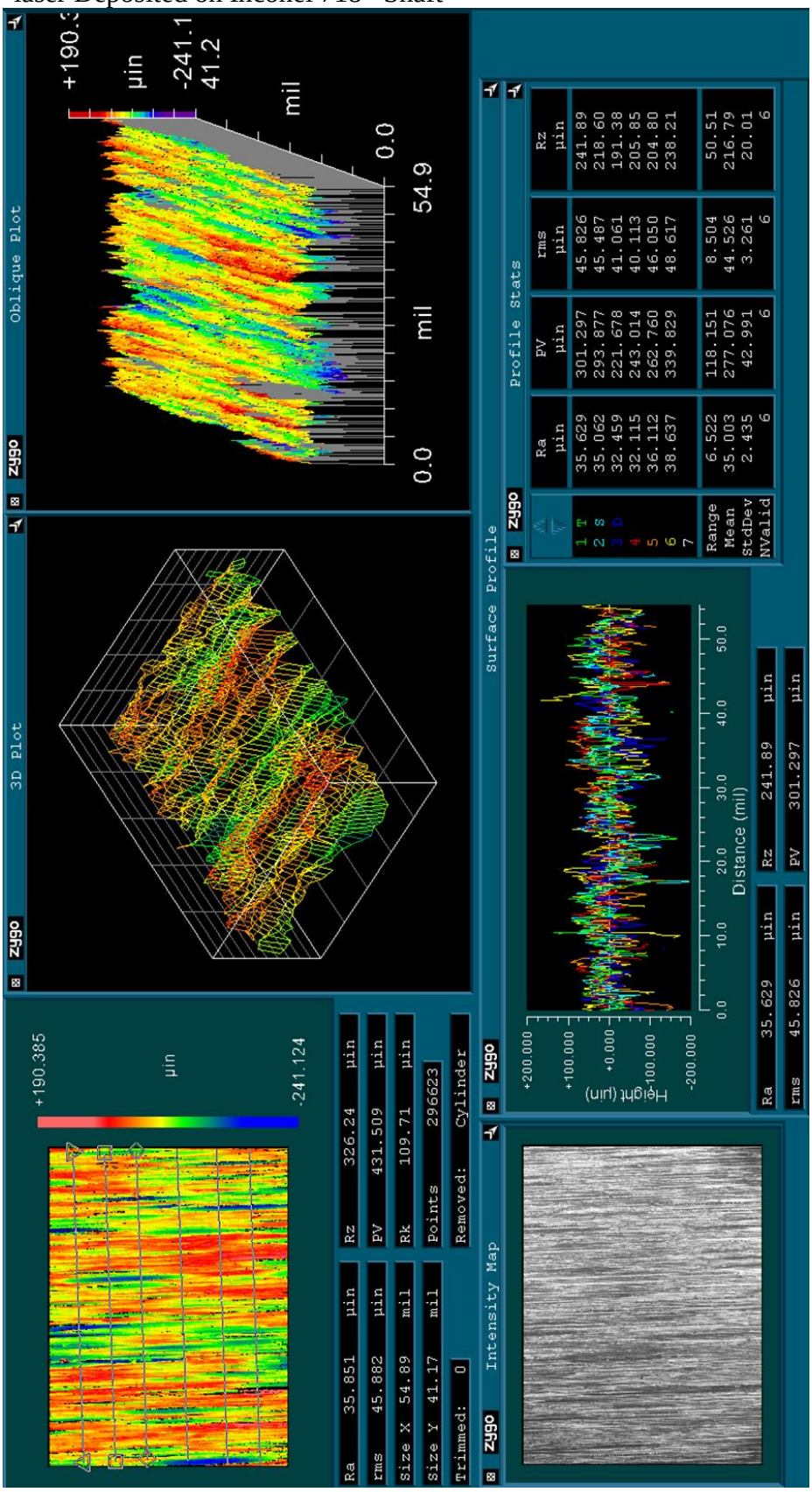

SS 431 laser Deposited on Inconel 718® Shaft

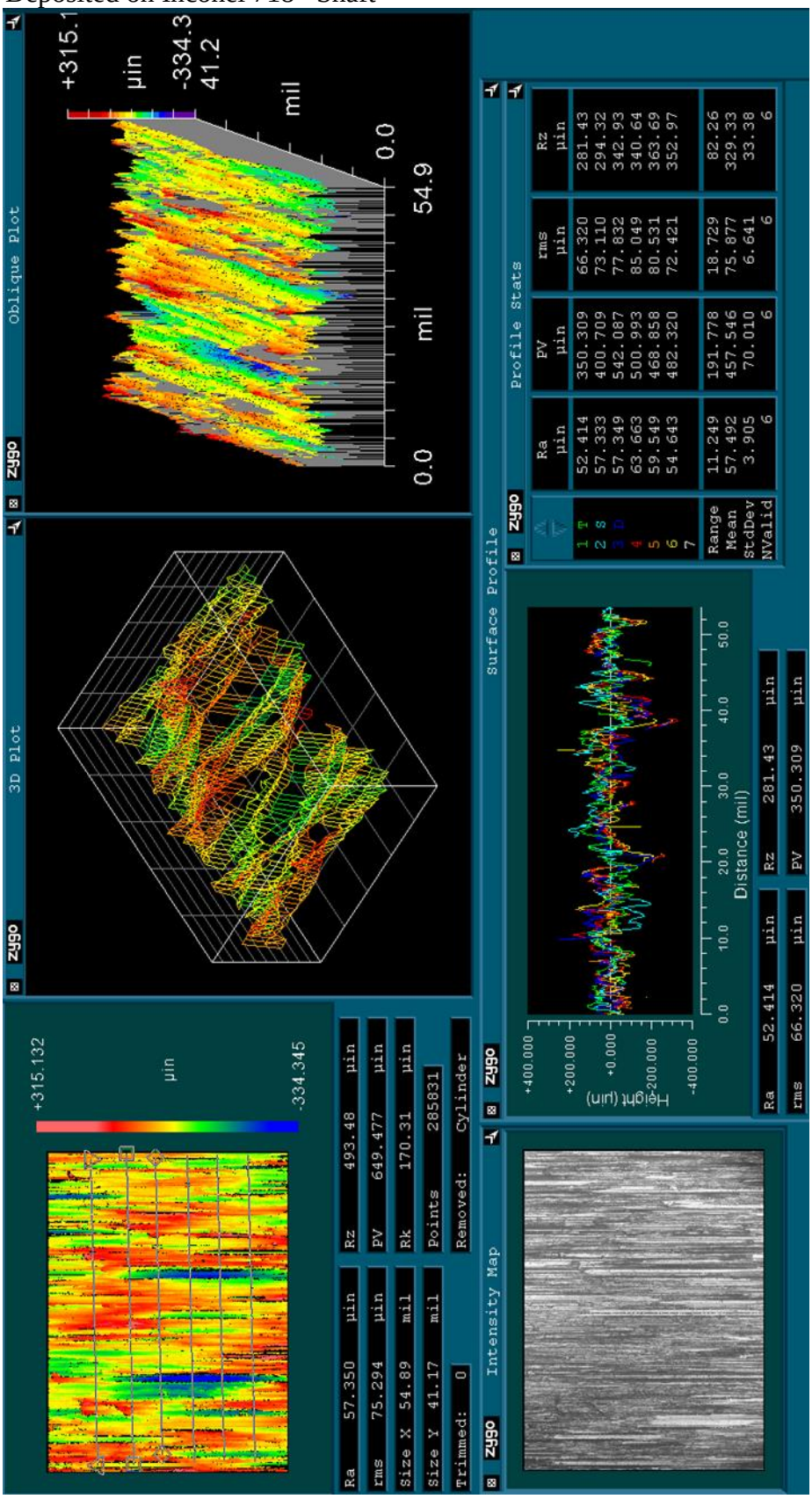

SS 431/20 TiC laser Deposited on Inconel 718® Shaft

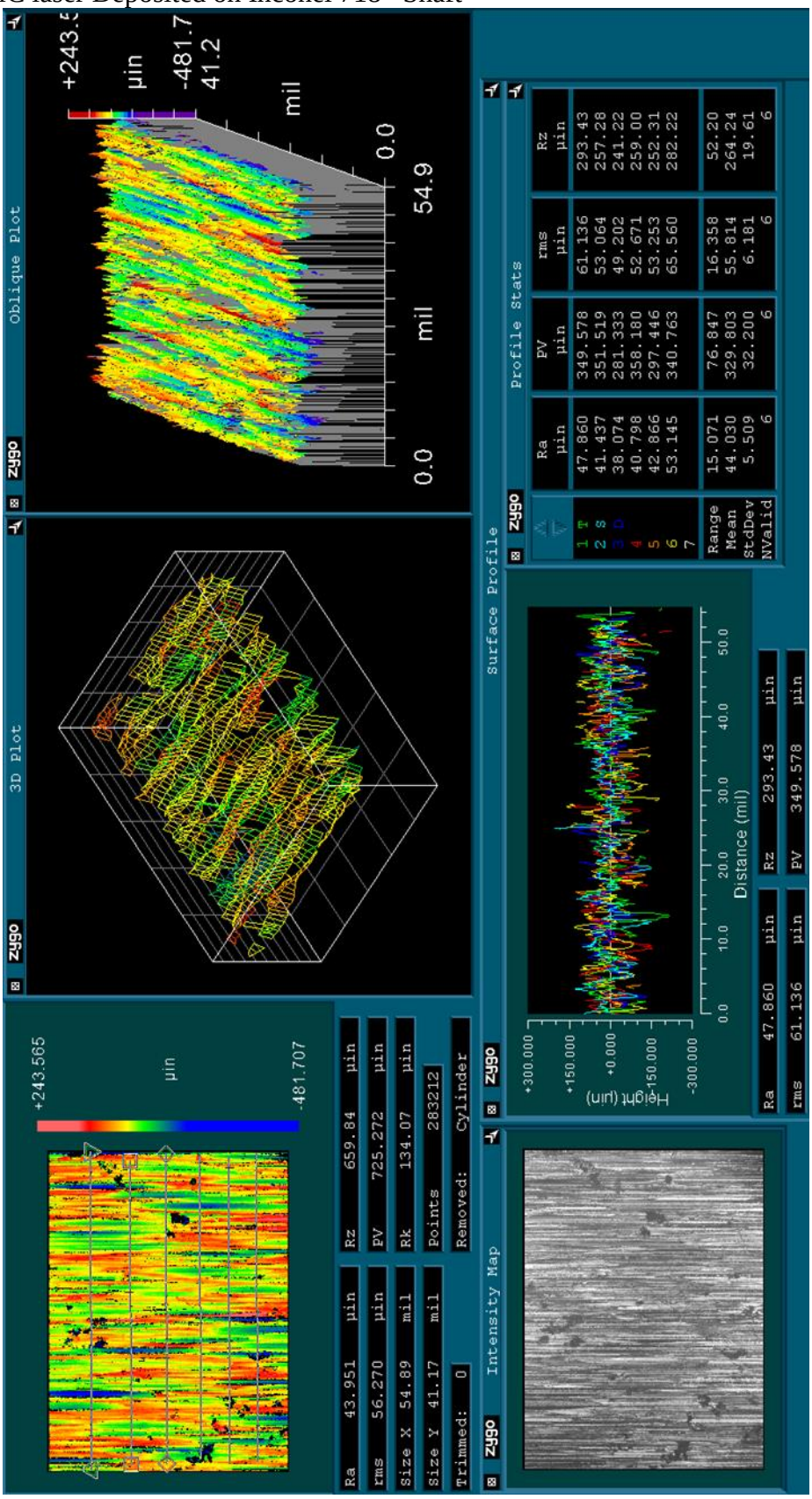

SS 431/40 TiC laser Deposited on Inconel 718® Shaft